LBL-12520
SAC-37
UC-70

SWEDISH-AMERICAN COOPERATIVE PROGRAM ON RADIOACTIVE WASTE STORAGE IN MINED CAVERNS IN CRYSTALLINE ROCK

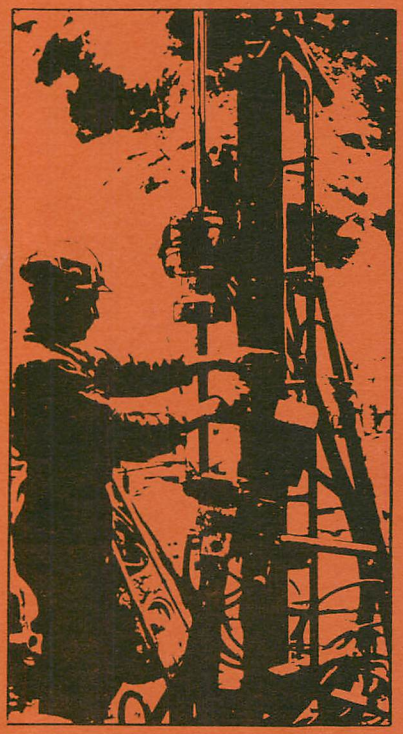

GEOHYDROLOGICAL DATA FROM THE MACROPERMEABILITY EXPERIMENT AT STRIPA, SWEDEN

Charles R. Wilson, Jane C. S. Long,
Robert M. Galbraith, Kenji Karasaki,
Howard K. Endo, Andrew O. DuBois,
Malcolm J. McPherson, and Gunnar Ramqvist

Lawrence Berkeley Laboratory
University of California
Berkeley, California 94720

March 1981

A Joint Project of

Swedish Nuclear Fuel Supply Co.
Fack 10240 Stockholm, Sweden

Operated for the Swedish
Nuclear Power Utility Industry

Lawrence Berkeley Laboratory
Earth Sciences Division
University of California
Berkeley, California 94720, USA

Operated for the U.S. Department of
Energy under Contract DE-AC03-76SF00098

This report was prepared as an account of work sponsored by the United States Government and/or the Swedish Nuclear Fuel Supply Company. Neither the United States nor the U.S. Department of Energy, nor the Swedish Nuclear Fuel Supply Company, nor any of their employees, nor any of their contractors, subcontractors, or their employees, makes any warranty, express or implied or assumes any legal liability or responsibility for the accuracy, completeness or usefulness of any information, apparatus, product or process disclosed, or represents that its use would not infringe privately owned rights.

Printed in the United States of America
Available from
National Technical Information Service
U.S. Department of Commerce
5285 Port Royal Road
Springfield, VA 22161
Price Code: A09

Lawrence Berkeley Laboratory is an equal opportunity employer.

LBL-12520
SAC-37
UC-70

GEOHYDROLOGICAL DATA FROM THE MACROPERMEABILITY EXPERIMENT AT STRIPA, SWEDEN

Charles R. Wilson, Jane C.S. Long, Robert M. Galbraith,
Kenji Karasaki, Howard K. Endo, Andrew O. DuBois,
Malcolm J. McPherson, and Gunnar Ramqvist

Lawrence Berkeley Laboratory
University of California
Berkeley, California 94720

March 1981

This work was supported by the Assistant Secretary for Nuclear Energy, Office of Waste Isolation of the U.S. Department of Energy under Contract DE-AC03-76SF00098. Funding for this project is administered by the Office of Nuclear Waste Isolation at Battelle Memorial Institute.

PREFACE

This report is one of a series documenting the results of the Swedish-American cooperative research program in which the cooperating scientists explore the geological, geophysical, hydrological, geochemical, and structural effects anticipated from the use of a large crystalline rock mass as a geologic repository for nuclear waste. This program has been sponsored by the Swedish Nuclear Power Utilities through the Swedish Nuclear Fuel Supply Company (SKBF), and the U.S. Department of Energy (DOE) through the Lawrence Berkeley Laboratory.

The principal investigators are L.B. Nilsson and O. Degerman for SKBF, and N.G.W. Cook, P.A. Witherspoon, and J.E. Gale for LBL. Other participants will appear as authors of the individual reports.

Previous technical reports in this series are listed below.

1. Swedish-American Cooperative Program on Radioactive Waste Storage in Mined Caverns by P.A. Witherspoon and O. Degerman. (LBL-7049, SAC-01).

2. Large Scale Permeability Test of the Granite in the Stripa Mine and Thermal Conductivity Test by Lars Lundstrom and Haken Stille. (LBL-7052, SAC-02).

3. The Mechanical Properties of the Stripa Granite by Graham Swan. (LBL-7074, SAC-03).

4. Stress Measurements in the Stripa Granite by Hans Carlsson. (LBL-7078, SAC-04).

5. Borehole Drilling and Related Activities at the Stripa Mine by P.J. Kurfurst, T. Hugo-Persson, and G. Rudolph. (LBL-7080, SAC-05).

6. A Pilot Heater Test in the Stripa Granite by Hans Carlsson. (LBL-7086, SAC-06).

7. An Analysis of Measured Values for the State of Stress in the Earth's Crust by Dennis B. Jamison and Neville G.W. Cook. (LBL-7071, SAC-07).

8. Mining Methods Used in the Underground Tunnels and Test Rooms at Stripa by B. Andersson and P.A. Halen. (LBL-7081, SAC-08).

9. Theoretical Temperature Fields for the Stripa Heater Project by T. Chan, Neville G.W. Cook, and C.F. Tsang. (LBL-7082, SAC-09).

10. Mechanical and Thermal Design Considerations for Radioactive Waste Repositories in Hard Rock. Part I: An Appraisal of Hard Rock for Potential Underground Repositories of Radioactive Waste by N.G.W. Cook; Part II: In Situ Heating Experiments in Hard Rock: Their Objectives and Design by N.G.W. Cook and P.A. Witherspoon. (LBL-7073, SAC-10).

11. Full-Scale and Time-Scale Heating Experiments at Stripa: Preliminary Results by N.G.W. Cook and M. Hood. (LBL-7072, SAC-11).

12. Geochemistry and Isotope Hydrology of Groundwaters in the Stripa Granite: Results and Preliminary Interpretation by P. Fritz, J.F. Barker, and J.E. Gale. (LBL-8285, SAC-12).

13. Electrical Heaters for Thermo-Mechanical Tests at the Stripa Mine by R.H. Burleigh, E.P. Binnall, A.O. DuBois, D.O. Norgren, and A.R. Ortiz. (LBL-7063, SAC-13).

14. Data Acquisition, Handling, and Display for the Heater Experiments at Stripa by Maurice B. McEvoy. (LBL-7063, SAC-14).

15. An Approach to the Fracture Hydrology at Stripa: Preliminary Results by J.E. Gale and P.A. Witherspoon. (LBL-7079, SAC-15).

16. Preliminary Report on Geophysical and Mechanical Borehole Measurements at Stripa by P. Nelson, B. Paulsson, R. Rachiele, L. Andersson, T. Schrauf, W. Hustrulid, O. Duran, and K.A. Magnussen. (LBL-8280, SAC-16).

17. Observations of a Potential Size-Effect in Experimental Determination of the Hydraulic Properties of Fractures by P.A. Witherspoon, C.H. Amick, J.E. Gale, and K. Iwai. (LBL-8571, SAC-17).

18. Rock Mass Characterization for Storage in Nucler Waste in Granite by P.A. Witherspoon, P. Nelson, T. Doe, R. Thorpe, B. Paulsson, J.E. Gale, and C. Forster. (LBL-8570, SAC-18).

19. Fracture Detection in Crystalline Rock Using Ultrasonic Shear Waves by K.H. Waters, S.P. Palmer, and W.F. Farrell. (LBL-7051, SAC-19).

20. Characterization of Discontinuities in the Stripa Granite--Time Scale Heater Experiment by R. Thorpe. (LBL-7083, SAC-20).

21. Geology and Fracture System at Stripa by A. Okliewicz, J.E. Gale, R. Thorpe, and B. Paulsson. (LBL-8907, SAC-21).

22. Calculated Thermally Induced Displacements and Stresses for Heater Experiements at Stripa by T. Chan and N.G.W. Cook. (LBL-7061, SAC-22).

23. Validity of Cubic Law for Fluid Flow in a Deformable Rock Fracture by P.A. Witherspoon, J. Wang, K. Iwai, and J.E. Gale. (LBL-9557, SAC-23).

24. Determination of In-Situ Thermal Properties of Stripa Granite from Temperature Measurements in the Full-Scale Heater Experiments: Methods and Primary Results by J. Jeffry, T. Chan, N.G.W. Cook and P.A. Witherspoon. (LBL-8424, SAC-24).

25. Instrumentation Evaluation, Calibration, and Installation for Heater Tests Simulating Nuclear Waste in Crystalline Rock, Sweden by T. Schrauf, H. Pratt, E. Simonson, W. Hustrulid, P. Nelson, A. DuBois, E. Binnall, and R. Haught. (LBL-8313, SAC-25)

26. Part I: Some Results From a Field Investigation of Thermo-Mechanical Loading of a Rock Mass When Heater Canisters are Emplaced in the Rock by M. Hood. Part II: The Application of Field Data from Heater Experiments Conducted at Stripa, Sweden for Repository Design by M. Hood, H. Carlsson, and P.H. Nelson. (LBL-9392, SAC-26).

27. Progress with Field Investigations at Stripa by P.A. Witherspoon, N.G.W. Cook, and J.E. Gale (LBL-10559, SAC-27).

28. A Laboratory Assessment of the Use of Borehole Pressure Transients to Measure the Permeability of Fractured Rock Masses by C.B. Forster and J.E. Gale. (LBL-8674, SAC-28).

29. Thermal and Thermomechanical Data for In Situ Heater Experiments at Stripa, Sweden by T. Chan, E. Binnall, P. Nelson, O. Wan, C. Weaver, K. Ang, J. Braley, and M. McEvoy. (LBL-11477, SAC-29).

30. The Effect of Radon Transport in Groundwater Upon Gamma Ray Borehole Logs by P.H. Nelson, R. Rachiele, and A. Smith. (LBL-11180, SAC-30).

31. Strength and Permeability Tests on Ultra-Large Stripa Granite Core by R. Thorpe, D.J. Watkins, W.E. Ralph, R. Hsu, and S. Flexser. (LBL-11203, SAC-31).

32. Ultrasonic and Acoustic Emission Results from the Stripa Heater Experiments. Part I: A Cross-Hole Investigation of a Rock Mass Subjected to Heating by B.N.P. Paulsson and M.S. King. Part II: Acoustic Emission Monitoring During Cool-Down of the Stripa Heater Experiment by R. Rachiele. (LBL-10975, SAC-32).

33. Numerical Modeling to Assess Possible Influence of the Mine Openings on Far-Field In Situ Stress Measurements at Stripa by T. Chan, V. Guvanasen, and N. Littlestone (LBL-12469, SAC-33).

34. A Field Assessment of the Use of Borehole Pressure Transients to Measure the Permeability of Fractured Rock Masses by C.B. Forster and J.E. Gale. (LBL-11829, SAC-34).

35. Water Inflow into Boreholes During the Stripa Experiments by P.H. Nelson, R. Rachiele, J.S. Remer and H.S. Carlsson (LBL-12547, SAC-35).

36. Petrology and Radiogeology of the Stripa Pluton by H. Wollenberg, S. Flexser, and L. Andersson. (LBL-11654, SAC-36).

CONTENTS

	Page
LIST OF FIGURES	vii
LIST OF TABLES	ix
LIST OF MICROFICHE FILES	xi
MATHEMATICAL NOTATION	xiii
ABSTRACT	xvii
1.0 INTRODUCTION	1
1.1 Objectives and Scope of Report	1
1.2 Objectives of the Experiment	2
2.0 GENERAL DESCRIPTION OF THE EXPERIMENT	5
2.1 Test Facility	5
2.2 General Experimental Procedures	16
2.3 Supplementary Tests	23
3.0 DATA ACQUISITION AND STORAGE PROCEDURES	29
3.1 General Data Handling	29
3.2 Ventilation System Data Acquisition	30
3.3 Water Pressure Data Acquisition	44
3.4 Rock-Water Temperature Data Acquisition	49
3.5 Geochemical Data Acquisition	54
4.0 DATA REDUCTION PROCEDURES	55
4.1 Introduction	55
4.2 Reduction of Ventilation System Data	55
4.3 Computation of Net Moisture Pickup	55
4.4 Reduction of Water Pressure Data	61
4.5 Reduction of Temperature Data	80
4.6 Example Computation of Hydraulic Conductivity	83
5.0 ERROR AND SENSITIVITY ANALYSIS	89
5.1 Theory of Error Analysis	89
5.2 Error Analysis of Net Moisture Pickup Data	98
5.3 Sensitivity Analysis of Net Moisture Pickup	105
5.4 Error Resulting From Use of a Simplified Head	108
5.5 Error in Temperature Data	120
6.0 PRESENTATION OF DATA	123
6.1 Organization	123
6.2 Water Pressure Data	123
6.3 Borehole Water Temperature Data	127
6.4 Ventilation System Data	127
6.5 Shunting Test Data	130
6.6 Rock Temperature Data from Temperature Hole	134

Page

6.7 Rock Temperature Data from Drift Walls 134
6.8 Exhaust Duct Temperature Data 134
6.9 Differential Duct Temperature Data 140
6.10 Room Air Temperature Data 142
6.11 Air Flow Data 142
6.12 Geometric Data 142
6.13 Tracer Test Data 146
6.14 Geochemical Data 151

ACKNOWLEDGMENTS 153

REFERENCES 155

APPENDIX A. COMPUTATION OF NET MOISTURE PICKUP A-1

APPENDIX B. EQUATIONS FOR SENSITIVITY OF NET MOISTURE PICKUP TO VARIOUS INPUT PARAMETERS B-1

LIST OF FIGURES

		Page
1.	Location of experimental rooms in granite rock mass at Stripa .	6
2.	Schematic view of experimental setup	9
3.	Plan view of experimental area	12
4.	Plan view of Stripa site showing surface holes	15
5.	Charts used to assist in operation of the ventilation system for assumed inlet conditions of 14.5° dry bulb temperature and 65% relative humidity	18
6.	Schematic drawing of pipe string packers and water pressure and temperature sensing ports installed in boreholes	22
7.	Block diagram of ventilation data collection system	31
8.	Sample data sheet for ventilation system measurements	32
9.	Sample data sheet for water pressure and temperature measurements	45
10.	Sample data sheet for two zone shunting tests	47
11.	Sample data sheet for three zone shunting tests	48
12.	Sample data sheet for salt tracer test	50
13.	Sample data sheet for temperature hole measurements	52
14.	Sample data sheet for wall temperature measurements	53
15.	Flow chart for determination of net moisture pickup	60
16.	Net moisture pickup for the period 19 November 1979 to 22 September 1980	62
17.	Borehole layout in ventilation drift	70
18.	Cross-section of the ventilation drift showing boreholes R01 to R05	71
19.	Cross-section of the ventilation drift showing boreholes R06 to R10	72
20.	Section showing boreholes HG1, HG2 and HG4	73
21.	Section showing boreholes HG1, HG3 and HG5	74

Page

22. Perspective view of the HG boreholes 75

23. Arrangement of water pressure gauges on the gauge panels 77

24. Alignment and zone locations in borehole DBH-2 78

25. Average temperature vs. vertical distance from floor in time-scale drift 81

26. Distance-drawdown plot of initial 20° test results 87

27. Types of errors occurring in experiments 90

28. Hypothetical results of repeated measurements of a constant parameter 92

29. Examples of two Gaussian error curves with different values of mean (μ) and variance (σ^2) 94

30. Illustration of standard error 95

31. Flow chart for determination of experimental error in net moisture pickup 99

32. Experimental error bars for net moisture pickup data 104

33. Geometric information for computing hydraulic head in R04 zone 3 112

34. Temperature variation with distance from drift wall for R04 and temperature hole on 25 July 1980 113

35. Sources of error in the hydraulic head 116

36. Example of exhaust duct circular chart temperature data 139

37. Example of differential duct circular chart temperature data . . 141

38. Example of room air temperature circular chart data 143

39. Example of air flow rate circular chart data 144

A1. Air flow monitor calibration for test period of August 1979 to 22 April 1980 . . . . . A- 9

A2. Air flow monitor calibration for test period of 14 May 1980 to 27 May 1980 . . . . . A-10

A3. Air flow monitor calibration for test period of 28 May 1980 to 29 July 1980 . . . . . A-11

A4. Air flow monitor calibration for test period of 2 August 1980 to 22 September 1980 . . . . . A-12

LIST OF TABLES

Page

1. Approximate minimum distances from ventilation drift to nearby openings 14

2. Shunting test zones 23

3. Equipment specifications 33

4. Periods of use for air velocity metering systems 41

5. Net moisture pickup data 63

6. Error in simplified hydraulic head for selected zones on July 25, 1980 85

7. Sensitivity of net moisture pickup to input parameters: examples for data of 20°C and 45°C tests 109

8. Organization of microfiche data files 124

9. Sample water pressure data 125

10. Sample early water pressure data 126

11. Sample borehole water temperature data 128

12. Sample ventilation system data 129

13. Sample data from two-zone shunting tests 131

14. Sample data from three-zone shunting tests 132

15. Tubing lengths between monitored zones and pressure gauges . . . 133

16. Tubing lengths between gauges and common for shunting tests 135

17. Sample data for rock temperature from temperature hole 137

18. Sample data for rock temperature from drift walls 138

19. Sign conventions for differential duct temperature records on circular charts 140

20. Sample data for zone ends and pressure port locations in R and HG holes 145

21. Conductance data for 31 March 1980 before tracer injection . . . 147

Page

22. Conductance data for 31 March 1980 after tracer injection . . . 148

23. Conductance data for 22 September 1980 149

24. Conductance data for zone 6 of borehole HG3 following tracer injection 150

A1. Latent heat of water A-3

LIST OF MICROFICHE FILES

		Microfiche No.
1.	Water pressure data	001 - 005
2.	Water temperature in boreholes	006 - 009
3.	Ventilation system data	010
4.	Shunting test data	011
5.	Rock temperature in temperature hole	012
6.	Rock temperature on drift walls	013
7.	Exhaust duct temperature	014
8.	Differential duct temperature	015
9.	Room air temperature	016
10.	Air flow measurements	017
11.	Location of water temperature monitoring zones in the R and HG boreholes	018

Note: Microfiche files are not included in this report but are available upon request from

Earth Sciences Division
Lawrence Berkeley Laboratory.
University of California
Berkeley, CA 94720

MATHEMATICAL NOTATION

Symbol	Definition
b	length along axis of drift over which seepage enters drift
C_h	correction due to simplifying assumption that the specific weight of water is constant; used in determining the hydraulic head
C_t	experimental error in thermocouples; used to calibrate temperature transducers
C_{zone}	conductance of water in zone
CH	chart reading
$\overline{CH}$	mean of all chart readings made during calibration test
CH_o	a particular value of CH
C_{pa}	specific heat of air at constant pressure
C_{pm}	specific heat of moist air at constant pressure
C_{pv}	specific heat of water vapor at constant pressure
DH	differential pressure head between inlet and exhaust ducts
E_i	voltage drop across reference resistor
E_w	voltage drop across electrodes in monitored zone
e	vapor pressure of water at ambient conditions
e_{sw}	saturation vapor pressure of water
f	function of a measured variable
g	acceleration of gravity
h	hydraulic head
h_G	part of hydraulic head resulting from the pressure at the gauge
h_p	hydraulic head at pressure ports in boreholes

Symbol	Definition
h_s	simplified hydraulic head
I	integral term in the hydraulic head; also electric current
k	zone where pressure head is evaluated
K	constant; also coefficient of hydraulic conductivity
L	latent heat of vaporization
LE	latent heat transfer
L_{zi}	elevation change in length i
MP	net moisture pickup
m	mass of gas
n	number of measurements
P	pressure
Pr	probability
P_G	pressure at gauge
P_z	pressure at port
p	normal density function
Q	volumetric water flow rate
Q_{act}	actual volumetric air flow rate
Q_{st}	standard volumetric air flow rate
q	sensible heat transfer
r	radial distance from drift axis
R_a	gas constant for air
R_m	gas constant for moist air
R_v	gas constant for water vapor
R_{ref}	resistance of reference resistor

Symbol	Definition
R_{zone}	resistance of water in zone
S	standard deviation
S_{yo}	estimate of the standard error for a particular value of the chart reading
$S_{y/x}$	mean squared deviation about the calibration curve
t	temperature
t_d	dry bulb temperature
t_r	measured temperature
t_w	wet bulb temperature
V	volume
v	volumetric flowrate of moisture
X	ratio of mass of water vapor to mass of dry air at ambient conditions
X_s	ratio of mass of water vapor to mass of dry air at saturated air conditions
Y_i	ith actual measurement of the standard air flow during the calibration test
Y_i	regression estimate of the ith measurement of standard air flow during the calibration test
Z	Z coordinate
Z_D	Z coordinate of datum
Z_G	Z coordinate of gauge
Z_H	elevation head
Z_P	Z coordinate of pressure port
Z_i	incremental length of ith increment
$Z_{i,i+1}$	Z coordinate between length i and i+1
γ_H	constant specific weight of water used in calculation of simplified hydraulic head

Symbol	Definition
γ_w	specific weight of water
γ_{wz}	specific weight of water at pressure port
γ_{zi}	specific weight of water in length i
Δ	experimental error
δL	percentage error in the latent heat of vaporization
μ	true value of a given parameter in Gaussion error calculations
$\rho_{m(act)}$	mass of moist air per unit volume of moist air
$\rho_{m(app)}$	mass of moist air per unit volume of dry air fraction
ρ_{st}	standard density of water
ρ_w	density of water
ρ_{zi}	density of water in length i
σ	standard error
σ^2	variance
$\hat{\sigma}^2$	uniformly minimum variance unbiased estimate of the variance
X	measured variable
$\bar{X}$	mean of observations

Commonly Used Subscripts	Definition
a	air
E	exhaust
i	ith individual measurement of a parameter
I	inlet
m	moist air
v	water vapor

ABSTRACT

The Macropermeability Experiment was conducted in a granite body adjacent to a recently abandoned iron ore mine at Stripa, Sweden. This experiment was conducted to measure the permeability of a large volume of low permeability, fractured rock. The experiment was conducted over 11 months in an approximately 4m x 4m x 33m drift at the 335 m level of the mine.

Groundwater seepage into the drift was measured as the net moisture pickup of the ventilation system. Water pressure and temperature were monitored at 95 locations in the rock surrounding the drift. The data collection system was designed to provide in-situ averaging of the measured parameters, to ultimately estimate the hydraulic conductivity of the rock as if it were a porous medium.

This report is limited to data presentation. It describes the types of data collected, the methods of measurement, and procedures used for data collection, storage, and reduction. Experimental errors are reviewed for all principal types of data.

The data presented are sufficient to estimate (1) the rate of seepage of moisture into the drift; (2) the three-dimensional distribution of hydraulic head in the rock mass to a radial distance of 30 m from the drift; and (3) the three-dimensional distribution of temperature in the rock mass, also to a radial distance of 30 m. These data can in turn be used to estimate the intrinsic permeability of the monitored rock mass.

Analysis and interpretation of these results will be presented in subsequent reports.

1.0 INTRODUCTION

1.1 Objectives and Scope of Report

The Macropermeability Experiment is part of a series of studies evaluating the possibility of using a large crystalline rock mass as a geologic repository for nuclear waste. This experiment was conducted to measure the permeability of a large volume of low-permeability, fractured granite. The site was an approximately 4 m x 4 m x 33 m drift called the ventilation drift at the 335 m level of the Stripa mine in Sweden. Water inflow to the drift and pressure in the surrounding rock were monitored. The experiment began in November 1979, following completion of primary instrumentation, and ended in September 1980.

This report presents the data file obtained from the Macropermeability Experiment so that the data and the primary data reduction can be evaluated and used by others. Analysis of data beyond the primary reduction is not included here but will be presented in later reports. Data acquisition, storage, and reduction procedures are discussed in detail in this report. The errors inherent in the data are examined, and procedures for obtaining the original field data are presented.

Additional information required for complete data analysis would have to include detailed descriptions of the test equipment, installation procedures, operating procedures, and such daily events as temperature fluctuations, power outages, and equipment malfunctions that affected the experimental results. Although general descriptions of the test facility and experimental procedures are given here, detailed descriptions will be presented in subsequent reports.

1.2 Objectives of the Macropermeability Experiment

The primary objective is to improve techniques for characterizing the permeability of large volumes of low permeability rock in regional groundwater studies. In meeting this objective, we expect the results at Stripa to enable us to:

- directly measure the hydraulic conductivity of as much as 10^5 m^3 of rock;
- confirm analysis of earlier small-scale borehole permeability tests;
- improve our ability to monitor in situ water pressures in fractured rock;
- evaluate the ventilation technique of flow measurement.

The theoretical basis for the experiment and the need for this type of research were discussed in earlier papers (Witherspoon, et al., 1979 and 1980; Long et al., 1980). The theory will be reviewed in the light of our experimental results in a subsequent report.

The experiment was conceived as part of the fracture hydrology research program at the Stripa test station. This program was designed to evaluate two alternative methods of characterizing rock mass permeability. Interconnected networks of fractures play a dominant role in conducting fluid through low permeability, crystalline rocks. The characterization of rock mass permeability is therefore very closely interrelated with the geometry of the fracture system.

One approach to characterizing permeability is to measure the geometric and hydrologic characteristics of large numbers of single fractures or small groups of fractures, and to mathematically integrate the results to determine the effective permeability tensor of the rock mass. Snow (1965)

gave one of the first descriptions of this discrete approach. It relies upon many small-scale tests on single fractures to adequately estimate the bulk properties of the rock mass.

The other approach is to perform tests on a scale sufficiently large to average, in the field, the individual effects of many fractures. This large-scale "macro approach" thus attempts to simulate in a fractured medium the testing conditions of porous medium studies, where every field measurement represents the averaged flow in many individual conduits.

Both approaches attempt to investigate the possibility of identifying a porous medium-type of permeability tensor for the rock mass. This permeability tensor represents the averaged effect of the multitude of individual fractures. The primary difference is in the method of averaging. The discrete approach requires a mathematical averaging, while the macro approach relies upon in situ averaging. The discrete approach was applied at Stripa by performing approximately 1,000 small-scale tests in both surface and underground boreholes. The results of these experiments will be reported separately. The macro approach was applied in the Macropermeability Experiment. We are also planning an integrated report comparing the results of the two approaches.

2.0 GENERAL DESCRIPTION OF THE EXPERIMENT

2.1 Test Facility

The Stripa test facility is located at the Stripa mine near Lindesberg in south central Sweden, approximately 150 km west of Stockholm. Iron ore mining had been carried out there for hundreds of years but stopped several years ago. A massive body of granite is adjacent to the underground workings. A test facility was excavated in the granite at about the time that mining operations ceased and was expanded in 1977 into the full experimental area shown in Fig. 1. The Macropermeability Experiment was conducted in the ventilation drift, an isolated, 45-m long drift at the end of the experimental area. A summary of the experiments performed in the test facility is presented by Witherspoon and Degerman (1978).

Determining the average intrinsic permeability of the rock mass surrounding the ventilation drift required measurement of net moisture seepage into the drift and of the water pressures and temperatures in the surrounding rock. The systems developed to measure these three basic parameters constitute the primary instrumentation of the experiment. Supplementary short-term tests such as shunting tests, a tracer test, and earth tide measurements were also performed during the experiment. These supplementary tests were not essential to the main objectives of the experiment and they did not require significant modifications of the primary instrumentation.

2.1.1 Seepage Measurement System

In most permeability tests, the water can be collected in a tube or pipe and the flow rate measured directly. However, in the low permeability rock of this experiment, the flow rate into the drift is so low and the

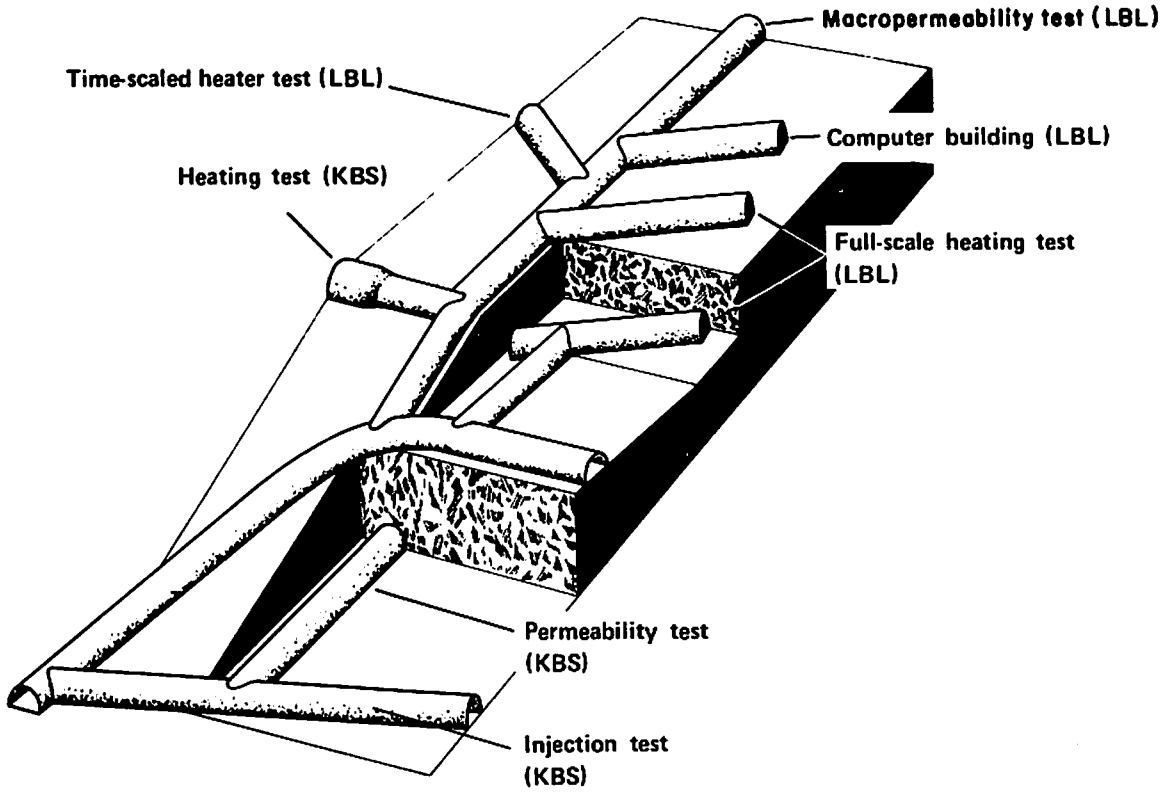

XBL787-2596B

Fig. 1. Location of experimental rooms in granite rock mass at Stripa.

surface area so great that a significant proportion of the inflow would be lost to evaporation and the remainder would collect on the floor of the drift too slowly to be measured in a reasonable amount of time. For these reasons, it was decided to attempt evaporating all water entering the drift and determine seepage rates by measuring the net moisture pickup in the air of the ventilation system.

For a ventilation system employing the circulation of outside air, it is necessary to measure: (1) the air velocity in the exhaust duct; (2) the wet and dry bulb temperatures of the incoming and exhaust air streams; and (3) the barometric pressures at each temperature measurement station. These measurements enable the calculation of both incoming and exhaust water vapor mass flow rates. The difference between the incoming and exhaust water vapor flow rates is the rate at which water has evaporated from the surfaces of the drift. The floor of the drift and the surfaces of the walls were observed to assure that all water inflow was being evaporated without puddling. Use of such visual checks required that any given tests be conducted long enough to allow significant nonequilibrium conditions to be detected.

Tests were run at room temperatures of about 20°C, 30°C, and 45°C, followed by a cool-down test back to 20°C. A room temperature of 20°C most closely reproduced the conditions under which earlier discrete borehole permeability tests were performed, while still permitting complete removal of incoming moisture by the ventilation system. Tests at the two higher temperatures provided a higher accuracy of measurement and will permit investigation of the effects of temperature on the measured groundwater inflow and on the ventilation techniques.

A sketch of the experimental setup is shown in Fig. 2. An air-tight and vapor-tight bulkhead was constructed to seal off a 33-m length of the ventilation drift. This bulkhead consisted of a structural wooden frame covered with a 0.15-mm thick sheet of polyvinylchloride (PVC) as a vapor barrier, and with insulating fiber glass to prevent condensation. The bulkhead was keyed into a 20-cm-deep notch on all four sides; a foamed plastic sealed the notch and prevented the loss of water through blast-damaged surface rock. An insulated metal door provided access through the bulkhead.

The general mine ventilation system delivered about 1.4 m^3/s of fresh air to a point just outside the bulkhead. A portion of this fresh air was admitted into the sealed room to pick up (as vapor) the water that flowed into the sealed room through the surrounding rock. The fan for this secondary ventilation system was located in an exhaust duct so that a slightly negative pressure could be maintained in the sealed room. Any air leakage through the bulkhead was inward and therefore would have the same properties as air coming through the inlet duct. Thus, the inlet wet and dry bulb measurements were considered representative of both leaking and intentionally admitted air. The flow measuring station as well as the exhaust wet and dry bulb sensors were in the exhaust duct. These sensors monitored the total air flow, including leakage.

After entering the sealed room, the air passed through a 45-kW electric duct heater and was then distributed through an insulated duct with multiple openings along the length of the room. Since most of the water arrived by seeping along discrete fractures, the air issuing from these openings was directed preferentially onto any damp spots on the rock surface. The walls

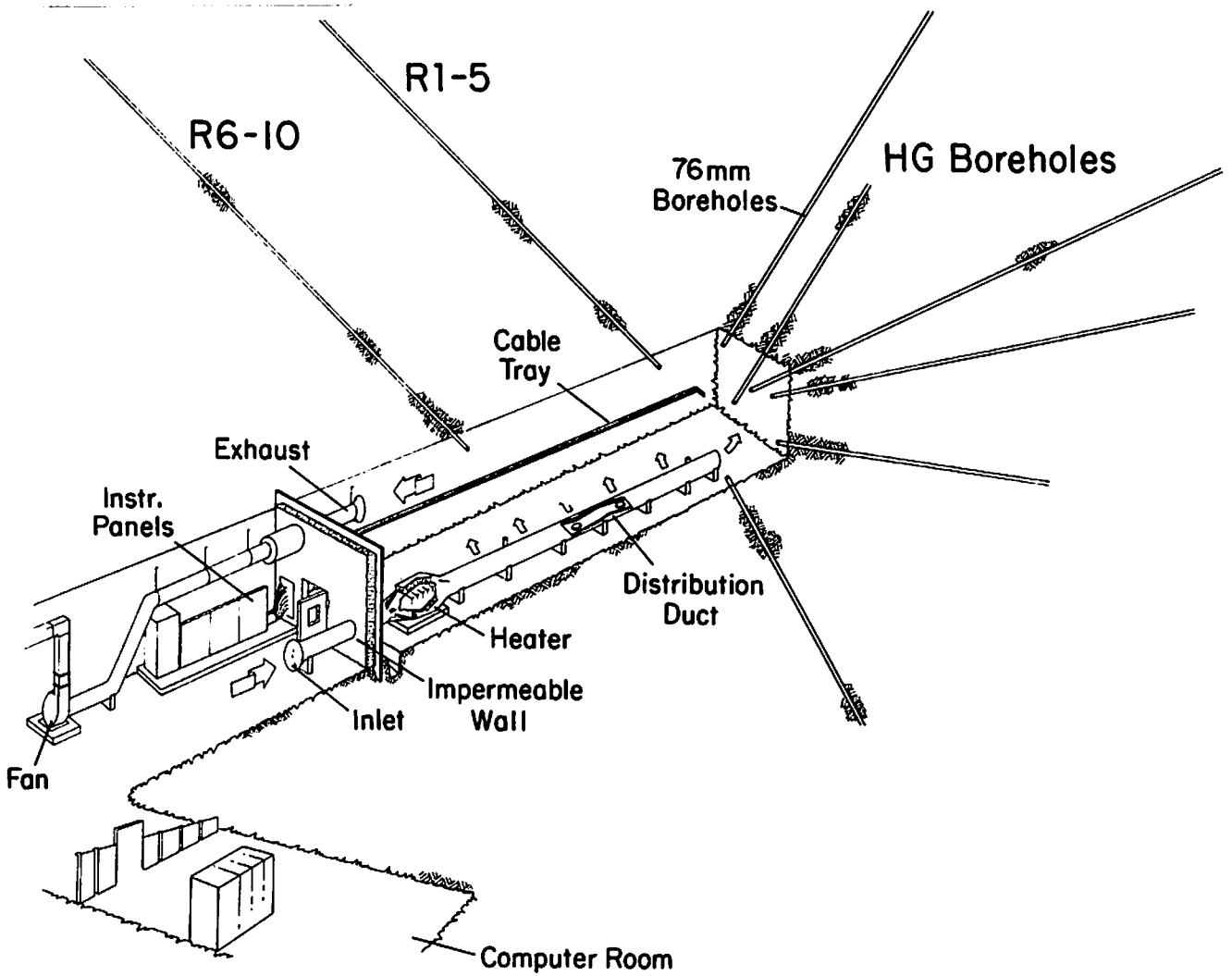

Fig. 2. Schematic view of experimental setup.

of the drift were then maintained in an almost dry condition, using auxiliary fans to provide a high air velocity over particularly damp spots. For the higher-temperature experiments, the inlet duct was modified to allow partial recirculation of room air through the heater.

Climatic conditions in the room were controlled by adjusting a damper on the fan exhaust (thus selecting a suitable air flow rate) and then adjusting the heater power to maintain the desired air temperature. The energy input from the heater was used to provide: (1) the heat required to increase the air temperature; (2) the heat of vaporization for the seepage water; and (3) the heat to increase the rock temperature. The 45-kW duct heater was divided into six separately controlled sections. Five sections were under manual control and one was thermostatically controlled. Heater voltage was regulated to isolate it from the large fluctuations of the mine power system.

A 75-cm deep trench was cut across the floor of the drift, just inboard of the bulkhead, to intercept any water that might otherwise flow under the bulkhead through fractures in the floor of the drift. No significant volume of water appeared in this trench, indicating that lateral flow beneath the floor was negligible.

2.1.2 Water Pressure and Temperature Measurement Systems

An isolated drift can be idealized as a long but finite cylindrical sink. The inner boundaries of this flow system are reasonably well defined. The wall of the drift is the inner boundary, and the pressure at this boundary is essentially atmospheric since the drift is kept dry.

The outer boundaries are more difficult to characterize. Several possible approaches can be taken. One is to assume that at some distance from the drift the flow field is undisturbed and the hydraulic potential is constant. However, the hydrology of the region surrounding the drift is affected by the other drifts of the test facility or by other mine workings. Piezometric profiles in the vicinity of the ventilation drift at Stripa are irregular, and an assumption of undisturbed conditions would not be valid.

Another method is to define a convenient boundary surface and measure the pressure distribution on this surface. Alternatively, pressures could be measured at an array of points such that an isopotential surface could be located in space. In an ideal, homogeneous porous medium this method would present few problems. The open interval of the piezometer would intersect a large number of pores and grains and the measured pressure would be a physically averaged value. In a fractured system, however, the piezometer interval may intersect only a few fractures and the measurement may reflect the local rather than the average gradient. If the average gradient cannot be determined, the equivalent permeability cannot be calculated. The problem is equivalent to predicting the permeability of a porous medium from measurements of pressure in only a few pores.

The rock mass surrounding the ventilation drift was instrumented with a three-dimensional array of pressure sensors, so as to measure boundary conditions at various radial distances into the rock. Water pressure was monitored in 15 boreholes 30 to 40 m long drilled from the ventilation drift into the surrounding rock. These boreholes are shown schematically in Fig. 2 and their locations in the drift in Fig. 3. They were divided into three

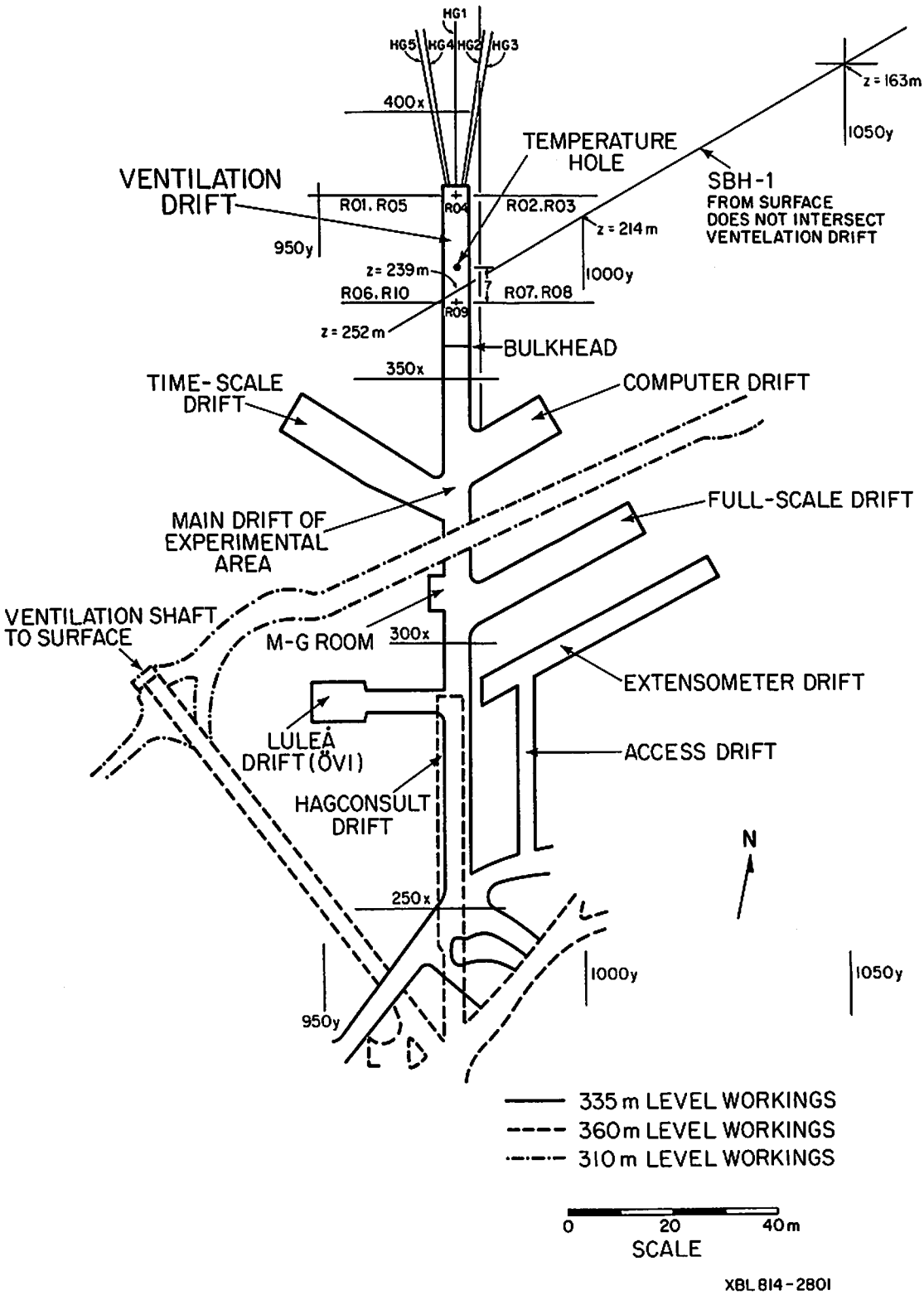

Fig. 3. Plan view of experimental area.

groups of five holes each. Two groups are radial (R) holes and one group, the hydrological-geophysical (HG) holes, extend from the face of the drift. A total of 94 packers were installed at approximately 5-m intervals. The open interval length had to be long enough to contain sufficient numbers of fractures to permit measurement of average local water pressures, yet short enough to prevent the boreholes from acting as major fluid conductors. Some 15 to 20 fractures, on average, were exposed in each open interval. The instrumented holes created a three-dimensional array of 94 zones, 90 of which were individually connected by tubing to pressure gauges.

In addition, a 97-m long horizontal borehole called DBH-2 was instrumented to isolate five test zones, each approximately 10 m long. This borehole is parallel with the axis of the drift. It is at about mid-drift height and 1.5 m behind the wall on the inlet duct side, as shown in Fig. 3. All test zones in DBH-2 lie beyond the end of the ventilation drift. The first 46 m of DBH-2, including the portion lying just behind the wall of the drift, have been continuously sealed with packers to prevent water movement along the hole, as such movement might have disrupted natural seepage conditions.

All zones instrumented for water pressure were also instrumented for temperature, except for borehole DBH-2. In addition, temperature was monitored in temperature hole TG-1 at eight logarithmically spaced depths ranging from 0.07 m to 10 m beneath the floor of the drift. This hole is 10.5 m deep, drilled vertically in the center of the ventilation drift floor, and parallel to and approximately 7 m north of hole R09, (Fig. 3). TG-1 was instrumented only for temperature measurements, and thermally conductive

materials for all components except the electrical leads were avoided. Seven additional temperature gauges monitored rock wall temperature. These gauges were cemented to the rock near the collars of boreholes R01, R02, R04, R06, R07, R09, and TG-1. One other gauge was mounted beside a mercury thermometer on an instrument panel outside the sealed portion of the drift to measure air temperature and serve as a control for long-term stability. Air temperature was monitored inside the sealed part of the drift at three separate locations, one of which served as input to the heater control unit. Air temperature data are presented in the discussion of the seepage measurement system.

The relationship of the ventilation drift to the other experimental drifts, boreholes, and mine workings is indicated in Figs. 3 and 4. The nearest source of perturbation outside the immediate experimental area is a drift at the 310-m level which passes within about 30 m of the ventilation drift. Minimum distances from the ventilation drift to nearby openings are presented in Table 1. The hydraulic gradients due to these openings were taken into account by directly measuring the actual in situ groundwater heads around the ventilation drift.

Table 1. Approximate minimum distances from ventilation drift to nearby openings.

Opening	Distance (m)
Computer Drift	17
Time Scale Drift	20
310 Level Workings	30
360 Level Workings	79
Borehole SBH-1	83
Borehole SBH-2	95
Borehole SBH-3	113

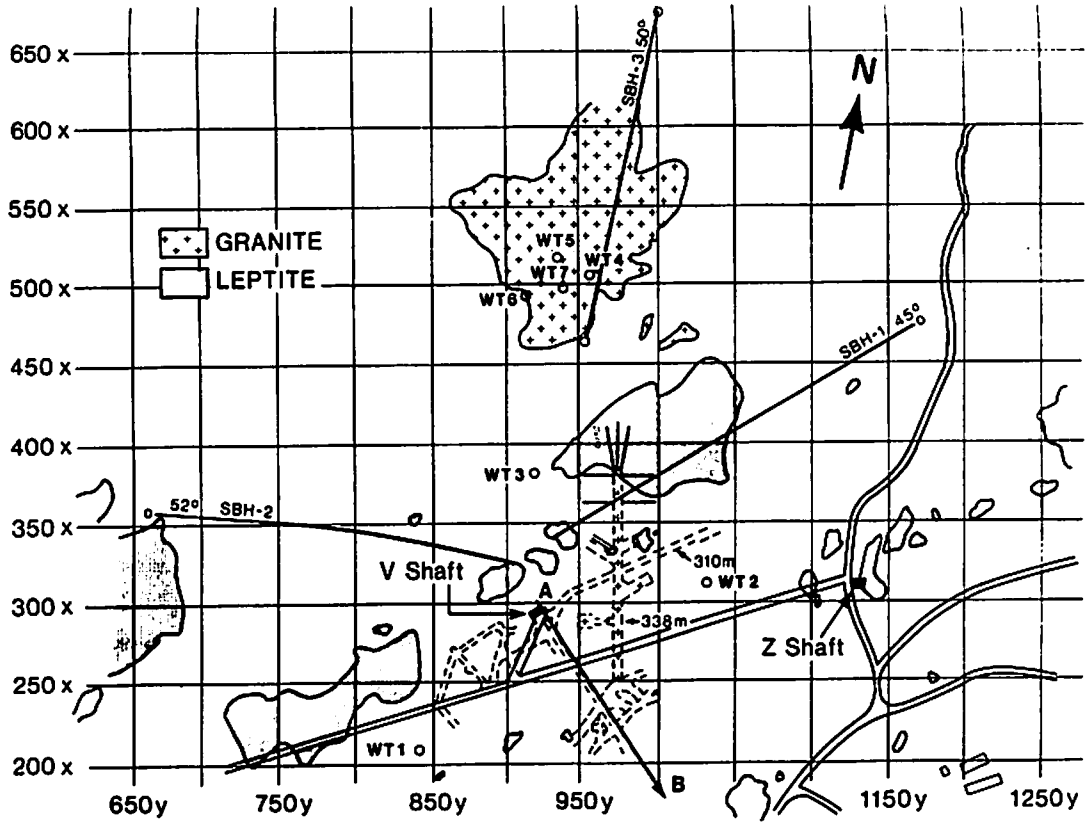

XBL 804-9434

Fig. 4. Plan view of Stripa site showing surface holes.

2.2 General Experimental Procedures

The Macropermeability Experiment concurrently measured the seepage rate, water pressure, and rock mass temperature. These parameters were repeatedly measured at nominal ambient room air temperatures of 20°C, 30°C, and 45°C, followed by a cool-down back to 20°C. The accuracy of seepage rate measurements was improved by increasing the air temperature; it also determined the degree to which results were temperature-dependent. An attempt was made to allow each constant temperature run to continue until essentially steady conditions were approached, but this was not always possible because of time constraints.

Activities associated with the Macropermeability Experiment continued over two years, from October 1978 through September 1980. The sequence of events in broad outline was as follows:

10/78 to 5/79	Experiment design, fabrication and shipping of equipment.
6/79 to 11/79	Installation of equipment.
12/79 to 3/80	Stabilization of operating conditions and performance of initial 20°C test.
4/80 to 5/80	Equipment modification and performance of 30°C test.
6/80 to 7/80	Performance of 45°C test.
8/80 to 9/80	Equipment modification and performance of 20°C cool-down test.

Each constant-temperature operation will be referred to as a separate test. Each test followed approximately the same procedure of increasing (or decreasing) the air temperature, adjusting the fan speed, and waiting for quasi-equilibrium conditions to be established. This process normally

required about six to eight weeks. Because the general procedures for the seepage, pressure, and temperature measurements were quite different from one another, they will be discussed separately.

2.2.1 Ventilation System Operation

Estimates of seepage rates were based upon the net moisture pickup of the ventilation air within the sealed portion of the drift. The ventilation system was therefore operated to maximize the measurement accuracy of net moisture pickup. This was primarily achieved by assuring that at any given temperature the volume of moisture evaporated per unit volume of circulating air was as high as reasonably possible. Since the final net moisture pickup computation was to be based upon the difference between the mass flow rates of moisture in the inlet and exhaust air streams, the greater the contrast in these values, the greater would be the accuracy of the measurement.

Charts prepared to assist in operating the ventilation system are shown in Fig. 5. These drawings helped to anticipate the duct air flow rates required to maintain a given level of experimental accuracy. The air flow rate, inlet air conditions, and moisture evaporation rate also determined the amount of additional heat required to perform the evaporation, and thus served as a guide for designing the heating system for the inlet air duct. The inlet duct heaters served three distinct purposes: (1) since the equilibrium seepage rate could not be accurately estimated in advance of the experiment, the heaters assured that the moisture-carrying capacity of the air could be increased to permit evaporation of unexpectedly large seepage rates; (2) heating the inlet air permitted the operators to increase measurement accuracy; and (3) the effect of room air temperature on the results of

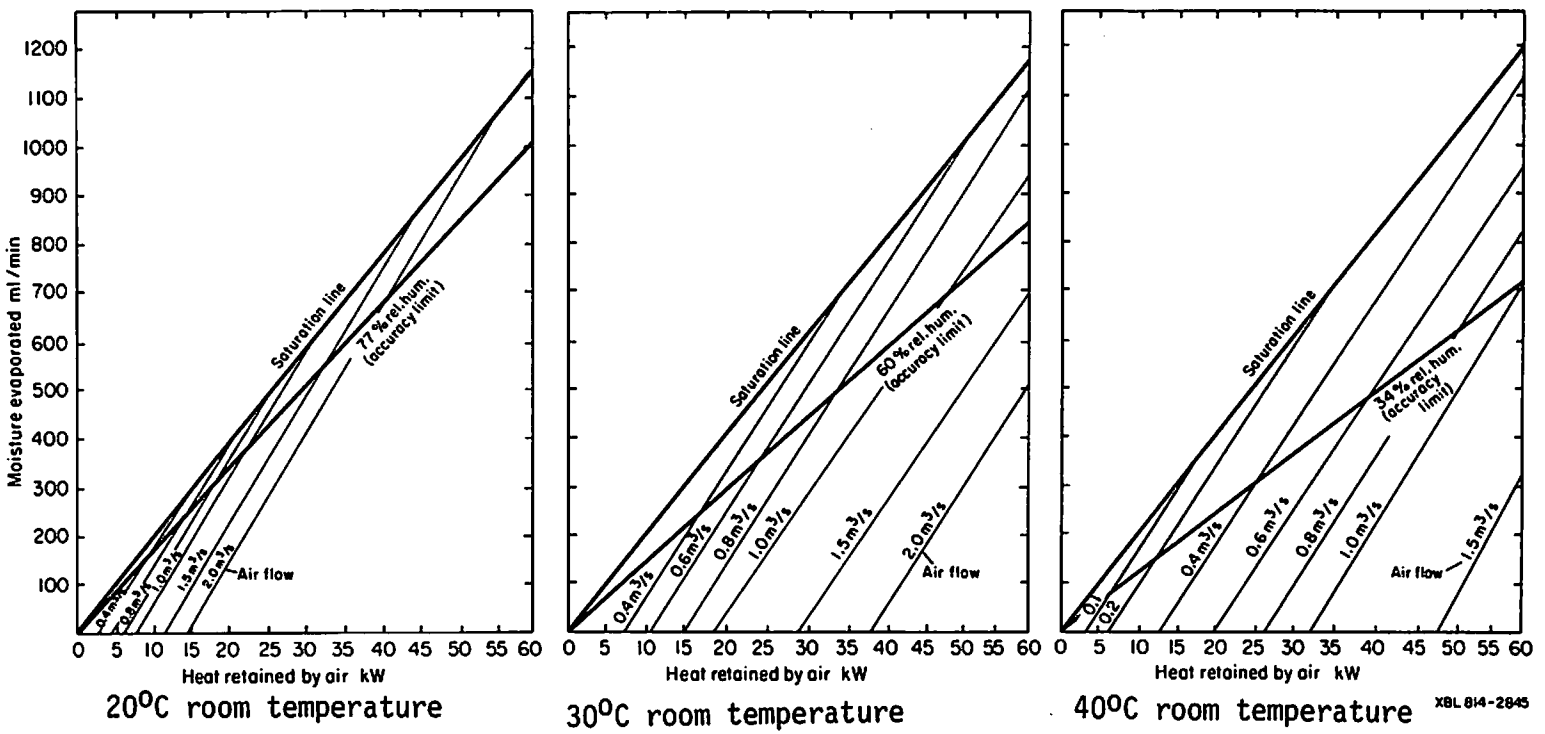

Fig. 5. Charts used to assist in operation of the ventilation system for assumed inlet conditions of 14.5°C dry bulb air temperature and 65% relative humidity.

the experiment could be investigated.

The dark band on the Fig. 5 charts show the operating ranges initially targeted for achieving a resolution of at least 20% in computation of net moisture pickup, based on a preliminary sensitivity analysis of the ventilation system. Regarding humidity and room temperature, these initial studies showed, for example, that the relative humidity of the exhaust duct air should be at least 77% at 20°C, 60% at 30°C, and 34% at 40°C. This increasing width in the band of acceptable operating conditions graphically demonstrates the effect of room temperature on the accuracy of measurement.

In practice, the charts of Fig. 5 could not be used directly because of changing inlet air conditions and because of the difficulty of evaporating all incoming moisture when the relative humidity of the room air exceeded about 65%. One problem was a persistent drip from the collar of borehole R05. A hot plate was installed to evaporate this source of moisture, and, to increase air velocities (thus improving evaporation), ceiling fans were added. Improved air circulation was especially necessary for the higher-temperature runs, where duct air velocities were reduced considerably. Even for these runs, however, it was easier to keep the room dry by operating at or below 65% relative humidity.

Further constraints were placed upon the ventilation system by a much lower seepage rate than was initially expected. Before they were instrumented and sealed, the 15 R and HG holes penetrating the rock mass from the ventilation drift were open and drained water into the drift. Several holes, particularly R01, had penetrated fairly permeable zones in the rock, and the total yield from all holes was about 800 ml/min. Sealing the bore-

holes was expected to reduce inflow into the drift for at least one of the following reasons: (1) permeable fractures which intersect the boreholes do not also intersect the drift; (2) flow was diverted to other drifts or boreholes in the mine; or (3) sealing reduced the effective radius of the drift and hence the net seepage. The ventilation system was designed to handle up to 600 ml/min of moisture inflow, with an expected inflow of 200 to 400 ml/min. Actual equilibrium moisture inflow was much less, on the order of 50 ml/min.

The relatively low seepage rates encountered forced us to operate near the low end of the charts shown on Fig. 5. The primary problem this generated was in air flow monitoring for the initial and cool-down 20°C tests, where we operated at the lower end of the linear portion of the instrument range. A low-velocity air flow monitoring system was installed for the two higher-temperature tests, thereby avoiding this problem. However, the lower air velocities required the installation of plates that reduced the cross section of the ducts near the recording wet bulb thermometers. The reduced cross section was necessary to maintain a required 3 to 10 m/s air flow rate across these instruments.

Net moisture pickup of the ventilation system was found to be very sensitive to changes in room temperature and air flow rates. This was particularly true during the higher-temperature tests, where duct air velocities were low. Achievement of quasi-equilibrium conditions within the sealed room therefore required maximum stability in fan speed and room air temperature. Events that would have been minor during the 20°C test, such as the accidental loss of heater power for about 4 hours, caused perturbations that took about a week to eliminate during the 45°C test. Because of this

sensitivity, access to the sealed room was restricted throughout the experiment and changes in operating conditions were minimized for the duration of each constant-temperature test.

2.2.2 Water Pressure and Temperature System Operation

Each borehole used for monitoring water pressure within the rock mass was equipped with 5 to 8 packers that sealed the boreholes at known intervals and precluded further movement of water within the borehole past the packer. Between the packers were pressure and temperature measurement zones where water movement was unrestricted. A schematic drawing of this system is shown in Fig. 6.

All boreholes were filled with native groundwater prior to final packer inflation and hole sealing. Mechanical packers were used in all holes except DBH-2, where pneumatic packers were used. The packers were activated by dry nitrogen gas, maintained at a pressure of about 5 MPa throughout the experiment. Small leaks caused some of the nitrogen gas to escape into the boreholes because measured water pressure in the boreholes was always less than in the packers. In several instances, such gas leakage became significant and affected the water pressure being monitored. In such cases, it was necessary to stop testing in the zone and periodically bleed off excess pressure to avoid damage to the water pressure gauge. The equipment in one hole, RIO, was twice removed and reinstalled during the experiment because of an unusually large number of gas leaks. All other borehole installations remained undisturbed. Except for packer pressure maintenance and the incidental tests described below, operation of the water pressure and temperature monitoring system required only the periodic reading of gauges.

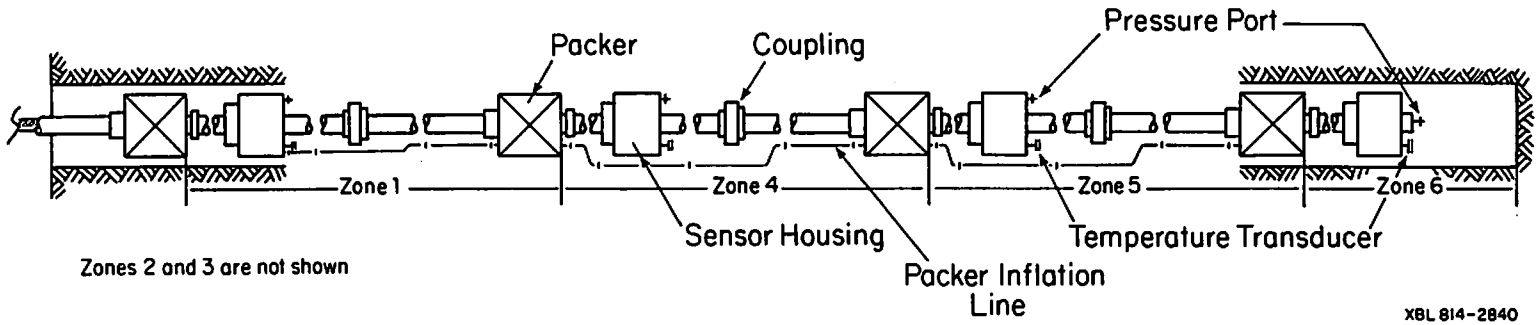

Fig. 6. Schematic drawing of pipe string packers and water pressure and temperature sensing ports installed in boreholes.

2.3 Supplementary Tests

Several supplementary short-term hydrologic tests were performed that were only peripherally related to the Macropermeability Experiment's objectives. These were the shunting tests, borehole withdrawal tests, a salt tracer test, and earth tide measurement. They did not significantly alter the primary test facility. Also, geochemical tests were made of fracture-filling materials and precipitates from evaporated groundwater. Each of these tests is briefly described below.

2.3.1 Shunting Tests.

The purpose of the shunting tests was to measure the average water pressure over two or three adjacent zones in a borehole to determine the effect of zone length on pressure measurement, and thus on the boundary conditions used in data analysis. Zones that had pressure differences greater than approximately 0.1 MPa (10 psi) were selected for shunting and the tests were performed during a one-week period following the end of the 20°C cool-down test. The boreholes and zones used are listed in Table 2.

Table 2. Shunting test zones.

Borehole	Two-Zone Tests	Three-Zone Tests
R01	6 - 7	6 - 7 - 8
R02	5 - 6	4 - 5 - 6
R06	7 - 8	6 - 7 - 8
R07	4 - 5	not tested
R09	4 - 5	4 - 5 - 6

The shunting tests were performed by hydraulically interconnecting the shunted zones through the tubing used to monitor water pressure in each zone. Average pressure at the gauge panel and flow velocities in the tubing were monitored. These data and a knowledge of the resistance to flow offered by the tubing permit computation of the water pressure in each zone.

2.3.2 Borehole Withdrawal Tests.

The borehole withdrawal tests were intended to measure the hydraulic conductivity of each zone in boreholes R04 and R07 by simultaneously opening all pressure measurement tubing to the atmosphere and independently measuring the rate of flow from each zone. These tests were to be performed both before and after the higher-temperature macropermeability tests to serve as a crude measurement of possible changes in local hydraulic conductivity caused by heating the rock. Three days of withdrawal and four days of recovery were allowed for the tests. The initial withdrawal test was performed during the week of 24 March 1980, following the end of the initial 20°C test.

The results of the initial withdrawal tests were disappointing. A continuous flow of water was achieved in only 5 of the 12 zones tested, and none of these were from the two zones nearest the drift, where heating of the rock was expected to be measurable. The intermittent water flow observed from most zones is thought to be the result of gas in the water coming out of solution upon pressure release and from leaks in the packer inflation system. This lack of data from the zones of greatest interest indicated that hydraulic conductivity changes could not be measured in this way. The subsequent test under heated rock conditions was therefore not performed.

An unrelated series of similar tests was performed early in the experiment to check for possible leaks in packer seals between adjacent zones showing essentially identical water pressures. Water pressure was maintained at atmospheric levels on one side of the suspect seal while in situ water pressure was monitored in the zone on the other side of the seal. It was reasoned that if a significant leak did exist, the water pressure in the monitored zone would fall rapidly as water escaped past the faulty seal into the lower pressure zone. Such tests were performed in: (1) zone 5 in R09; (2) zone 6 in R09; and (3) zone 5 in R08. Each test was run for 2 to 6 hours, but no evidence of significant water leaks past the packers was found. Although it is not possible to make a definitive conclusion, it is believed that the similarity in water pressures was due to hydraulic interconnection through fractures in the rock mass.

2.3.3 Salt Tracer Test.

The purpose of this experiment was to determine the pattern of water flow in the rock beyond the face of the drift under the prevailing hydraulic gradient. A tracer solution of NaCl was introduced into zone 6 of borehole HG3 on 31 March 1980. This zone was specially equipped with two tubes for this purpose, so that a tracer could be circulated into the zone in one tube, and excess fluid drained from the zone in the other tube. In this way, the tracer could be introduced rapidly at a lower pressure than the ambient pressure of the zone and would not be injected into the rock. A 50,000 mg/l NaCl feed solution was used, and injection continued until the concentration of salt in the drainage tube became about 80% of the injection concentration. Thus the final NaCl concentration in the zone was approximately 40,000 mg/l. The injection process required about 75 minutes to complete.

Borehole HG3 and zone 6 were selected because the local hydraulic conductivity appeared to be relatively high, based upon injection test data obtained from Dr. John Gale of the University of Waterloo (Gale, 1981), and because our pressure data indicated a hydraulic gradient away from that zone toward the other HG holes and borehole R01.

In addition to the usual pressure tubing and temperature sensor, each zone in the HG holes and zone 4 of borehole R01 (the most conductive zone in that hole) were instrumented with an electrode to monitor the conductance of water in the zone. Baseline conditions were established by monitoring daily for several months before injecting the tracer.

The tracer monitoring system was operated for six months, from 31 March through 22 September, 1980, but no movement of the tracer from the injection zone into any other monitored zone was detected. Because this test failed to produce substantive information, the data obtained will be presented only in summary form (Tables 21-24).

2.3.4 Earth Tide Measurement.

Earth tide data were obtained over a period of about 2 months during the latter part of the experiment, using pressure transducers and a data logger. The transducers were connected to the pressure tubing at the pressure gauges, and were not put into the boreholes. As these measurements were not directly related to the objectives of the Macropermeability Experiment, the results will be published separately.

2.3.5 Geochemical Tests.

Geochemical studies were made of natural groundwater precipitates and fracture fillings to provide information on the nature of the precipitates being deposited on the rock and in fracture and pore voids by the evaporating groundwater. Three sets of samples were taken: (1) accumulated precipitates left from the evaporation of excess water dripping from the collar of borehole R05; (2) fracture-filling material from the wall of the drift collected at drift midheight between R02 and R07; and (3) filling materials from natural, open fractures in the first meter of core from borehole HG-2.

3.0 DATA ACQUISITION AND STORAGE PROCEDURES

3.1 General Data Handling

This chapter discusses in detail the raw data collection procedures. Subsequent chapters present the procedures and equations used to convert the raw data into the desired output and assess the possible errors involved.

The primary data collection systems were based upon manual readout of dial or digital displays and entry on a standard data sheet. Automatic electronic data collection was not employed because of the limited volume of data anticipated, the long duration of expected transients, the greater stability of readout from mechanical instrumentation, and the higher cost of automatic collection. As a backup to the manual system, the air flow rate, exhaust and differential duct temperatures, and room air temperature were continuously recorded on circular charts.

Data readings were made every working day in the early morning. This time provided the most stable results, unperturbed by short-term transients in mine air temperature resulting from the activities of personnel and motorized equipment in the adjacent experimental area. The circular charts were changed every Tuesday following the morning readings. Copies were made of all data and mailed weekly to LBL in Berkeley. Copies of the ventilation and temperature data were also mailed to the project's consultant on mine ventilation systems, Dr. Malcolm McPherson, at the University of Nottingham in the United Kingdom. All original data were maintained on file at the Stripa test station.

Data which were not collected routinely and which had no standard formats were entered into the daily log. These included calibration data

and early pressure transient data, which were collected during the period between installation of borehole equipment and use of standard data sheets.

3.2 Ventilation System Data Acquisition

The purpose of the ventilation system data was to permit computation of the net moisture pickup of the ventilation air within the sealed portion of the ventilation drift. The variable data required for this computation are as follows:

t_{Id} = inlet duct dry bulb temperature

t_{Iw} = inlet duct wet bulb temperature

t_{Ed} = exhaust duct dry bulb temperature

t_{Ew} = exhaust duct wet bulb temperature

P_m = barometric pressure outside the sealed room

P_r = barometric pressure inside the sealed room

V_a = flow velocity of air entering and leaving the room.

Also required were calibration curves for air flow velocity measurement, the cross section area of the exhaust duct at the point of airflow velocity measurement, the density of water, and the specific heats of water and air. Other measurements were used to control the operation of the ventilation system, but they do not directly enter into the computation of moisture pickup. These included air temperature in the sealed room, air temperature in the control area outside the room, and total electric power usage in the room. A block diagram of the ventilation data collection system is shown on Fig. 7, and Table 3 lists equipment specifications. Ventilation data were recorded on a data sheet as shown in Fig. 8.

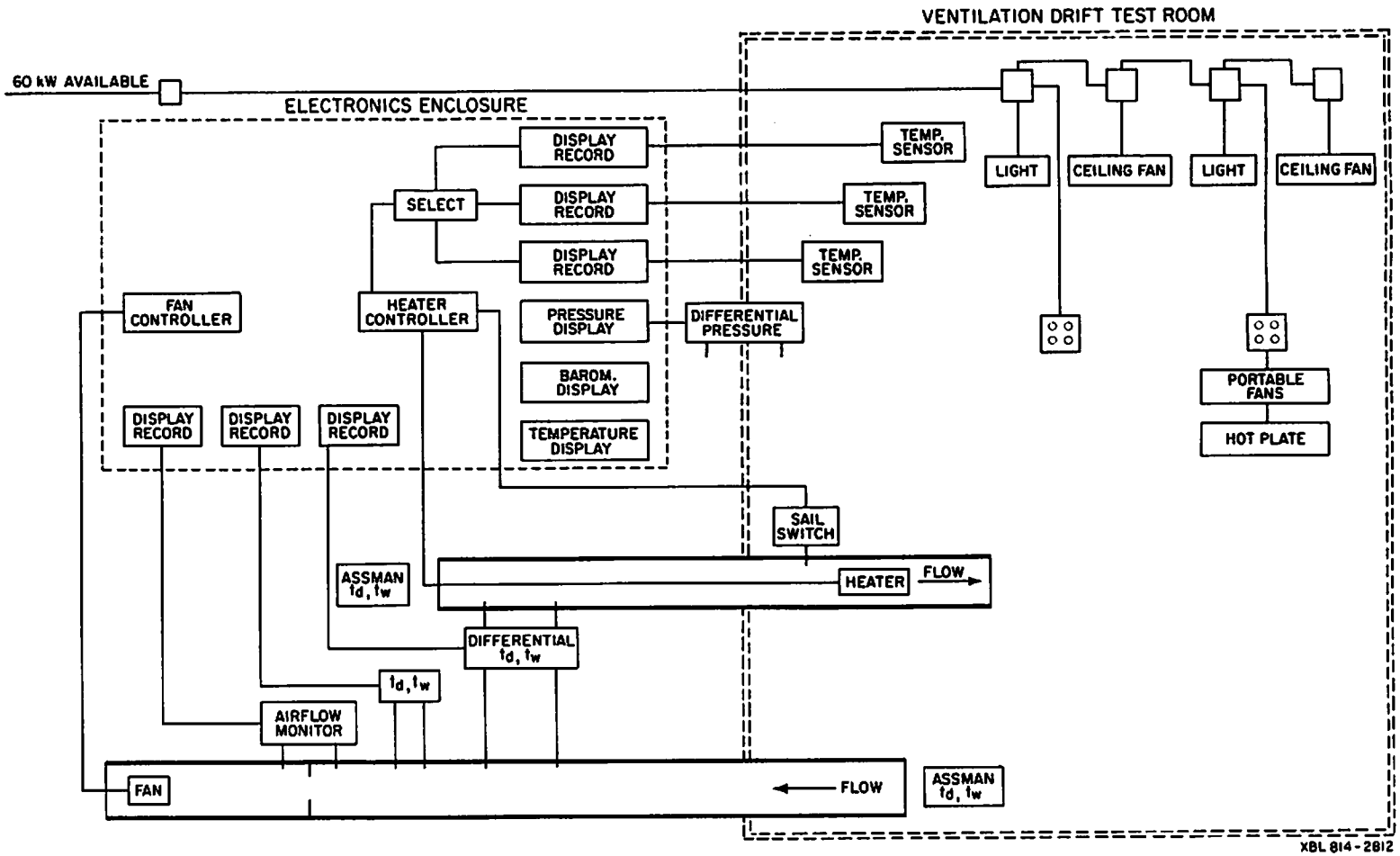

Fig. 7. Block diagram of ventilation data collection system.

LBL FIELD ENGINEER R. Galbraith

MONTH AND YEAR July 1980

LBL MACROPERMEABILITY EXPERIMENT

VENTILATION SYSTEM DATA SHEET

Date	Time	Inlet Duct: Assman Readings t_w (°C)	Inlet Duct: Assman Readings t_d (°C)	Inlet Duct: Barometric Pressure (mb)	Inlet Duct: Chart Recorder[1] Δt_w (°C)	Inlet Duct: Chart Recorder[1] Δt_d (°C)	Exhaust Duct: Assman Readings t_w (°C)	Exhaust Duct: Assman Readings t_d (°C)	Exhaust Duct: Pressure across bulkhead[2] (in.H_2O)	Exhaust Duct: Chart Recorder t_w (°C)	Exhaust Duct: Chart Recorder t_d (°C)	Exhaust Duct: Chart Recorder Air Flow (chart div.)	Heater Control Room Temp. (°C)	Cumulated Energy Use (watt-hours)	Mine Air Temperature: Electronic (°K)	Mine Air Temperature: Mercury (°C)
2	7:15	11.0	14.3	1032.0	16.0	25.1	27.0	40.2	.09	27.2	39.4	76.0	42.0	628134	287.3	14.4
3	7:19	11.0	14.2	1035.1	16.0	25.5	27.1	40.5	.09	27.2	39.7	76.0	42.0	635713	287.2	14.3
4	7:22	11.0	14.2	1036.6	16.4	25.6	27.5	41.0	.07	27.6	40.0	70.0	42.0	642967	287.3	14.3
4	13:57	10.9	14.3	1035.0	14.0	20.4	25.0	35.1	.09	25.1	34.6	75.5	36.0	643702	287.3	14.4
7	7:42	10.7	14.0	1033.0	14.5	22.0	25.6	36.7	.09	25.8	36.1	76.0	38.0	649307	286.9	14.1
8	7:41	10.9	14.3	1028.7	15.7	24.9	27.0	39.8	.085	27.3	39.3	76.0	41.0	656833	287.3	14.5

Footnotes:

[1] Positive Number indicates higher temperature in exhaust duct

[2] Positive Number indicates higher pressure outside room.

Fig. 8. Sample data sheet for ventilation system measurements.

Table 3. Equipment specifications.

1.	Ventilation System	
1.1	Air Flow Monitor	Brandt Industries, Inc., Fuquay, North Carolina
a.	Air Measuring Station	Brandt model 10 DSK1011-14-10 air flow measuring primary, 14 inch diameter, with 3/8 inch hexcell flow straightner, 8 total head pitots and 8 velocity head pitots.
b.	Pressure Transmitter	Brandt model 21 DPT2X2X-.5-SQR differential pressure transmitter.
c.	Square Root Extractor	Brandt model 40SQR411-0 pneumatic square root extractor, 3 to 15 psig output.
d.	Chart Recorder	Foxboro Co., Foxboro, Massachusetts. Model 40PR-RFM1 7 day mechanical one pen chart recorder, 0-100 paper scale.
e.	Air flow calibration	Alnor Instrument Co., Niles, Illinois. Thermo-anemometer type 8500, range of air stream temperatures 20°F to 150°F. Accuracy the larger of 2 FPM or 3% of air velocity. Used to calibrate the air flow monitoring systems at flow velocities less than 3 m/s.
		Dwyer Instruments, Inc., Michigan City, Indiana. Pitot tube, model 304, 12 inches long. Accuracy 2% of reading. Used to calibrate the air flow monitoring systems at flow velocities greater than 3 m/s.
1.2	Heater Control Assembly	
a.	RMS Voltage Readout	Analogic International, Wakefield, Massachusetts Series PI 4461 L 100x3 Serial 937984 digital voltage readout, used for heater control.
b.	Voltage Regulator	Variac automatic voltage regulator, General Radio Co., Concord, Massachusetts. Type 1582AH, 230V±10%, 60Hz, 42.5 Amp., and type 1582AHS, 230V±5%, 60Hz, 85 Amp, used for heater control.

Table 3 (continued).

	c. Automatic Controller	Foxboro Co., Foxboro, Massachusetts. Model 43AP Style A. Pneumatic controller, used for heater control.
	d. Watt Hour Meter	Ohio Semitronics, Inc., Columbus, Ohio. W-H Series, Model WH3-66, 220/380 VAC, 50Hz, 100 Amp.
1.3	Psychrometric Measurements	
	a. Portable Hygrometer	C.F. Casella & Co., Ltd., London. Aspirated hygrometer (Assman psychrometer). Catalog No. T 8900/1 to T 8913/1, spring driven fan in metal sleeve, 4 m/s minimum air flow rate. Thermometers in °C, with 0.5°C subdivisions. Range -5°C to 50°C. Accuracy 0.1°C. Used to measure wet and dry bulb temperatures.
	b. Duct Thermometer	Foxboro Co., Foxboro, Massachusetts. Two liquid filled 6 inch long bulbs with 60 feet of tubing each, 0 to 40°C range, Class 1A system. Bulb code 4442; tubing code D-FS-SS. One porous sleeve, part no. 44938. Used for continuous measurement of exhaust duct wet and dry bulb temperatures. Output displayed on Foxboro model 40PR-PFM2 7-day mechanical 2 pen chart recorder, 0 to 40 paper scale.
	c. Differential Duct Thermometer	Foxboro Co., Foxboro, Massachusetts. Four liquid filled 6 inch long bulbs each with 20 feet of tubing to differential pressure block, then 2 tubes 50 feet long to chart recorder. 0 to 40°C range, class 1A system. Bulb code 4442, tubing code D-FS-SS. Two porous sleeves part nos. 44938. Used for continuous measurement of differential wet and dry bulb temperatures. Output displayed on Foxboro model 40PR-PFM2, 7 day mechanical 2 pen chart recorder, 0 to 40 paper scale.

Table 3 (continued).

1.4	Ambient Air Temperature	
	a. Room Air Thermometer	Foxboro Co., Foxboro, Massachusetts. Nickel resistance temperature detector model DB-21B-227W part no. E 0119ZC with resistance pneumatic transmitter model 34C-AN, 10 to 70°C range, part no. NR-227W-CURVE. 120 V, 60 Hz, 3 to 15 psi. "Dynatherm" resistance bulbs provide electrical output proportional to temperature. Range -215 to 320°C. Accuracy 0.3°C. Used to monitor air temperature in sealed portion of drift. Output displayed on Foxboro model 40 PR-RFM3 7 day mechanical 3 pen chart recorder, 0-70 paper scale.
	b. Control Area Air Thermometer	Fisher Scientific, Pittsburg, Pennsylvania Air Thermometer (distributors). Mercury thermometer model 15-043A range -1 to 51°C, 0.1°C subdivision. Accuracy 0.2°C.
1.5	Air Pressure	
	a. Control Area Barometer	Belfort Instrument Co., Baltimore, Maryland. Aneroid barometer, range 910 to 1060 millibars, catalog no. 6079-1; serial no. 072. Minimum subdivision 0.5 mb. Accuracy 0.8 mb.
	b. Differential Air Pressure Gauge	Dwyer Instrument Co., Michigan City, Indiana. "Magnehelic" differential pressure gauge, 0 to 6 inches water. Minimum subdivision 0.2 inches water. Series 2000. Accuracy 0.12 inches water. Used for differential pressure measurement across bulkhead during 20°C tests. Dwyer differential pressure manometer, Mark II model no. 25. Range - 0.05 to 3 inches water. Accuracy 0.09 inches water. Minimum subdivision 0.01 inches water. Used for 30°C and 45°C tests.

Table 3 (continued).

2. Water Pressure

a. Pressure Meters	Dresser Industries, Inc., Ashcroft Gauge Division, Stratford, Connecticut. Series 1082A Bourdon type gauge, 0 to 300 psi range, 6 inch diameter dial. Minimum subdivision 1 psi. Accuracy 0.75 psi. Used to measure water pressure in R holes.
	AMETEK, U.S. Gauge Division, Sellersville, Pennsylvania. Model 1403 Bourdon type gauge, 0 to 300 psi range, 6 inch diameter dial. Minimum subdivision 1 psi. Accuracy 0.75 psi. Used to measure water pressure in HG holes and DBH-2.
b. Packer	Cobbs Engineering, Tulsa, Oklahoma. Borehole packer model 275126, for use in 76mm diameter R and HG holes. Seal length 19.4cm.

3. Water and Rock Temperatures

a. Voltmeter	John Fluke Mfg. Co., Mountlake Terrace, Washington. Digital multimeter model 8040A, 5 ranges for voltage, 6 ranges for resistance. Voltage range minimum 0 to 200 mV AC and DC; resistance range minimum 0 to 200 ohms. 5-digit readout. Accuracy 0.05% of DC voltage reading for temperature transducers; 0.5% of AC voltage reading for tracer test, and 0.2% of resistance reading. Used to monitor temperature transducers on drift walls, in temperature hole, in boreholes, and in control area. Also used to monitor conductance for tracer test.
b. Temperature sensors	Analog Devices, Norwood, Massachusetts Two terminal IC temperature transducer, models AD590L (for use in R and HG boreholes on drift walls, and in control area) and AD590K (for use in temperature hole). Accuracy 1.6°C for model L and 2.0°C for model K.

Table 3 (continued).

4.	Shunting Test	
	a. Flow Meter	Fischer and Porter Co., Warminster, Pennsylvania. Purge flow meter model 10A3135, tube FP 1/8-20-P-3, with 1/8 BG float. Range 0 to 29 ml/min, accuracy 2.9 ml/min.
	b. Nylon tubing	The Polymer Corporation, Reading, Pennsylvania. Nylaflow high pressure nylon tubing, 1/4" type H, 2500 psi burst rating, 0.150 inches ID, for use between gauge and boreholes; 3/16" type H, 2500 psi burst rating, 0.110 inches ID, for use within R and HG boreholes; 1/8" type H, 2500 psi burst rating, 0.078 inches ID, for use within DBH-2 borehole.
5.	Salt Tracer Test	The voltmeter used was the same as for water and rock temperature measurements described in item 3.a above.

3.2.1 Duct Air Temperature

Preliminary sensitivity analysis showed that the accuracy of the moisture pickup computation was quite sensitive to minor variations in duct air temperature, particularly wet bulb temperature. Because of this, two independent systems monitored these parameters.

The primary system consisted of a portable Assman psychrometer which was used once daily for spot measurements of wet and dry bulb temperatures in both the inlet and exhaust ducts. This instrument contained two mercury thermometers. The measurements were made by suspending the psychrometer in front of the duct intakes, first the inlet and then the exhaust duct. Data were recorded daily (Fig. 8).

The backup system consisted of continuous wet and dry bulb monitors permanently installed in the inlet and exhaust ducts. The signals recorded on continuous, 7-day circular chart records, were sent through factory-sealed liquid-filled tubes. The wet bulb monitors were equipped with porous ceramic sleeves that were continuously moistened by a controlled-drip filtered water feed. One set of sensors monitored the absolute temperatures in the exhaust duct, which were logged by a two-pen chart recorder. A second set monitored the differential temperatures between the inlet and exhaust ducts; these data were also logged by a two-pen chart recorder. Inlet air was filtered to minimize dust buildup on the porous sleeves.

Sensitivity and accuracy problems were encountered with the backup system. It therefore served primarily as a monitor for unexpected, large-scale fluctuations not detected by the primary system.

The main difficulty was in maintaining the correct wet bulb water feed. Ideally, there should be just enough water to keep the ceramic wet-bulb sleeve saturated but not dripping. The flow rate required to maintain this equilibrium varied with air temperature and the age of the ceramic sleeves. The sleeves tended to become clogged with precipitates and dust from the air despite the use of air filters. Although the wet bulb water feeds were adjusted regularly, some departure from the ideal did occasionally occur. This problem was avoided with the Assman psychrometer because its wet bulb sleeve, which was cloth, not cereamic, could be moistened to the appropriate degree prior to each reading. Manufacturer's calibrations were used for the Assman psychrometer, and the continuous monitor detectors and readout system were calibrated against the Assman unit.

3.2.2 Air Pressure

Air pressure was monitored with daily spot measurements made at the same time as the psychrometric readings. A continuous readout was not deemed necessary for pressure measurements because the net moisture pickup was found to be relatively insensitive to air pressure fluctuations. Inlet pressure conditions were read from a dial-gauge aneroid barometer in the control area. Exhaust pressure conditions were determined from a differential pressure gauge that indicated the difference in pressure between the control area and the sealed room. Daily measurements from both instruments were entered on a data sheet (Fig. 8). Manufacturers' calibrations were used.

3.2.3 Air Flow Velocity

Air flow velocity was continuously monitored in the exhaust duct approximately 1.5 m downstream of the bulkhead. Pressure measurements made in the duct were converted to velocity head and thence to velocity through a system of pneumatic control devices. Output displayed in "chart division" units was continuously recorded on a circular chart, from which daily readings were made at the same time that the psychrometric data were taken. These spot readings were recorded on a data sheet (Fig. 8). The only exception to this procedure was temporarily using a 76-mm-diameter duct as an air flow monitor; this change will be described below. For this duct, the circular chart could not be used because pressure drops were outside the range of input pressures measured by the recording instrument. Spot readings of pressure drop along this duct were converted directly to velocity. Continuous records of air velocity therefore do not exist for the two-week period that the 76-mm duct was used.

The air velocity monitoring device was changed several times to meet the changes in air flow rates that occurred at different temperatures. The various devices and dates of use are listed on Table 4.

The original air flow monitor consisted of a honeycomb flow straightener to reduce turbulence, followed by an array of 16 Pitot tubes to measure static and total air pressure. This device was operated at the lower end of its linear range for the initial 20°C test. Calibration was performed in August 1979, several months before the experiment began, using a Pitot-static tube and hot wire anemometer traverses within a long straight section of the 377-mm-diameter exhaust duct. The results of this and subsequent calibrations of the air flow monitor system are presented in Appendix A.

Table 4. Periods of use for air velocity metering systems.

Metering system	Period of Use
Flow straightener with pitot tubes in 377 mm diameter duct	August 1979 to 22 April 1980 (20° & 30° test)
Modification of system-air flow unmetered	23 April to 13 May 1980 (30° test)
76 mm (3 inch) diameter duct	14 May to 27 May 1980 (30° test)
100 mm orifice in 146 mm diameter duct	28 May to 29 July 1980 (30° & 45° test)
Modification of system-air flow unmetered	30 July to 1 August 1980
Flow straightener with pitot tubes in 377 mm diameter duct	2 August to 22 September 1980 (20° test)

The ventilation system was modified in late April and early May 1980 to accommodate higher room temperatures (the 30°C test was in progress) and considerably lower air flow rates. A 100-mm orifice plate was intended to replace the Pitot tube unit, but, because of delays in delivery, a 76-mm (3-inch) diameter, 305-mm (12-inch) long duct was used as a temporary replacement. This duct was calibrated as a flow metering device in May 1980 and remained in service for approximately two weeks.

The 100-mm orifice plate was installed on 27 May and remained in service through the end of the 30°C test and for all of the 45°C test. It was calibrated in early June in a special 165-mm duct section that replaced a part of the original 377-mm exhaust duct. This special calibration duct improved the accuracy of measurement by increasing the air velocity.

The 100-mm orifice was replaced by the original Pitot tube unit in early August 1980, in order to measure the higher air velocities of the 20°C cool-down test. This unit was recalibrated shortly after reinstallation using the original 377-mm calibration duct section, and was found to be virtually unchanged from the original calibration. The Pitot tube unit was used for air flow monitoring during the balance of the experiment.

3.2.4 Room Air Temperature

Three nickel resistance temperature detectors were mounted at midheight inside the sealed room to measure air temperature. These temperature detectors were used for both room temperature and heater control, but not for moisture pickup computations. The detectors were located at approximately even intervals within the room. Pneumatic transmitters were used to remotely actuate a three-pen circular chart recorder. Although one of the three

temperature detectors could also serve as automatic control for a portion of the duct air heater, manual control of the heater power was sufficient to provide constant room air temperature. The detectors, transmitters, and readout were calibrated in the field according to manufacturer's instructions. A spot readout of the central room air temperature detector, which was linked to the heater control unit, was recorded daily on a data sheet (Fig. 8).

3.2.5 Control Area Air Temperature

The control area was located outside the bulkhead and was open to free circulation of mine air. All measurements except the Assman psychrometer exhaust duct temperatures were read in the control area. Inlet duct air was drawn from the control area, so this duct temperature accurately reflected mine air temperature in the control area. Control area air temperature was also measured by a temperature transducer of the same type as was used in the boreholes and by a mercury thermometer. These were mounted side by side on top of a water pressure gauge panel. The manufacturer's calibration was used for the mercury thermometer, and the temperature transducer was calibrated against the mercury thermometer. This redundant measurement provided a check on the long-term stability of the temperature transducer. Control area mine air temperature was recorded daily from both devices on a data sheet (Fig. 8).

3.2.6 Electric Power Consumption

Total electric power consumption inside the sealed room was cumulatively recorded on a watt-hour meter, and daily spot readings were entered on a data sheet (Fig. 8). These measurements were intended to provide data needed to

model heat flow into the rock, and did not bear directly on the computation of net moisture pickup. The meter recorded the combined power consumption of all electric devices used in the room, including heaters, ceiling fans, lights, and an electric hotplate. The manufacturer's calibration was used.

3.3 Water Pressure Data Acquisition

The purpose of the water pressure data system was to provide information on the head of water in the rock around the drift as a function of time and location. The data required for computing water head are the pressure of the water and the geometry of the instrumentation system.

3.3.1 Water Pressure

Water pressure was monitored in 95 isolated zones within the rock mass throughout the experiment. Spot measurements were recorded daily on a data sheet (Fig. 9). Readings were taken from dial gauges mounted on four panels in the control room. Each gauge was independently connected to one of the monitored zones in the rock by means of a high-pressure nylon tube which passed through an airtight seal in the bulkhead wall. Specifications of the pressure gauges and tubing are shown in Table 3. Pressure gauge calibrations were checked in the field against a Heise Bourdon gauge and were found to fall within the manufacturer's stated accuracy limits, as given in Table 3.

3.3.2 Geometric Data

Conversion of pressure data into total head requires a knowledge of the elevations of the pressure gauges and monitored zones and the temperature in the monitored zones and the drift. Pressure gauge elevations were measured to the center of the gauge with reference to the surveyed elevation of either (a) the instrument platform for all R and HG boreholes or (b) the axis of the

LBL FIELD ENGINEER R. Galbraith

DATE 800617

TIME 8:10

LBL MACROPERMEABILITY EXPERIMENT

DATA TYPE Temp/Pressure

BOREHOLE NAME

Zone	R1	R2	R3	R4	R5	
1	319.9 / 196.0	291.0 / 152.5	X / 132.5	289.2 / 139.0	290.1 / 143.5	
2	X / 207.0	285.6 / 170.0	285.2 / 179.0	X / 148.0	X / 138.0	
3	X / 208.5	284.4 / 104.0	284.2 / 180.5	284.2 / 151.5	X / 131.5	
4	284.2 / 208.0	284.0 / 212.0	284.2 / 182.0	284.1 / 153.0	284.1 / 263.0	
5	284.1 / 234.0	284.2 / 217.5	284.1 / 186.0	284.0 / 152.5	X / 178.0	
6	284.1 / 246.0	284.1 / 227.0	X / 199.0	X / 155.0	X / 132.0	

Temp (°K) / Pressure (psi)

Temperature/Pressure

Temp (°K) / V_i / V_v / Cond.

Conductance

Conductance = $\frac{V_i}{V_v} \frac{1}{R_{ref}}$

Fig. 9. Sample data sheet for water pressure and temperature measurements.

hole at the collar for borehole DBH-2. Elevations of zones within boreholes were based upon borehole surveys conducted by the Swedish surveying firm VIAK AB. Local traverse points within the ventilation drift were identified by conventional roof markers. Details of the surveying techniques and an appraisal of accuracy are described by Kurfurst et al. (1978, pp. 28-33).

3.3.3 Shunting Data

Shunting test data consist of flow rate measurements in the tubes connected to shunted zones and pressure measurements within all zones of the borehole being tested. Flow rate measurements were made by a purge type of flow meter inserted in the shunting tubes. Flow rate is indicated by the height to which a calibrated weight is lifted by upward flow in a conical tube. Specifications for the flow meters used in the shunting tests are given in Table 3. The manufacturer's calibrations were used for these flow meters. Zone pressure measurements were made using the same pressure gauges as described in Section 3.3.1. Data were recorded on data sheets of the type shown on Fig. 10 for two-zone tests and Fig. 11 for three-zone tests.

The shunting tests were performed during the week of 22 September, 1980. This was the last week that the ventilation drift was available to LBL for experimentation. Shunting was continued for about 2 days on the two-zone tests and 5 days on the three-zone tests. The two-zone tests ran smoothly, primarily because it was clear from initial pressure conditions which direction the flow would take between zones. Difficulties were encountered in some of the three-zone tests because (1) the final orientation of flow is less well defined than in two-zone tests, and (2) the initial orientation of flow may not be the same as the final orientation. For these tests, therefore,

TWO ZONE SHUNTING DATA SHEET - MACROPERMEABILITY EXPERIMENT

LBL Field Engineer Charles R Wilson Month and Year 9/80

Hole	Flow		Date	Time	Pressure Data by Zone (psi)						Panel No.	Gauge No.	Flow Rate	
	From Zone	To Zone			~~1~~ 3	~~2~~ 4	~~3~~ 5	~~4~~ 6	~~5~~ 7	~~6~~ 8			% of Scale 1/	ml/min
R06	8	7	22	800	171.0	203.0	206.5	208.0	217.0	239.0	3	AB	0	0
START		TEST		1140	170.0	202.5	205.0	207.5	32.0	32.5			75	21.8
				1145					35.0	35.0			25	7.2
				1200	171.0	202.5	206.5	207.5	46.0	46.0			28	8.1
				1220	171.0	202.5	206.5	207.5	206.0	206.0			8	2.3
				1315	171.0	202.5	206.5	207.5	233.0	233.5			4	1.2
			23	730	171.0	202.5	206.5	207.5	237.0	237.5	3	AB	2	0.6
				1340	171.0	202.5	206.5	207.5	237.0	237.5			3	0.9
			24	730	171.0	203.0	206.0	208.0	237.0	238.0	3	AB	4	1.2

Notes:

1/ Full scale = 29 ml/min.

Fig. 10. Sample data sheet for two zone shunting tests.

THREE ZONE SHUNTING DATA SHEET - MACROPERMEABILITY EXPERIMENT

Hole	Flow Pattern			Date	Time	Pressure Data by Zone(psi)						Panel No.	Flow Rate					
	From Zone	~~Zone~~ 1/ To Zone	To Zone			~~1~~ 3	~~2~~ 4	~~3~~ 5	~~4~~ 6	~~5~~ 7	~~6~~ 8		Zone 6 1/ % of Scale 2/	Zone 6 1/ ml/min	Zone 7 3/ % of Scale 4/	Zone 7 3/ ml/min	Zone 8 5/ % of Scale 6/	Zone 8 5/ ml/min
R06	INITIAL CONDITIONS			22	800	171.0	203.0	206.5	208.0	217.0	239.0	3						
START TEST	8	7	6	24	1320	168.5	201.0	179.5	21.0	33.0	19.0	3	0	0	0	0	0	0
				24	1430	171.5	202.0	205.5	209.0	210.0	210.5	3	0	0	0	0	0	0
				25	10:22	171.5	203.0	208.0	208.5	208.5	209.0	3	0	0	0	0	20	5.8
				26	10:14	171.5	203.0	208.0	214.0	215.0	216.5	3	0	0	0	0	15	4.4
				29	12:04	171.5	203.5	208.5	214.5	216.0	216.0	3	15	4.4	0	0	15	4.4

LBL Field Engineer WILSON / RAMQVIST Month and Year Sept 1980

Notes:
1/ Gauge AB used for Zone 6. 3/ Gauge CD used for Zone 7. 5/ Gauge EF used for Zone 8.
2/ Full scale = 29 ml/min. 4/ Full scale = 29 ml/min. 6/ Full scale = 29 ml/min.

Fig. 11. Sample data sheet for three zone shunting tests.

flow was measured into or out of all three zones to provide an internal mass balance check. For unknown reasons mass balance was satisfied in only two of the four three-zone tests conducted.

3.3.4 Salt Tracer Test

The possible movement of a salt tracer was monitored by measuring the conductance of water in each zone of the HG holes and in zone 4 of borehole R01. Measurements were taken daily using a digital AC meter (see Table 3). Conductance was determined by comparing the voltage drop across the water gap with the voltage drop of the same current across a known resistor. Current was supplied by a square-wave generator operating at 100 Hz. Daily readings consisting of the two voltages and the resistance of the known resistor were entered on a data sheet of the type shown on Fig. 12. The manufacturer's calibration was used for the AC meter.

3.4 Rock-Water Temperature Data Acquisition

The purpose of the temperature data system was to measure ambient temperatures in the rock mass in order to monitor the transfer of heat from the room air into the rock. This section covers water temperature monitors in the R and HG boreholes, rock temperature monitors in the temperature hole, and rock wall temperature monitors. All monitoring stations used the same type of analog temperature transducer (specifications in Table 3). Each device was set so that the voltage read across a resistor in millivolts was numerically equal to the temperature in degrees K.

3.4.1 Water Temperature in the R and HG Boreholes

Each zone equipped for water pressure monitoring was also equipped for temperature monitoring, except for borehole DBH-2. The temperature

LBL FIELD ENGINEER R. Galbraith

DATE 800701

TIME 8:23

LBL MACROPERMEABILITY EXPERIMENT

DATA TYPE Conductance,

Before 10.10

After 10.10

BOREHOLE NAME

Zone	R1	HG1	HG2	HG3	HG4	HG5
1		116.51 / .3211 / 35.9	117.65 / .2522 / 46.2	117.57 / .2570 / 45.3	116.35 / .3317 / 34.7	117.44 / .2654 / 43.8
2	117.14 / .2829 / 41.0	116.93 / .2958 / 39.1	117.05 / .2885 / 40.2	116.99 / .3543 / 32.4	116.85 / .3008 / 38.5	117.10 / .2855 / 40.2
3		116.61 / .3153 / 36.6	116.27 / .3357 / 34.3	116.42 / .3267 / 35.3	116.63 / .3142 / 36.8	116.08 / .3497 / 37.8
4		116.72 / .3052 / 37.5	116.99 / .2926 / 39.6	116.43 / .3275 / 35.2	116.79 / .3052 / 37.9	116.80 / .3041 / 38.8
5		117.55 / .2582 / 45.1	116.26 / .3361 / 34.5	116.98 / .2925 / 39.6	116.38 / .3292 / 35.0	116.90 / .2939 / 38.9
6		117.36 / .2702 / 43.0	117.02 / .2909 / 39.8	121.29 / 30.99 / 387.5	116.98 / .2929 / 39.5	117.66 / .2513 / 46.4

Temp (°K) / Pressure (psi)

Temperature/Pressure

Temp (°C) / V_i / V_v / Cond.

Conductance

$$\text{Conductance} = \frac{V_i}{V_v}\,\frac{1}{R_{ref}}$$

Fig. 12. Sample data sheet for salt tracer test.

transducer was mounted at about the same depth in each zone as the open port of the water pressure sensing tube. The various components of the installed borehole equipment are shown in Fig. 6. Electric leads to each transducer were threaded through the bulkhead and terminals were mounted on the pressure gauge panels beside the pressure gauge for the corresponding zone. Temperatures were measured daily at the same time that water pressures were recorded. Data were entered on the same data sheet as water pressures (Fig. 9). All water temperature detectors were calibrated in the borehole immediately after installation, by setting them to a constant initial groundwater temperature of 284.0 K.

3.4.2 Rock Temperature in the Temperature Hole

Temperature hole TG-1 was instrumented with 8 temperature transducers of the type used in other boreholes. Readout was made from a panel in the control area. Data were recorded daily on a data sheet of the type shown in Fig. 13. Before sealing them in the borehole, the transducers were calibrated in air against a mercury thermometer of the same type as was mounted in the control room.

3.4.3. Rock Wall Temperature

Temperature transducers of the same type as was used in the boreholes were glued to the rock walls of the ventilation drift near the collars of boreholes R01, R02, R04, R06, R07, R09 and TG-1. Readout was made from a panel in the control area. Data were recorded daily on a data sheet (Fig. 14). The transducers were calibrated in air against the mercury thermometer mounted in the control room (see Section 3.2.5) before installation on the drift walls.

LBL FIELD ENGINEER G. Bangquist

MONTH AND YEAR Nov 1979

LBL MACROPERMEABILITY EXPERIMENT

TEMPERATURE DATA - TEMPERATURE HOLE

TEMPERATURE (°K)

Date/Time	Sensor Depth (m)							
	0.0	0.15	0.30	0.60	1.25	2.5	5.0	10.0
21 12:33	284.3	284.1	284.1	284.4	284.4	285.6	283.6	283.2
22 10:56	284.3	284.1	284.1	284.4	284.4	284.3	283.6	283.2
23 11:05	284.5	284.3	284.2	284.4	284.4	284.4	283.6	283.2
26 11:05	284.5	284.3	284.3	284.5	284.5	284.5	283.6	283.2
27 10:42	284.5	284.3	284.3	284.5	284.5	284.4	283.6	283.2

Fig. 13. Sample data sheet for temperature hole measurements.

LBL FIELD ENGINEER R Galbraith

MONTH AND YEAR Feb 1980

LBL MACROPERMEABILITY EXPERIMENT

WALL TEMPERATURE DATA SHEET

Date	Time	Wall Temperature (°K) at Borehole:						
		R-1	R-2	R-4	R-6	R-7	R-9	temp hole (TG-1)
27	8:06	288.2	287.5	288.6	286.6	286.6	286.9	287.4
28	7:57	288.3	287.5	288.6	286.7	286.6	286.9	287.4
29	7:58	288.6	287.8	288.9	286.8	286.8	287.1	287.6
29	12:00	289.3	288.2	289.8	287.0	286.9	287.4	287.9
03	8:10	289.6	288.7	290.0	287.4	287.3	287.7	288.3
04	8:25	289.6	288.7	290.1	287.4	287.3	287.8	288.4

Fig. 14. Sample data sheet for wall temperature measurements.

3.5 Geochemical Data Acquisition

Three geochemical samples were taken from walls and fractures of the drift to see what type of material was being deposited as the water was evaporated. The first sample consisted of precipitates collected on the bottom of an iron evaporating pan at borehole R05. The precipitates, a dry, white crystalline material, were collected on 11 June 1980 and shipped to LBL in a plastic sample jar. The second sample consisted of fracture-filling materials and adjacent rock removed from the drift wall with dry chisels. These materials were collected on 28 July 1980 under dry room conditions, before cooling the room for the final 20°C test, and were immediately wrapped and sealed in plastic and shipped to LBL. The third sample consisted of natural fracture fillings and adjacent rock found in the core of borehole HG-2. This hole was cored by conventional triple-tube drilling techniques, and the natural open fractures were exposed to the drilling fluids. This borehole was drilled during the week of 20 February 1978 and the core was stored in a wooden corebox in a surface storage shed at the Stripa mine until it was removed for shipment to LBL on 23 September 1980.

The sample of precipitates has been studied by x-ray diffraction techniques, and the results are presented in Chapter 6. The other samples will be studied with secondary ion mass spectrometry (SIMS) and Auger spectroscopy, which are expected to provide information on the types and relative amounts of elements present in the fracture fillings. These latter studies have not yet been completed.

4. DATA REDUCTION PROCEDURES

4.1 Introduction

Analysis of the rock properties governing the flow of groundwater in the fracture system surrounding the ventilation drift requires transforming the collected raw data into net moisture pickup in the ventilation drift, the hydraulic head distribution in the fractured medium surrounding the drift, and the temperature within the rock mass. This section describes the basic procedures involved in data reduction.

4.2 Reduction of Ventilation System Data

Ventilation system data were collected to compute the net moisture pickup of water by air in the sealed portion of the ventilation drift. As discussed earlier, these data can be used to estimate the seepage rate of groundwater into the drift. The net moisture pickup is the difference in moisture content of the air in the exhaust and inlet ducts.

The procedure for calculating net moisture pickup will be summarized here, and a detailed example computation is given in Appendix A. A sensitivity analysis of net moisture pickup to input variables and the determination of standard error will be discussed in Chapter 5.

4.3 Computation of Net Moisture Pickup

4.3.1 Introduction

The mass flow rate of water within the inlet or exhaust duct air is equal to the product of the density of water (ρ_W) and the equivalent volumetric flow rate of liquid water (v) for the moisture in the air moving through the duct. The mass flow rate is also equal to X, the ratio of water vapor mass to dry air mass, multiplied by the mass flow rate of dry air;

the latter is the produce the the density of dry air [$\rho_{m(app)}$] and the volumetric air flow rate (Q_{act}). From this mass flow rate relationship, the equivalent volumetric flow rate of liquid water in a duct is:

$$v = \frac{X \, \rho_{m(app)} \, Q_{act}}{\rho_w} .$$

Hence, the net moisture pickup (MP) within the drift is:

$$MP = v_E - v_I \quad ,$$

where v_E = equivalent volumetric flow rate of liquid water in the exhaust duct (water outflow),

v_I = equivalent volumetric flow rate of liquid water in the inlet duct (water inflow).

The determination of net moisture pickup requires the calculation of three quantities at both the inlet and exhaust ducts: X, $\rho_{m(app)}$ and Q_{act}. These quantities were determined from the following set of measurements made in the ventilation drift: (1) the wet bulb temperature (t_w) and the dry bulb temperature (t_d) in the inlet and exhaust ducts; (2) the barometric pressure in the inlet duct (P_I); (3) the differential pressure head (DH), between the inlet and exhaust ducts from which the barometric pressure in the exhaust duct is determined; and (4) the chart reading (CH), used in determining the air flow rate.

4.3.2 Determination of the Ratio of Mass of Water Vapor to Mass of Dry Air

The ratio of mass of water vapor to mass of dry air (X) is ascertained by using the theory of the wet bulb thermometer, in which a transfer of moisture, in the form of evaporation, takes place from the wet bulb to the air flowing past it. This transfer is assumed to occur at a rate sufficient

to saturate the air in the immediate vicinity of the bulb. The mass of water vapor evaporated into the air from the bulb, per unit mass of dry air, is $X_s - X$, where X_s is the ratio of mass of water vapor to mass of dry air at saturated condition. As a result of this evaporation, the energy level at the wet bulb is lowered. The latent heat transfer per unit mass of dry air (LE), from the bulb to the atmosphere, is:

$$LE = L(X_s - X) \quad , \tag{1}$$

where L is the latent heat of vaporization of water.

At equilibrium, the latent heat transfer is equal to the sensible heat transfer (q) due to the convection of air past the bulb which, for a unit mass of dry air is:

$$q = C_{pm}(1 + X)(t_d - t_w) \quad , \tag{2}$$

where C_{pm} is defined as the specific heat of moist air at constant pressure (see Eq. A6 for computing C_{pm}). By establishing values for X_s, C_{pm} and L, X can be determined upon equating (1) and (2).

The latent heat of vaporization (L) is calculated using an emprical equation (Eq. A1) found accurate to within 0.10% of the actual value of L for the temperature range 10°C to 50°C. The ideal gas law is used to determine X_s:

$$PV = mR_a t,$$

where

P = pressure,

V = volume,

m = mass of gas,

R_a = gas constant for air,

t = temperature.

In a volume occupied by water vapor/air mixture (termed moist air) at isothermal condition, the relationships between the gases are as follows:

(A) Moist air:

$$PV = mR_m t \quad , \tag{3}$$

where

m = total mass of water vapor and dry air,

R_m = gas constant for moist air.

(B) Water vapor:

$$eV = m_v R_v t \quad , \tag{4}$$

where

e = water vapor pressure,

m_v = mass of water vapor,

R_v = gas constant of water vapor.

(C) Dry air

$$P_a V = (P - e)V = m_a R_a t \quad , \tag{5}$$

where

P_a = pressure of dry air,

m_a = mass of dry air.

From (B) and (C) the ratio of mass of water vapor to mass of dry air $\frac{m_v}{m_a}$ can be resolved. Therefore:

$$X = \frac{R_a}{R_v}\left(\frac{e}{P - e}\right) \text{ and } X_s = \frac{R_a}{R_v}\left(\frac{e_{sw}}{P - e_{sw}}\right) \cdot \tag{6}$$

The Clausius-Clapeyron equation utilizing the empirical formula for L is used to ascertain the saturation vapor pressure of water (e_{sw}) (Eq. A2). Thus, all essential quantities required to calculate X are now known.

4.3.3 Determining the Density of Dry Air ($\rho_{m(app)}$)

From Eq. (5) in the previous section:

$$\rho_{m(app)} = \frac{m_a}{V} = \frac{P - e}{R_a t} \quad .$$

Having previously determined X, the density of dry air is ascertained by substituting the value of e as determined by Eq. (6) into the above equation.

The density of moist air $\rho_{m(act)}$ required in the next section can also be determined from Eq. (3) in the previous section as:

$$\rho_{m(act)} = \frac{m}{V} = \frac{P}{R_m t} \quad . \tag{7}$$

4.3.4 Determining the Actual Air Flow (Q_{act})

The actual air flow is determined by establishing the values of the density of moist air (Eq. (7)) and the standard air flow (Q_{st}). The standard air flow is based on a specific moist air density of 1.20 kg/m^3 and is obtained from the air flow monitor calibration curve, a relationship between Q_{st} and CH. Calibration curves were derived in the field for each air flow measuring device used in the experiment. A discussion of the derivation and use of the calibration curves is presented in Appendix A. Knowing Q_{st} and $\rho_{m(act)}$, the actual air flow (see McPherson, 1979b) is:

$$Q_{act} = Q_{st}\left[\frac{\rho_{st}}{\rho_{m(act)}}\right]^{1/2}$$

4.3.5 Presentation of Net Moisture Pickup

A systematic step-by-step procedure to determine the net moisture pickup is illustrated in Fig. 15. The results of the net moisture pickup

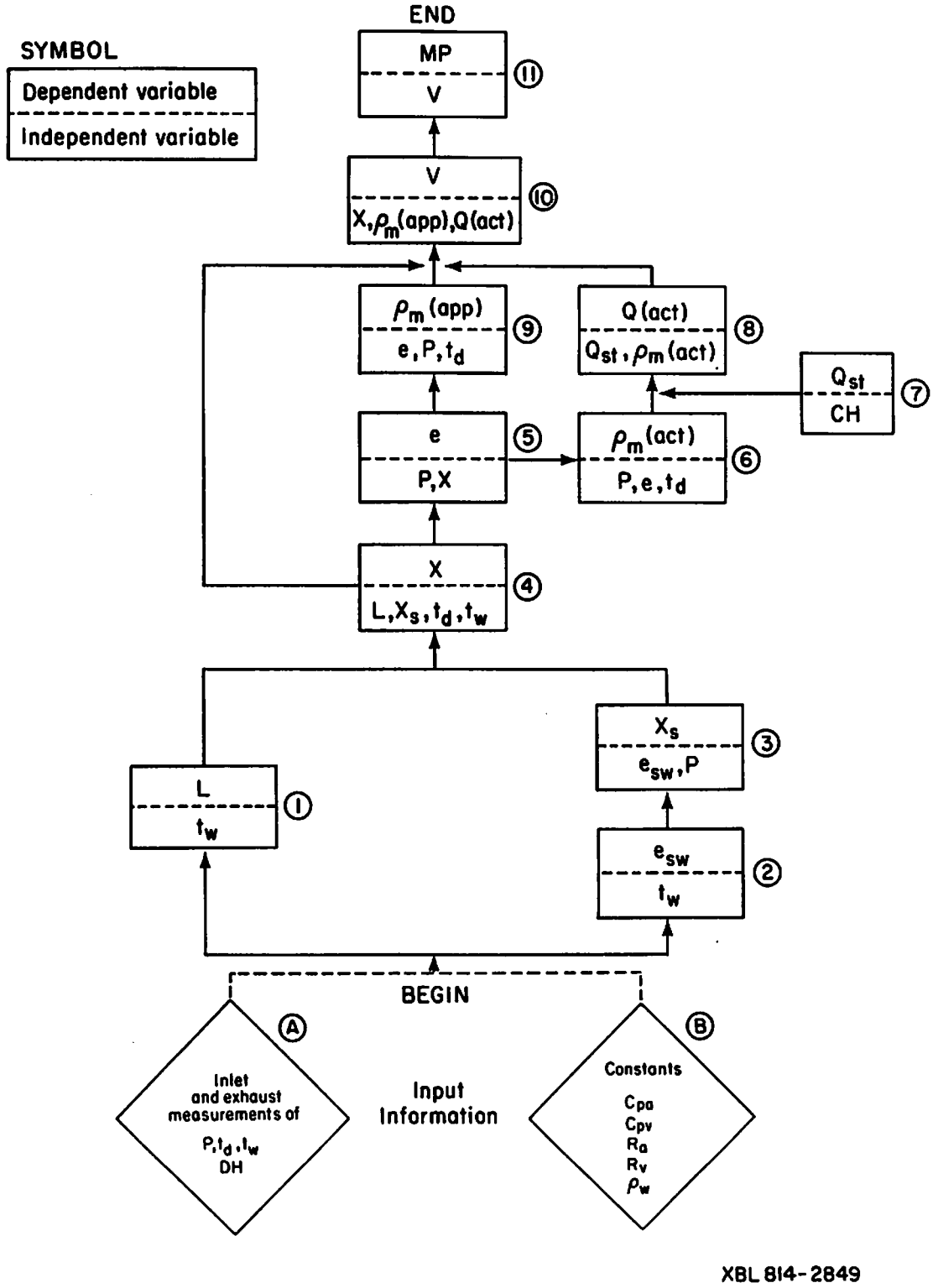

Fig. 15. Flow chart for determination of net moisture pickup.

computations, for each day that data were recorded, are shown in Fig. 16 and presented numerically in Table 5. Gaps in the record can be attributed to (1) change in equipment, (2) malfunction of equipment, or (3) weekends and holidays.

4.4 Reduction of Water Pressure Data

Darcy's law states that the mass flux of water in laminar flow is proportional to the hydraulic gradient. Consequently, to analyze the flow of water into the ventilation drift, pressures are measured in the rock surrounding the drift. Three sets of boreholes were drilled to measure pressures in the rock: (1) the HG boreholes, (2) the R boreholes, and (3) the DBH-2 borehole. Figure 17 shows the location and geometry of the three sets of boreholes in relation to the ventilation drift.

4.4.1 HG and R Boreholes

The HG and R boreholes are each 76 mm in diameter. Cross sections showing the borehole numbering system are illustrated in Figs. 18 to 21. Figure 22 is a perspective view showing the geometrical relations among the HG holes. Each borehole is 30 m long except for R01 and R06, which are 40 m long. Each 30 m borehole is subdivided into six zones approximately 5 m in length. The 40 m holes are subdivided into eight such zones. Packers are used to seal the boreholes and isolate the zones so that the pressure in each zone can be measured independently. For all boreholes except R01 and R06, the pressures are measured in zones 1 to 6. For R01 and R06 the pressures are measured in zones 3 to 8 (i.e., at locations farther away from the drift).

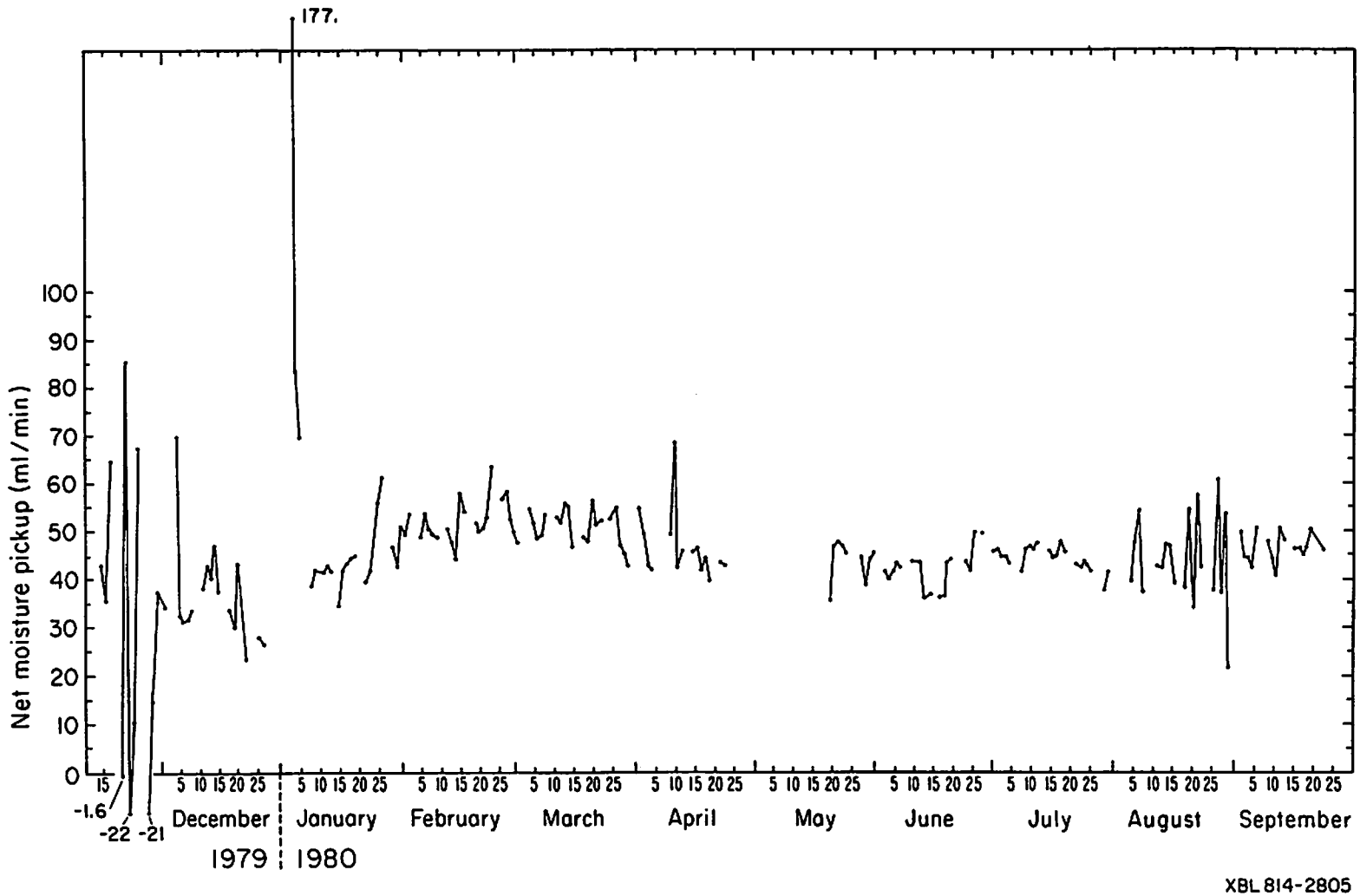

Fig. 16. Net moisture pickup for the period 19 November 1979 to 22 September 1980.

Table 5.

Net Moisture Pickup Data

DATE	AIR FLOW 3 (M /S)	TOTAL WATER INFLOW (ML/MIN)	EXPERIMENTAL ERROR IN WATER INFLOW (ML/MIN)	TOTAL WATER OUTFLOW (ML/MIN)	EXPERIMENTAL ERROR IN WATER OUTFLOW (ML/MIN)	NET MOISTURE PICKUP (ML/MIN)	EXPERIMENTAL ERROR IN NET MOISTURE PICKUP (ML/MIN)
11-14-79	1.251	548.9	8.2	591.7	8.4	42.8	12.
11-15-79	1.270	587.4	8.5	623.3	8.7	35.9	12.
11-16-79	1.270	521.0	8.2	585.2	8.5	64.3	12.
11-19-79	1.276	642.4	8.9	640.8	8.8	-1.6	12.
11-20-79	1.270	530.5	8.2	615.7	8.6	85.2	12.
11-21-79	1.276	589.7	8.5	567.7	8.4	-22.	12.
11-22-79	1.258	577.5	8.4	588.0	8.4	10.5	12.
11-23-79	1.245	568.0	8.3	635.5	8.7	67.4	12.
11-26-79	.309	165.2	5.2	144.5	4.6	-21.	6.9
11-27-79	.309	151.8	4.8	166.1	5.2	14.4	7.1
11-28-79	.321	134.1	4.2	171.7	5.2	37.6	6.7
11-29-79	.315	133.2	4.2	170.0	5.2	36.8	6.7
11-30-79	.309	133.1	4.3	167.1	5.2	34.0	6.8
12-03-79	.309	103.3	3.5	173.2	5.4	69.8	6.5
12-04-79	.309	140.7	4.5	172.8	5.4	32.0	7.0
12-05-79	.300	138.8	4.6	169.8	5.5	31.0	7.1
12-06-79	.303	139.5	4.5	170.8	5.4	31.3	7.1
12-07-79	.309	133.3	4.3	167.2	5.2	33.8	6.8
12-10-79	.303	103.5	3.5	141.7	4.6	38.2	5.8
12-11-79	.297	98.9	3.4	141.3	4.7	42.4	5.8
12-12-79	.297	88.2	3.1	128.2	4.3	40.1	5.3
12-13-79	.305	75.9	2.8	123.0	4.0	47.1	4.9
12-14-79	.300	84.9	3.0	122.2	4.1	37.3	5.1
12-17-79	.284	88.1	3.2	121.8	4.2	33.7	5.3
12-18-79	.283	87.8	3.2	117.8	4.1	29.9	5.2
12-19-79	.291	65.7	2.6	108.9	3.8	43.1	4.6
12-20-79	.297	86.9	3.1	121.1	4.1	34.1	5.1
12-21-79	.303	87.6	3.1	111.0	3.7	23.3	4.8
12-25-79	.297	108.7	3.7	136.5	4.5	27.8	5.9
12-26-79	.297	115.2	3.9	142.0	4.7	26.7	6.1

Table 5 (continued)

DATE	AIR FLOW 3 (M /S)	TOTAL WATER INFLOW (ML/MIN)	EXPERIMENTAL ERROR IN WATER INFLOW (ML/MIN)	TOTAL WATER OUTFLOW (ML/MIN)	EXPERIMENTAL ERROR IN WATER OUTFLOW (ML/MIN)	NET MOISTURE PICKUP (ML/MIN)	EXPERIMENTAL ERROR IN NET MOISTURE PICKUP (ML/MIN)
12-29-79	.291	116.5	4.0	154.3	5.2	37.8	6.5
01-02-80	1.245	545.1	8.1	722.0	9.2	177.	12.
01-03-80	1.233	461.8	7.6	545.3	8.0	83.5	11.
01-04-80	1.233	395.0	7.2	464.7	7.6	69.7	10.
01-07-80	.303	119.3	4.0	158.0	5.1	38.7	6.4
01-08-80	.321	125.2	4.0	167.0	5.1	41.8	6.4
01-09-80	.309	123.2	4.0	164.7	5.2	41.5	6.6
01-10-80	.309	121.8	4.0	163.0	5.1	41.3	6.5
01-11-80	.309	117.2	3.9	159.6	5.0	42.4	6.3
01-12-80	.309	118.4	3.9	159.8	5.0	41.4	6.4
01-14-80	.300	124.4	4.1	158.6	5.1	34.2	6.6
01-15-80	.291	109.9	3.8	151.5	5.1	41.7	6.4
01-16-80	.297	109.4	3.7	152.5	5.0	43.1	6.3
01-17-80	.297	108.6	3.7	152.7	5.0	44.1	6.2
01-18-80	.297	101.0	3.5	145.7	4.8	44.7	5.9
01-21-80	.297	111.6	3.8	150.9	5.0	39.3	6.3
01-22-80	.297	113.4	3.9	154.9	5.1	41.5	6.4
01-23-80	.511	203.7	4.4	261.1	5.2	57.4	6.8
01-24-80	.513	188.1	4.2	244.0	4.9	55.9	6.5
01-25-80	.450	138.3	3.6	199.3	4.6	61.0	5.8
01-28-80	.529	139.7	3.5	186.4	4.1	46.8	5.4
01-29-80	.529	160.5	3.8	203.1	4.3	42.6	5.7
01-30-80	.529	143.5	3.6	193.8	4.2	50.3	5.5
01-31-80	.529	157.8	3.7	206.9	4.4	49.1	5.7
02-01-80	.529	139.0	3.5	192.3	4.2	53.3	5.5
02-04-80	.529	191.4	4.2	240.1	4.8	48.7	6.4
02-05-80	.529	193.7	4.2	247.6	4.9	53.9	6.5
02-06-80	.641	234.9	4.6	285.5	5.1	50.6	6.9
02-07-80	.641	244.4	4.7	293.5	5.2	49.1	7.0
02-08-80	.579	218.6	4.5	267.0	5.0	48.4	6.7

Table 5 (continued)

DATE	AIR FLOW 3 (M /S)	TOTAL WATER INFLOW (ML/MIN)	EXPERIMENTAL ERROR IN WATER INFLOW (ML/MIN)	TOTAL WATER OUTFLOW (ML/MIN)	EXPERIMENTAL ERROR IN WATER OUTFLOW (ML/MIN)	NET MOISTURE PICKUP (ML/MIN)	EXPERIMENTAL ERROR IN NET MOISTURE PICKUP (ML/MIN)
02-11-80	.431	168.3	4.1	218.5	5.0	50.3	6.5
02-12-80	.431	171.6	4.2	218.9	5.0	47.4	6.6
02-13-80	.313	124.5	4.0	168.4	5.2	44.0	6.6
02-14-80	.816	346.5	5.7	404.5	6.2	58.0	8.4
02-15-80	1.270	561.3	8.3	615.1	8.6	53.8	12.
02-18-80	.664	280.6	5.1	332.3	5.6	51.7	7.6
02-19-80	.523	223.2	4.6	273.0	5.3	49.9	7.1
02-20-80	.526	225.7	4.7	275.9	5.4	50.2	7.1
02-21-80	.530	227.5	4.7	279.8	5.4	52.3	7.2
02-22-80	.529	209.2	4.4	272.4	5.3	63.2	6.9
02-25-80	.529	175.4	4.0	231.9	4.8	56.5	6.2
02-26-80	.529	175.5	4.0	233.6	4.8	58.1	6.2
02-27-80	.529	172.4	4.0	224.9	4.7	52.5	6.1
02-28-80	.529	182.1	4.1	231.9	4.8	49.8	6.3
02-29-80	.528	195.1	4.2	242.5	4.9	47.4	6.5
03-03-80	.522	182.6	4.1	237.0	4.9	54.4	6.3
03-04-80	.518	174.5	4.0	226.0	4.7	51.5	6.2
03-05-80	.526	179.6	4.0	228.0	4.7	48.4	6.2
03-06-80	.522	209.2	4.4	258.1	5.2	49.0	6.8
03-07-80	.521	204.8	4.4	257.8	5.2	53.0	6.8
03-10-80	.518	196.6	4.3	249.5	5.1	52.9	6.7
03-11-80	.521	200.3	4.3	252.1	5.1	51.8	6.7
03-12-80	.523	196.7	4.3	252.4	5.1	55.8	6.7
03-13-80	.528	205.2	4.4	255.2	5.2	50.0	6.8
03-14-80	.528	205.5	4.4	251.8	5.1	46.3	6.7
03-17-80	.529	188.9	4.2	237.3	4.9	48.4	6.4
03-18-80	.529	195.0	4.2	242.7	5.0	47.8	6.5
03-19-80	.529	189.2	4.2	245.4	5.0	56.2	6.5
03-20-80	.529	189.3	4.2	240.6	5.0	51.2	6.5
03-21-80	.530	193.9	4.2	245.9	5.0	52.0	6.6
03-24-80	.529	165.0	3.9	217.3	4.6	52.3	6.0
03-25-80	.529	170.1	3.9	224.9	4.7	54.9	6.1

Table 5 (continued)

DATE	AIR FLOW 3 (M /S)	TOTAL WATER INFLOW (ML/MIN)	EXPERIMENTAL ERROR IN WATER INFLOW (ML/MIN)	TOTAL WATER OUTFLOW (ML/MIN)	EXPERIMENTAL ERROR IN WATER OUTFLOW (ML/MIN)	NET MOISTURE PICKUP (ML/MIN)	EXPERIMENTAL ERROR IN NET MOISTURE PICKUP (ML/MIN)
03-26-80	.529	178.7	4.0	225.4	4.7	46.7	6.2
03-27-80	.526	178.3	4.0	223.3	4.7	45.0	6.2
03-28-80	.524	188.7	4.2	231.3	4.8	42.6	6.4
03-31-80	.523	206.7	4.4	261.2	5.3	54.5	6.9
04-01-80	.522	212.2	4.5	261.5	5.3	49.3	6.9
04-02-80	.521	211.4	4.5	253.6	5.2	42.2	6.8
04-03-80	.518	206.4	4.4	248.2	5.2	41.8	6.8
04-08-80	.517	210.0	4.5	259.1	5.4	49.1	7.0
04-09-80	.517	200.5	4.3	268.7	5.6	68.3	7.1
04-10-80	.516	186.7	4.2	229.3	5.1	42.6	6.6
04-11-80	.517	187.9	4.2	233.3	5.1	45.3	6.6
04-14-80	.517	186.1	4.1	231.6	5.1	45.5	6.6
04-15-80	.517	194.6	4.3	240.9	5.3	46.2	6.8
04-16-80	.517	200.9	4.4	242.4	5.3	41.5	6.9
04-17-80	.517	194.7	4.3	238.8	5.2	44.1	6.8
04-18-80	.515	195.9	4.3	235.5	5.2	39.6	6.7
04-21-80	.510	186.5	4.2	229.7	5.2	43.2	6.6
04-22-80	.529	191.1	4.2	234.0	5.2	42.9	6.7
05-14-80	.079	34.4	1.1	93.9	2.9	59.5	3.1
05-19-80	.078	36.3	1.2	71.7	2.3	35.5	2.6
05-20-80	.077	32.3	1.1	79.1	2.5	46.8	2.7
05-21-80	.077	30.7	1.0	77.9	2.5	47.3	2.7
05-22-80	.077	29.7	1.0	76.4	2.4	46.7	2.6
05-23-80	.071	29.4	1.1	74.5	2.6	45.1	2.8
05-27-80	.066	29.9	1.1	74.2	2.7	44.3	3.0

Table 5 (continued)

DATE	AIR FLOW 3 (M /S)	TOTAL WATER INFLOW (ML/MIN)	EXPERIMENTAL ERROR IN WATER INFLOW (ML/MIN)	TOTAL WATER OUTFLOW (ML/MIN)	EXPERIMENTAL ERROR IN WATER OUTFLOW (ML/MIN)	NET MOISTURE PICKUP (ML/MIN)	EXPERIMENTAL ERROR IN NET MOISTURE PICKUP (ML/MIN)
05-28-80	.056	25.0	1.3	63.4	3.1	38.4	3.4
05-29-80	.073	34.3	1.3	78.3	3.0	44.0	3.3
05-30-80	.073	34.2	1.3	79.3	3.0	45.1	3.3
06-02-80	.073	34.3	1.3	76.1	2.9	41.7	3.2
06-03-80	.067	31.3	1.3	71.3	2.9	40.0	3.2
06-04-80	.067	31.2	1.3	73.1	3.0	41.9	3.3
06-05-80	.067	30.7	1.3	73.8	3.0	43.1	3.3
06-06-80	.067	31.2	1.3	73.7	3.0	42.5	3.3
06-09-80	.068	31.7	1.3	75.3	3.1	43.6	3.3
06-10-80	.068	31.4	1.3	74.7	3.1	43.3	3.3
06-11-80	.068	32.0	1.3	75.2	3.1	43.2	3.3
06-12-80	.054	25.6	1.3	61.7	3.2	36.0	3.4
06-13-80	.054	25.3	1.3	61.9	3.2	36.5	3.4
06-16-80	.054	25.5	1.3	61.7	3.2	36.2	3.4
06-17-80	.054	25.3	1.3	61.8	3.2	36.5	3.4
06-18-80	.070	33.0	1.3	76.3	3.0	43.3	3.3
06-19-80	.069	32.0	1.3	76.0	3.0	44.0	3.3
06-23-80	.083	38.7	1.4	82.4	2.8	43.6	3.1
06-24-80	.083	40.4	1.4	82.2	2.8	41.8	3.1
06-25-80	.083	40.7	1.4	90.3	3.1	49.7	3.4
06-27-80	.083	40.8	1.4	90.0	3.0	49.2	3.3
06-30-80	.067	32.5	1.4	78.2	3.3	45.7	3.5
07-01-80	.067	32.0	1.4	78.0	3.2	46.0	3.5
07-02-80	.067	32.3	1.4	76.9	3.2	44.6	3.5
07-03-80	.067	32.4	1.4	76.9	3.2	44.5	3.5
07-04-80	.061	29.9	1.4	73.0	3.3	43.1	3.6
07-07-80	.067	31.5	1.3	73.0	3.0	41.5	3.3

Table 5 (continued)

DATE	AIR FLOW 3 (M /S)	TOTAL WATER INFLOW (ML/MIN)	EXPERIMENTAL ERROR IN WATER INFLOW (ML/MIN)	TOTAL WATER OUTFLOW (ML/MIN)	EXPERIMENTAL ERROR IN WATER OUTFLOW (ML/MIN)	NET MOISTURE PICKUP (ML/MIN)	EXPERIMENTAL ERROR IN NET MOISTURE PICKUP (ML/MIN)
07-08-80	.067	31.9	1.4	77.9	3.2	46.0	3.5
07-09-80	.067	31.7	1.3	78.0	3.3	46.4	3.5
07-10-80	.067	31.9	1.4	78.0	3.3	46.0	3.5
07-11-80	.067	31.0	1.3	78.4	3.3	47.4	3.5
07-14-80	.067	31.7	1.3	77.4	3.2	45.7	3.5
07-15-80	.067	31.9	1.4	76.4	3.2	44.5	3.5
07-16-80	.067	32.0	1.4	76.8	3.2	44.8	3.5
07-17-80	.067	32.2	1.4	80.1	3.3	47.9	3.6
07-18-80	.067	32.4	1.4	78.0	3.3	45.6	3.5
07-21-80	.067	31.5	1.3	74.7	3.1	43.1	3.4
07-22-80	.067	31.5	1.3	73.8	3.1	42.3	3.4
07-23-80	.067	31.4	1.3	74.8	3.1	43.5	3.4
07-24-80	.067	31.8	1.3	74.7	3.1	42.9	3.4
07-25-80	.067	31.7	1.3	74.2	3.1	42.5	3.4
07-28-80	.067	31.8	1.3	69.3	2.9	37.5	3.2
07-29-80	.067	31.4	1.3	72.9	3.0	41.5	3.3
08-04-80	.545	258.4	3.8	297.9	4.5	39.5	5.9
08-05-80	.545	256.8	3.8	304.6	4.5	47.8	5.9
08-06-80	.582	276.9	4.0	331.0	4.7	54.1	6.2
08-07-80	.851	406.3	5.5	443.5	6.1	37.2	8.2
08-08-80	.851	407.4	5.5	431.6	6.0	24.2	8.2
08-11-80	.857	420.9	5.6	463.6	6.1	42.7	8.3
08-12-80	.869	424.8	5.7	467.0	6.2	42.2	8.4
08-13-80	.875	424.5	5.7	471.6	6.2	47.1	8.4
08-14-80	.875	416.0	5.6	462.8	6.2	46.9	8.4
08-15-80	.875	422.8	5.7	461.9	6.2	39.1	8.4

Table 5 (continued)

DATE	AIR FLOW 3 (M /S)	TOTAL WATER INFLOW (ML/MIN)	EXPERIMENTAL ERROR IN WATER INFLOW (ML/MIN)	TOTAL WATER OUTFLOW (ML/MIN)	EXPERIMENTAL ERROR IN WATER OUTFLOW (ML/MIN)	NET MOISTURE PICKUP (ML/MIN)	EXPERIMENTAL ERROR IN NET MOISTURE PICKUP (ML/MIN)
08-18-80	.912	436.7	5.9	474.8	6.3	38.2	8.6
08-19-80	.887	445.3	5.8	499.8	6.3	54.5	8.6
08-20-80	.887	430.0	5.7	464.0	6.2	34.0	8.4
08-21-80	.887	442.8	5.8	500.4	6.3	57.6	8.5
08-22-80	.887	437.2	5.7	479.4	6.2	42.3	8.4
08-25-80	.887	452.4	5.9	489.9	6.3	37.5	8.6
08-26-80	.887	439.9	5.8	500.5	6.3	60.5	8.6
08-27-80	.893	448.6	5.9	485.6	6.2	37.1	8.6
08-28-80	.893	447.4	5.8	500.8	6.3	53.4	8.6
08-29-80	.503	271.1	3.9	292.5	4.2	21.4	5.7
09-01-80	.509	244.2	3.7	293.9	4.2	49.8	5.6
09-02-80	.509	249.7	3.7	293.9	4.2	44.2	5.6
09-03-80	.509	247.6	3.7	291.8	4.2	44.2	5.6
09-04-80	.509	250.3	3.7	292.7	4.2	42.3	5.6
09-05-80	.509	253.5	3.8	303.9	4.3	50.5	5.7
09-08-80	.509	252.6	3.8	300.5	4.2	47.9	5.7
09-09-80	.503	256.2	3.8	300.3	4.2	44.1	5.7
09-10-80	.503	255.7	3.8	296.2	4.2	40.5	5.6
09-11-80	.503	254.2	3.8	304.6	4.3	50.4	5.7
09-12-80	.503	255.2	3.8	303.3	4.3	48.1	5.7
09-15-80	.497	255.9	3.8	302.1	4.2	46.2	5.7
09-16-80	.503	253.8	3.8	299.7	4.2	46.0	5.7
09-17-80	.509	262.6	3.8	307.5	4.3	44.9	5.8
09-18-80	.503	256.2	3.8	302.7	4.2	46.5	5.7
09-19-80	.509	257.6	3.8	308.2	4.3	50.6	5.7
09-22-80	.503	253.9	3.8	299.8	4.2	46.0	5.7

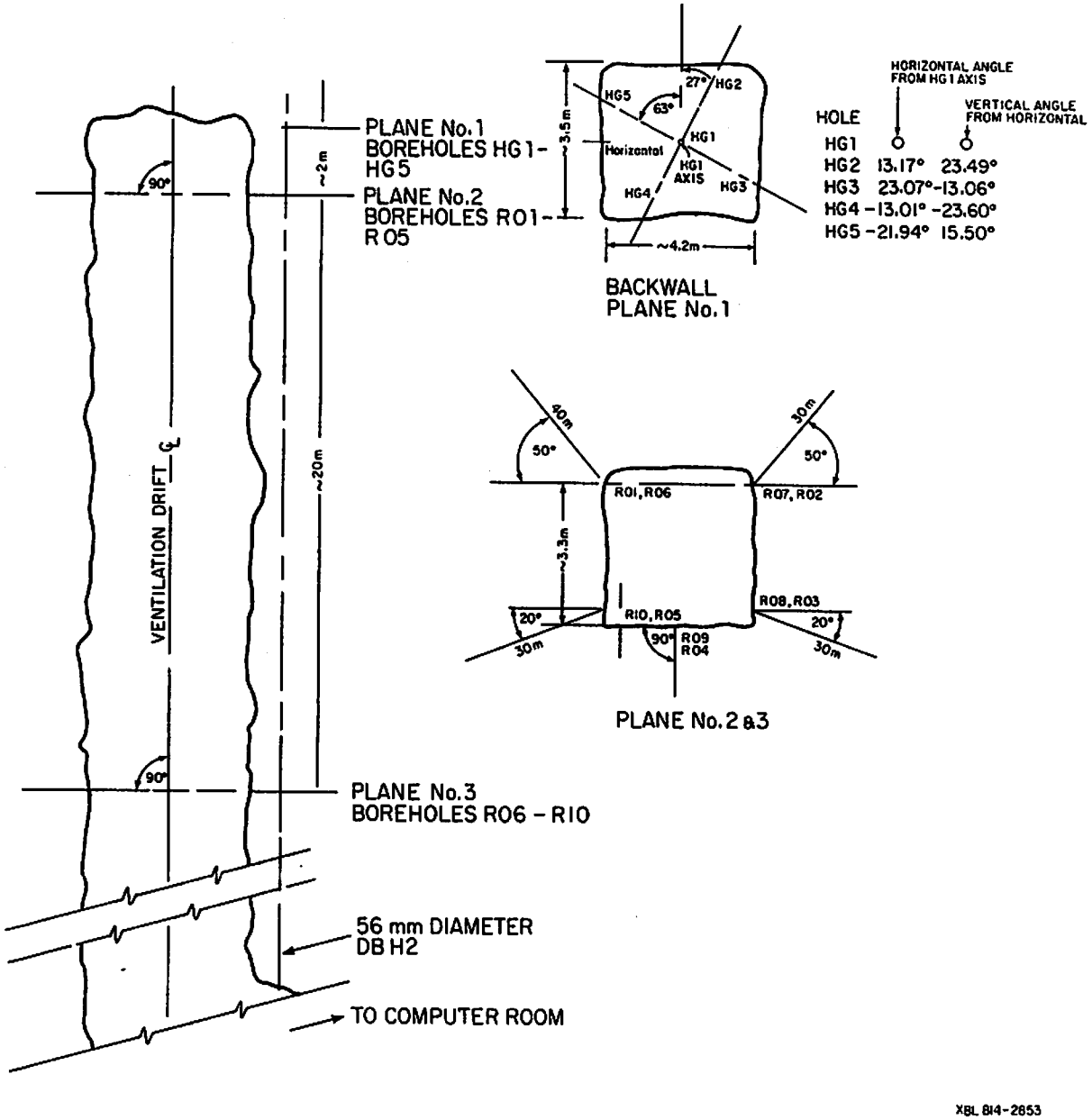

Fig. 17. Borehole layout in ventilation drift.

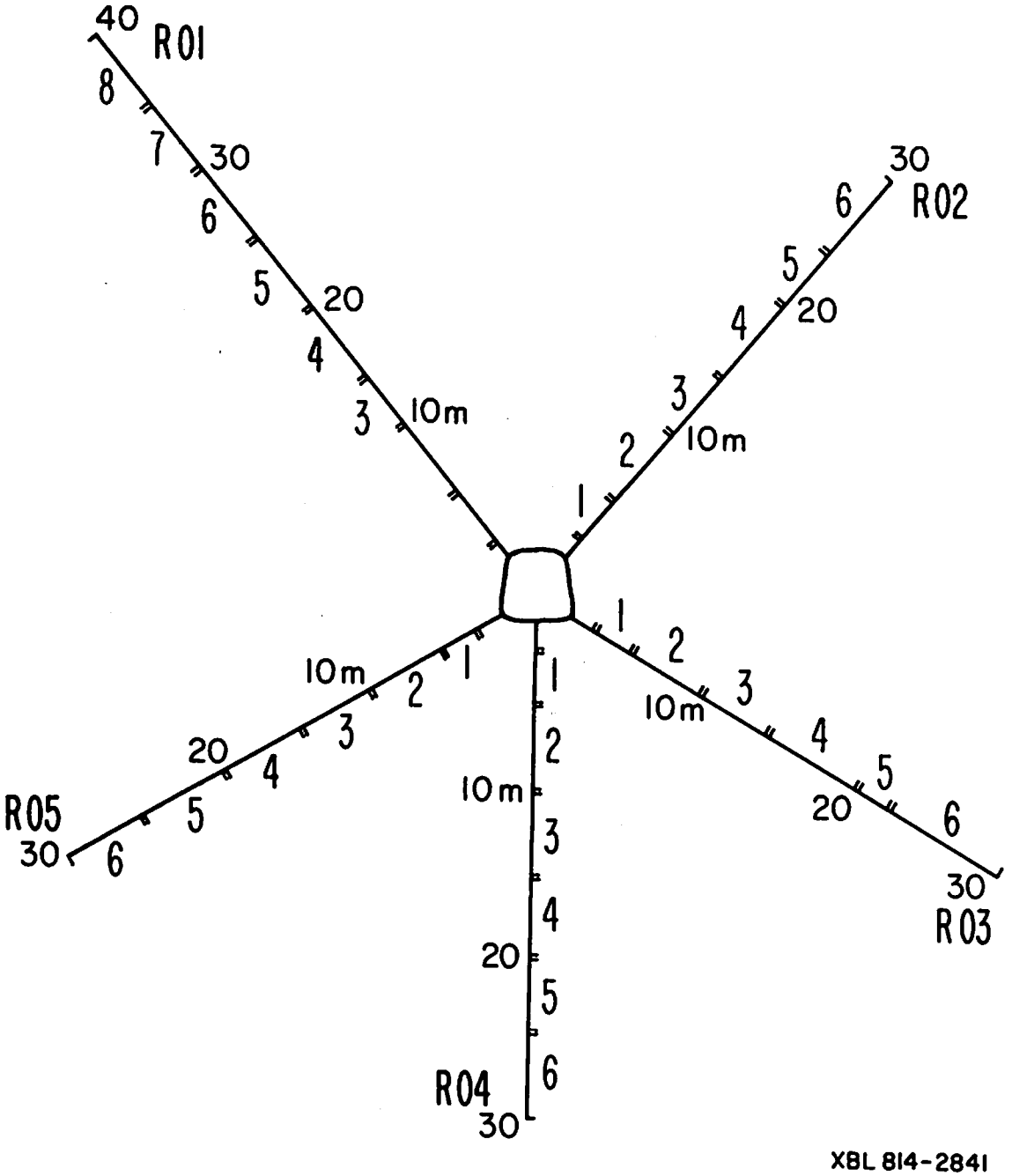

XBL 814-2841

Fig. 18. Cross-section of the ventilation drift showing boreholes R01 to R05.

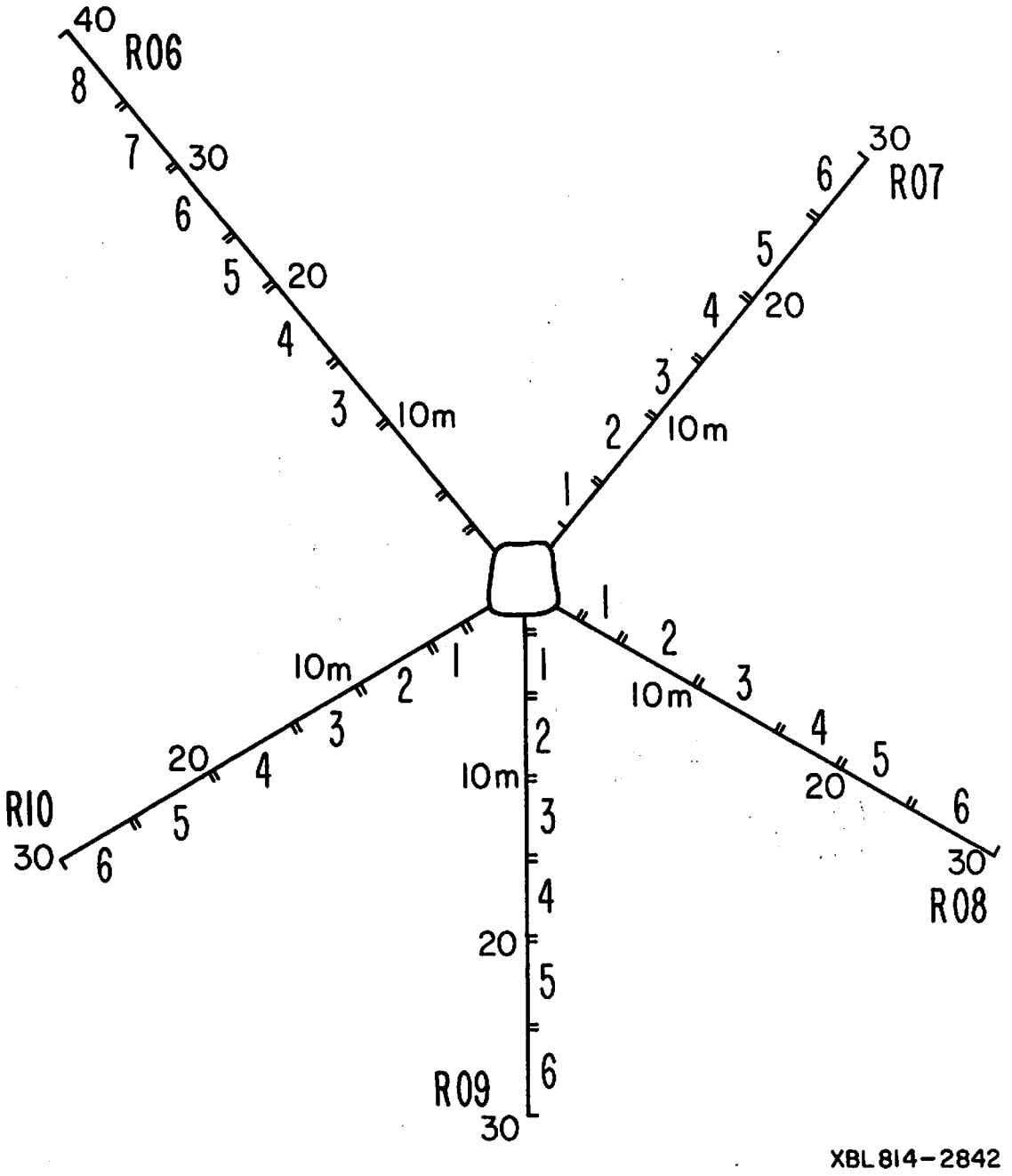

XBL814-2842

Fig. 19. Cross-section of the ventilation drift showing boreholes R06 to R10.

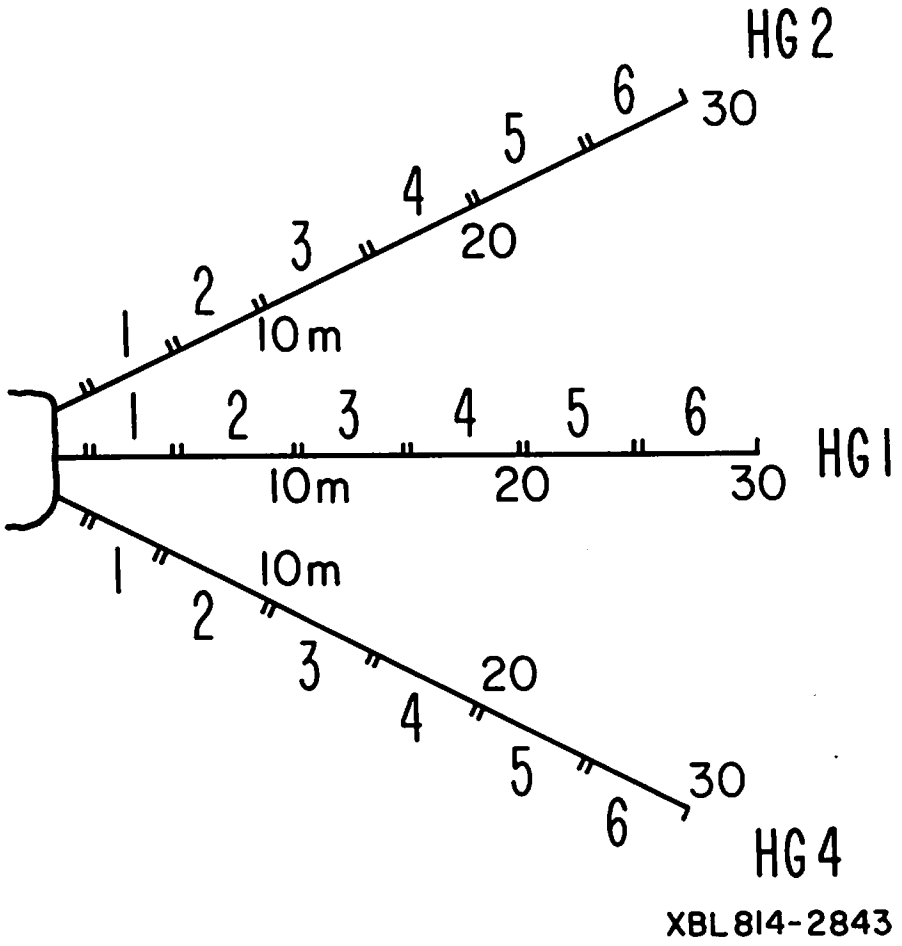

Fig. 20. Section showing boreholes HG1, HG2, and HG4.

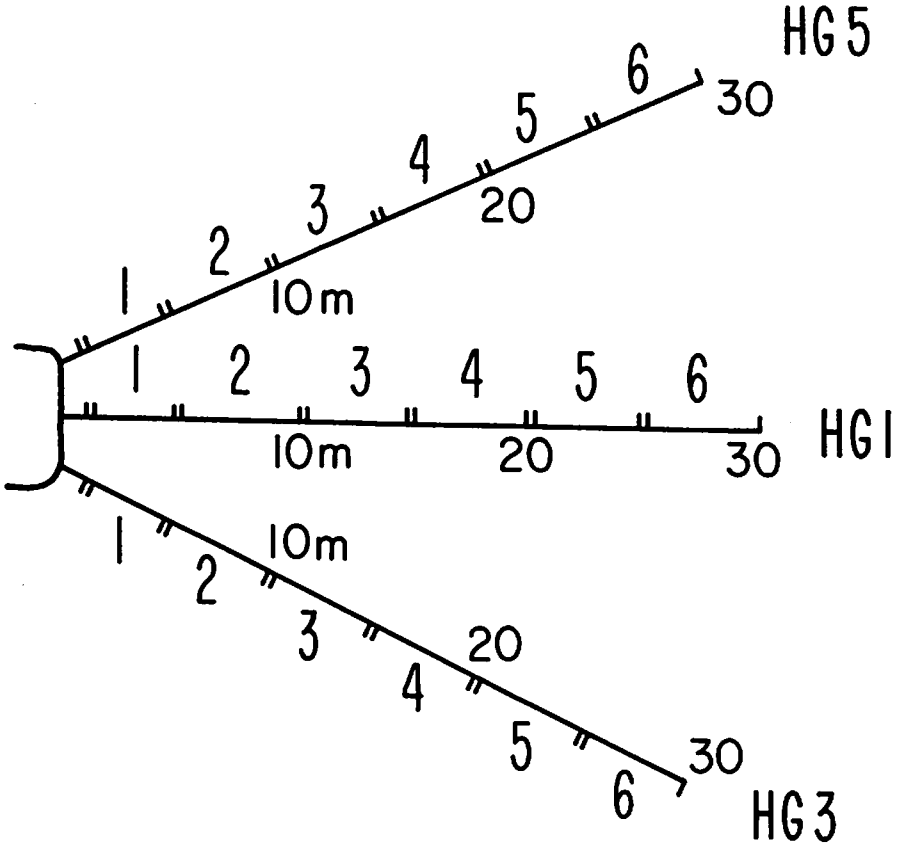

XBL 814-2844

Fig. 21. Section showing boreholes HG1, HG3 and HG5.

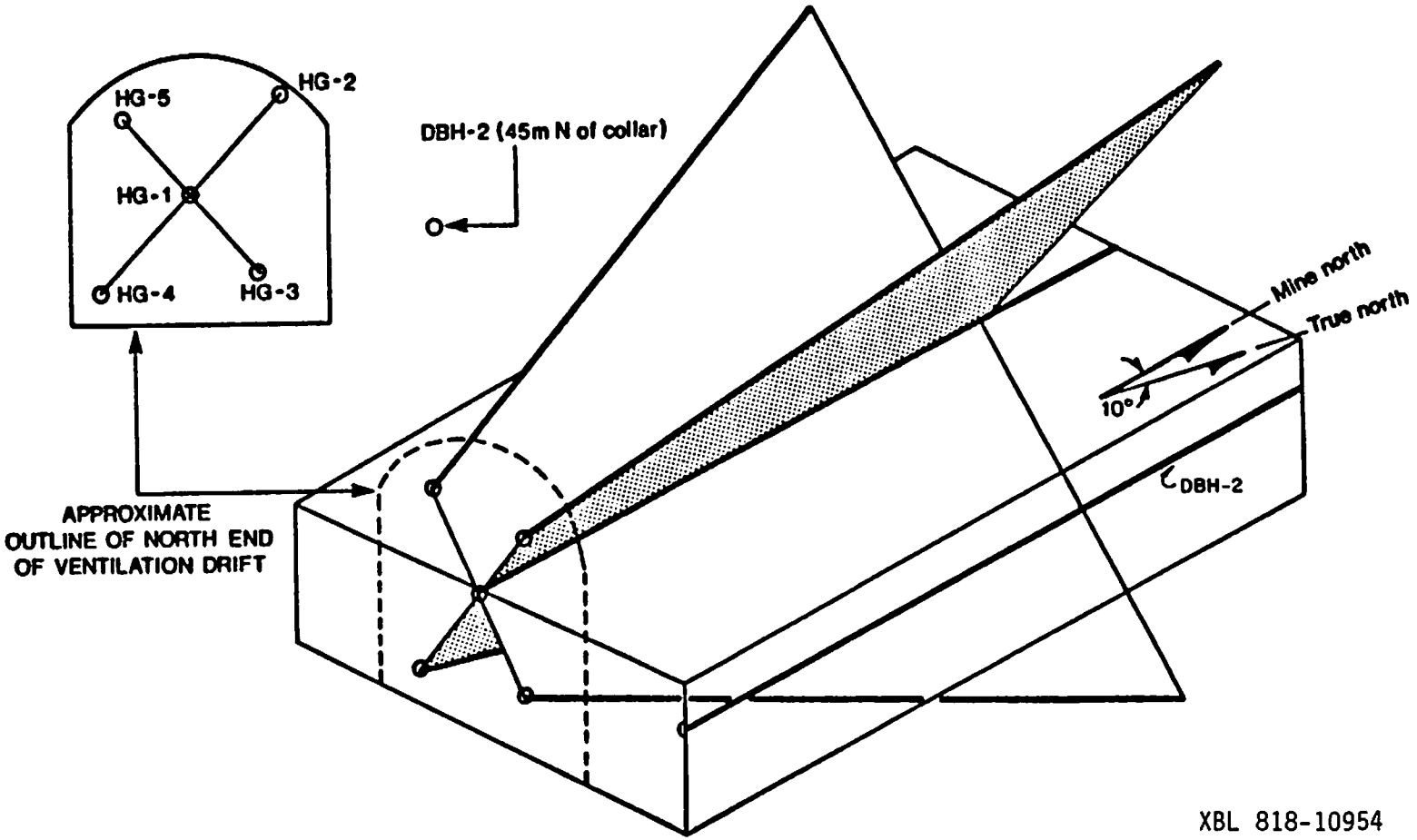

Fig. 22. Perspective view of the HG boreholes.

The pressure in each zone is measured by a gauge located in the control area outside the sealed room. The arrangement of the gauges for the R boreholes 1 to 5 is shown in Fig. 23. The same type of arrangement was used for the remaining R boreholes and HG boreholes.

4.4.2 DBH-2 Borehole

DBH-2 is a single, nearly horizontal, 56-mm-diameter, 97-m-long borehole. The vertical alignment and zone locations for DBH-2 are shown in Fig. 24. The five pressure gauges for DBH-2 were installed horizontally in the drift just above the hole collar at mine Z coordinate of 336.391 meters. Note that the Z coordinate increases with depth below surface in the mine coordinate system.

The original length of DBH-2 was 100 m, but the hole length was later shortened to 97.05 m when the computer room was enlarged to accommodate an air conditioning unit. The data shown in Fig. 24 all refer to the shorter hole, as it existed during the Macropermeability Experiment.

4.4.3 Determination of Hydraulic Head

The hydraulic head at a pressure port (h_p), is the sum of the pressure head P_z/γ_{wz}, and the elevation head Z_H. Thus:

$$h_p = \frac{P_z}{\gamma_{wz}} + Z_H \quad , \tag{8}$$

where P_z = Pressure at the port,

γ_{wz} = Specific weight of water at the port,

Z_H = Elevation head (vertical distance between the datum and the pressure port).

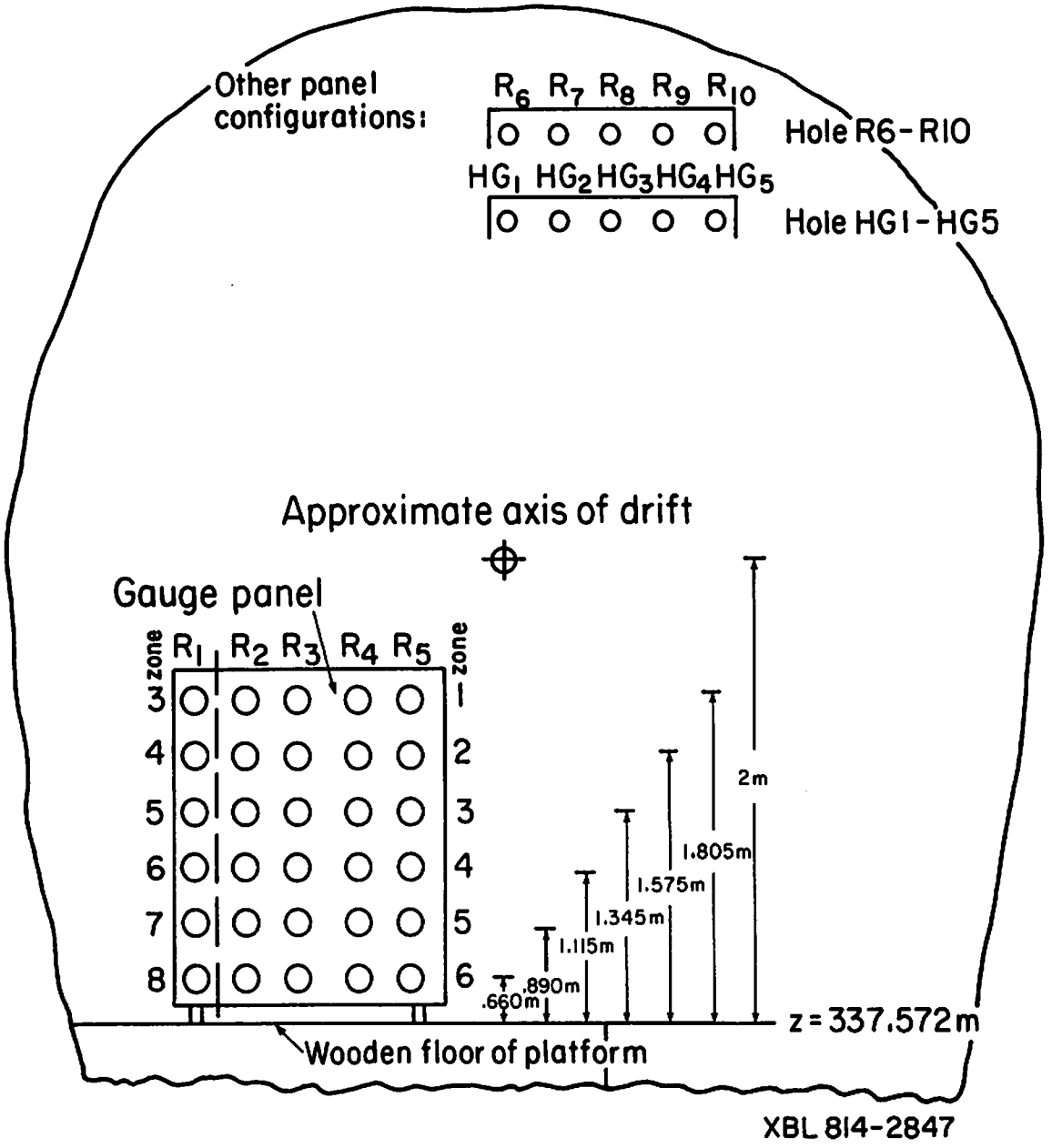

Fig. 23. Arrangement of water pressure gauges on the gauge panels.

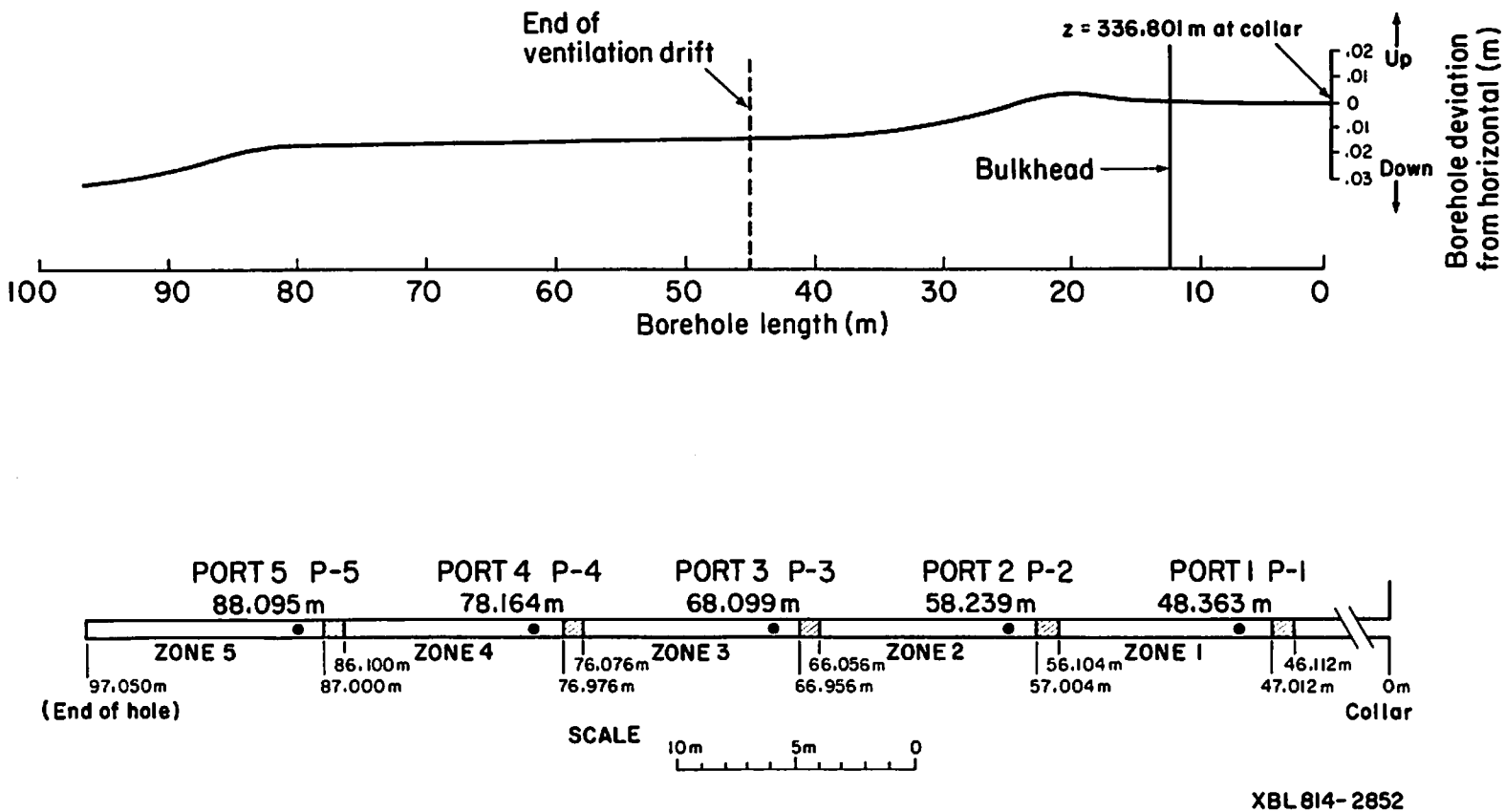

Fig. 24. Alignment and zone locations in borehole DBH-2.

The datum will be the approximate axis of the drift, which is defined as being 2 m above the floor of the drift at $Z = Z_D = 335.572$ m. The pressure throughout a zone will be assumed constant and equal to the pressure existing at the pressure port (see Fig. 6). To determine the pressure at the port (P_Z) from the pressure at the gauge (P_G), the following relationship from fluid statics is used:

$$P_Z = P_G + \int_{Z_G}^{Z_P} \gamma_W(Z)dZ \quad , \tag{9}$$

where Z_P = Z coordinate of pressure port in the zone (increases downward),

Z_G = Z coordinate of gauge in the drift.

Substituting Eq. (9) into Eq. (8), the hydraulic head is:

$$h_P = \frac{P_G}{\gamma_{WZ}} + \frac{\int_{Z_G}^{Z_P} \gamma_W(Z)dZ}{\gamma_{WZ}} + (Z_D - Z_P) \quad . \tag{10}$$

To simplify Eq. (10), the specific weight of water is assumed to be a constant equal to γ_H. The pressure in the zone then is:

$$P_Z = P_G + \gamma_H(Z_P - Z_G)$$

and the equation for h_S, the simplified hydraulic head in the zone, is:

$$h_S = \frac{P_G + \gamma_H(Z_P - Z_G)}{\gamma_H} + (Z_D - Z_P)$$

or

$$h_S = \frac{P_G}{\gamma_H} + (Z_D - Z_G) \quad . \tag{11}$$

4.5 Reduction of Temperature Data

Temperatures were measured with temperature transducers in the HG and R boreholes, in the temperature hole, and on the walls of the drift near selected boreholes. Model L temperature transducers (see Table 3) were installed in the HG and R boreholes as well as on the walls of the drift while model K transducers were utilized in the temperature hole. The voltage across the temperature transducer was read with a digital volt meter and converted to temperature.

4.5.1 Temperature Measurements in the HG and R Boreholes

Temperature transducers measured the temperature in each zone in the R and HG boreholes. The transducers were calibrated in the early stages of the experiment by assuming that the temperature of the rock mass was constant at 284 K. To determine the ambient temperature of the rock mass around the ventilation drift, the first temperature reading (i.e. prior to heating of the drift) from the 12 temperature holes in the floor of the adjacent time-scaled drift were used. Each hole had five thermocouples installed at different vertical elevations. The average initial temperature versus vertical distance from the floor of the drift is shown in Fig. 25. This figure shows that temperature changes were limited to the first 10 m below the floor of the drift, beyond which the temperature was constant at 10°C. Although these measurements were made approximately one year before the ventilation study began, the ambient rock temperature at this depth below the surface remains relatively constant.

Before the R and HG boreholes were plugged with packers for the Macro-permeability Experiment, they were freely draining the rock mass. Most of

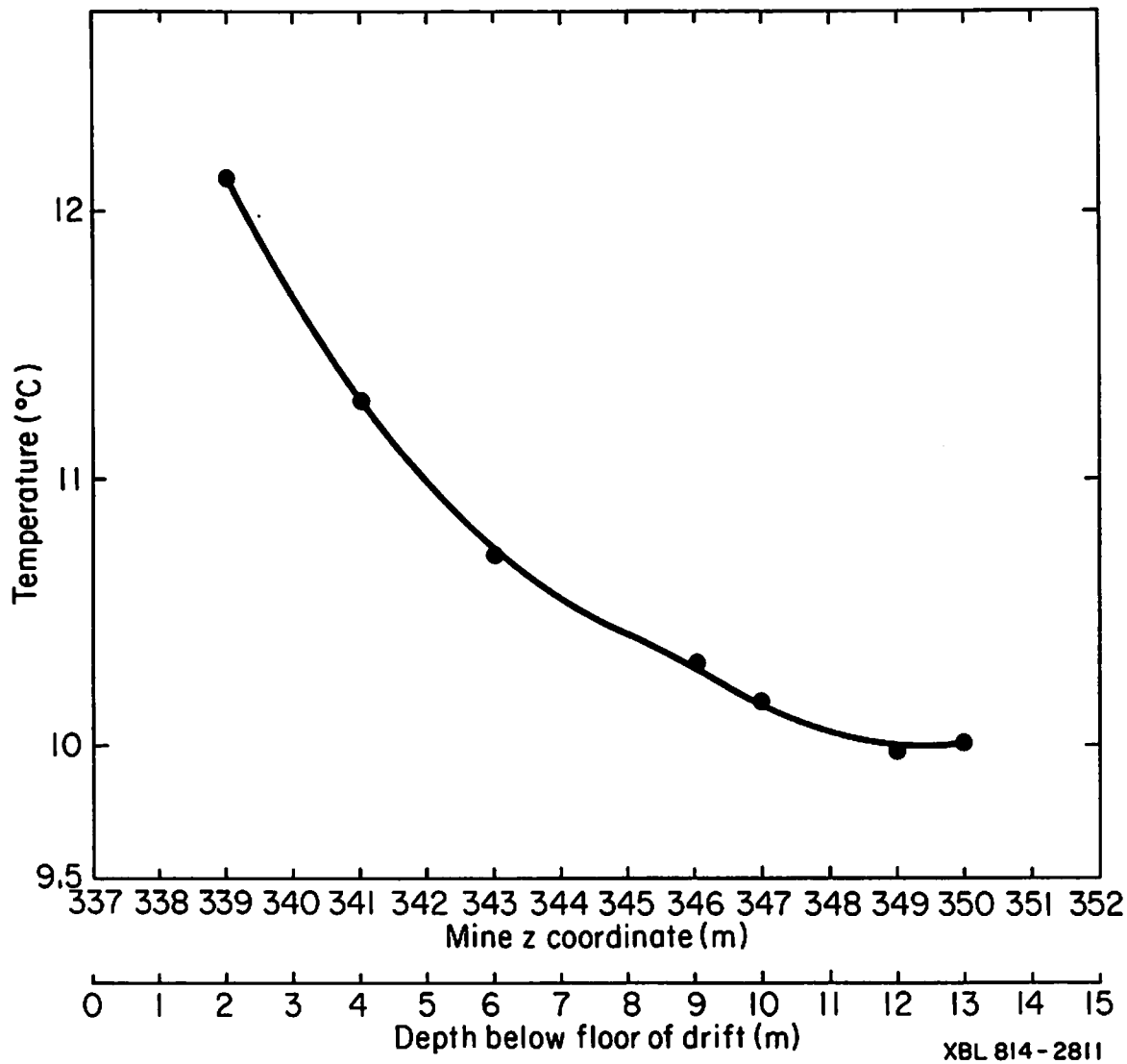

Fig. 25. Average temperature vs. vertical distance from floor in time-scale drift.

the flow of water into these boreholes occurred in the 20 m of hole farthest from the drift. Consequently, the water flowing from the boreholes was from an ambient rock temperature of 10°C and tended to maintain the rock around the boreholes in the first 10 m at this same temperature. Because of this, the water in the boreholes at the time of packer emplacement was assumed to be a constant temperature of 10°C or 283.2 K, instead of 284 K as originally calibrated. Thus, a correction of -0.8 K must be applied to all temperature measurements made in the R and HG boreholes. That is:

$$t = t_r - C_t \quad ,$$

where

t = actual temperature ,

t_r = measured temperature ,

C_t = 0.8.

4.5.2 Drift Wall Temperature Measurements

The same type of temperature transducers that were used in the R and HG boreholes were mounted flush to the wall of the drift at boreholes R01, R02, R04, R06, R07, R09, and the temperature hole, TG-1. The wall temperature sensors were calibrated with the reference mercury thermometer which was mounted on the gauge panel in the control area. At the time of calibration, this thermometer read 287.9 K in air.

4.5.3 Temperature Hole Measurements

The temperature hole sensors were calibrated in air at 286 K using a mercury thermometer of the same type as was used to calibrate the wall temperature sensors. A different model sensor was used in the temperature hole than was used for wall temperature measurements.

4.6 Example Computation of Hydraulic Conductivity

An example computation of hydraulic conductivity for the rock mass is provided to show how the reduced data can be used. For this example, a simple steady-state, radial-flow model will be used.

4.6.1 Analytical Model for Steady Radial Flow

The Thiem equation for steady radial flow to a long cylindrical opening in a homogeneous, isotropic porous medium is (Ferris et al. 1962, p. 91):

$$K = \frac{Q \ln\left(\frac{r_2}{r_1}\right)}{2\pi\, b\, (h_2 - h_1)} ,$$

where: K = coefficient of hydraulic conductivity,

Q = volumetric water flow rate into cylindrical opening,

r_1 and r_2 = radial distances from the drift axis to the first and second water head measuring points,

h_1 and h_2 = water head at radial distances r_1 and r_2,

b = length along axis of cylindrical opening over which seepage enters.

In applying the Thiem equation to the Macropermeability Experiment, Q is that portion of the total moisture inflow which occurs along the side walls of the drift, excluding inflow from the face. Water head is the head measured in the radial boreholes, and the length of the opening (b) is the length of the enclosed portion of the drift. Data obtained in the initial 20°C test will be used in this example.

4.6.2 Computation of Water Flow Rate

Total water inflow into the enclosed portion of the drift is determined from net moisture pickup data shown in Fig. 16. Moisture pickup and water

pressure data indicate that a state of relatively steady flow had been achieved for the period 26 February through 21 March 1980, during the initial 20°C temperature test. Net moisture pick up varied irregularly during this period about a mean value of 50.5 ml/min with a standard deviation of 3.1 ml/min. A linear regression applied to check for trends gave a slope of -0.014 ml/min per day, which is considered insignificant. For purposes of computation, a rounded value of 50 ml/min total water inflow will be used.

An analysis of flow into the drift was conducted using Fourier techniques to model measured boundary conditions around both the side walls and the face. This analysis showed that if the medium is considered to be homogeneous and isotropic, approximately 20% of total inflow would occur at the face, while the remaining 80% would occur through the side walls. This proportion would indicate that of the 50 ml/min total measured water inflow from all surfaces, approximately 80% or 40 ml/min, entered through the side walls.

4.6.3 Computation of Hydraulic Head

Computation of hydraulic head from the borehole pressure data is explained in Section 4.4. For purposes of this example, the specific weight of water will be assumed constant, and the simplified hydraulic head will be determined for a water temperature of 12°C using Eq. (11). All heads will be referenced to the approximate axis of the drift, as shown on Fig. 23.

Examples of computed hydraulic heads are given in Table 6 for data of 25 July 1980. Similar computations for the pressure data of 21 March 1980 were used to analyze the results of the initial 20°C test, this date being the last day of the test. Only the R-hole pressure data are used in this

Table 6. Error in simplified hydraulic head for selected zones on 25 July 1980.

Borehole	Zone	Actual Head h (m)	Simplified Head h_s(m)	Error (%)	Correction C_h(m)
RO4	1	100.84	100.68	0.16	0.16
RO4	3	107.98	108.02	-0.04	-0.04
RO4	6	109.72	109.77	-0.05	-0.05
RO7	1	73.52	73.36	0.22	0.16
RO7	3	96.58	96.55	0.03	0.03
RO7	5	121.93	121.90	0.02	0.03
HG1	1	85.45	85.27	0.21	0.18
HG1	3	137.22	137.22	0	0
HG1	6	142.16	142.16	0	0
DBH-2	1	137.58	137.52	0.04	0.06
DBH-2	5	160.70	160.73	-0.02	-0.03

radial flow analysis.

4.6.4 Computation of Hydraulic Conductivity

If assumptions inherent in the Thiem equation such as homogeneity and isotropy are met in the field, a plot of hydraulic head against the logarithm of the radius of the measurement point will produce a straight line with a slope proportional to K. All usable data from the 20°C test have been plotted in this manner in Fig. 26. The number of the radial borehole is used to plot the data point, and the radial distance is taken as the midpoint of the measurement zone. A linear regression analysis of the data points from each individual borehole yielded straight line correlation coefficients ranging from 0.64 for R05 to 0.98 for R04. Eight of the ten radial boreholes yielded correlation coefficients greater than 0.8. The best fit lines for individual boreholes with coefficients of 0.9 or better (R01, R04, R06, R07 and R08) are shown on Fig. 26. This degree of linearity exceeded our expectations, as we had anticipated that the fractured rock mass would behave much more irregularly.

An advantage of using an analytical approach such as the Thiem equation is that it permits graphical display and weighting of the array of data. It was necessary to weight the head data when computing average values because the data were taken at varying radial distances from the drift and because the boreholes were not symmetrically located along the length of the drift. Six weighted average data points were computed, representing weighted average head values for zones 1 through 6. These average values are plotted as small open circles in Fig. 26. Linear regression to these points yielded a straight line with a slope of 73.8 m per $\log_{10}$ cycle and a correlation coefficient of 0.98.

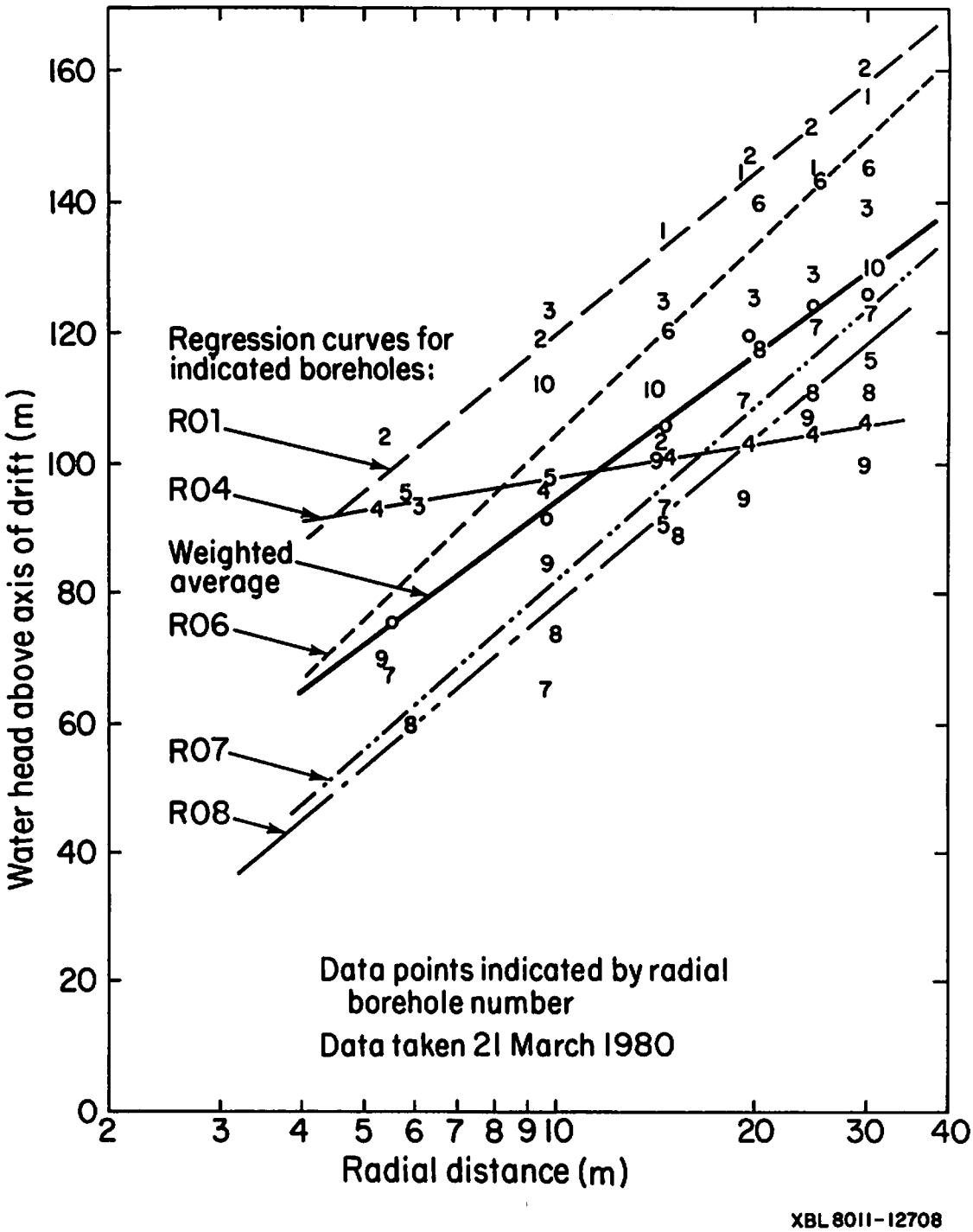

Fig. 26. Distance-drawdown plot of initial 20° test results.

To compute the average hydraulic conductivity, the following parameters are used:

volumetric water flow rate (Q) = 40 ml/min

length of drift (b) = 33 m

ratio $(h_2 - h_1)/\log_{10}(r_2/r_i)$ = 73.8 m

Inserting these values into the Thiem equation and including conversion factors, we compute the equivalent porous medium permeability of the rock mass for radial flow:

$$K = \frac{Q}{2\pi b}\left(\frac{\ln \frac{r_2}{r_1}}{h_2 - h_1}\right) = \frac{(40)\ (10^{-6})}{(2\pi)(33)(60)}\left(\frac{2.3}{73.8}\right)$$

$$K = 1.0 \times 10^{-10}\ \text{m/s}$$

The best fit lines for both individual borehole data and weighted average data in Fig. 26 project a higher hydraulic head at the radial distance corresponding to the wall of the drift than actually existed at the wall. For example, the weighted average line predicts a head of about 50 m at a radius of 2 to 2.5 m (the radius of the drift), while the actual head at the wall should be close to zero, because the head datum was taken as the axis of the drift. This abnormally high projected value indicates that the head loss between the zone 1 measurements and the drift is greater than would be expected from a homogeneous medium. It also indicates that the permeability of the rock close to the drift wall may be less than the average permeability of the rock mass; this finding was the reason that geochemical analysis of samples from the drift walls were added to the experiment.

5.0 ERROR AND SENSITIVITY ANALYSIS

This section is presented in five parts. Section 5.1 discusses the approach to error analysis that was applied to the Macropermeability Experiment data. Section 5.2 describes the error analysis of the ventilation data. Section 5.3 includes a sensitivity analysis of the ventilation data that helps to account for the change in magnitude of the error for different temperature tests. Section 5.4 describes the error analysis of the pressure data, and Section 5.5 the error analysis for the temperature data.

5.1 Theory of Error Analysis

5.1.1 Types of Errors

Figure 27 illustrates a classification of different types of errors that can occur in an experiment: (1) determinant, (2) indeterminant, and (3) illegitimate. Determinant errors are those that can be evaluated by a theoretical or experimental procedure; indeterminant errors cannot be determined by any available analysis within the constraints of the experiment; and illegitimate errors are mistakes, such as errors in computation, transcription, and experimental procedure.

Determinant errors may be subdivided into experimental and systematic errors. Experimental errors are random and irregular. Systematic errors are constant or vary regularly. Systematic and illegitimate errors can be identified and reduced or eliminated by careful experimental techniques. Every effort was made to eliminate systematic and illegitimate errors from the Macropermeability Experiment, and when such errors were observed, the appropriate corrections were made. Consequently the treatment of experimental errors will be of prime concern in this report.

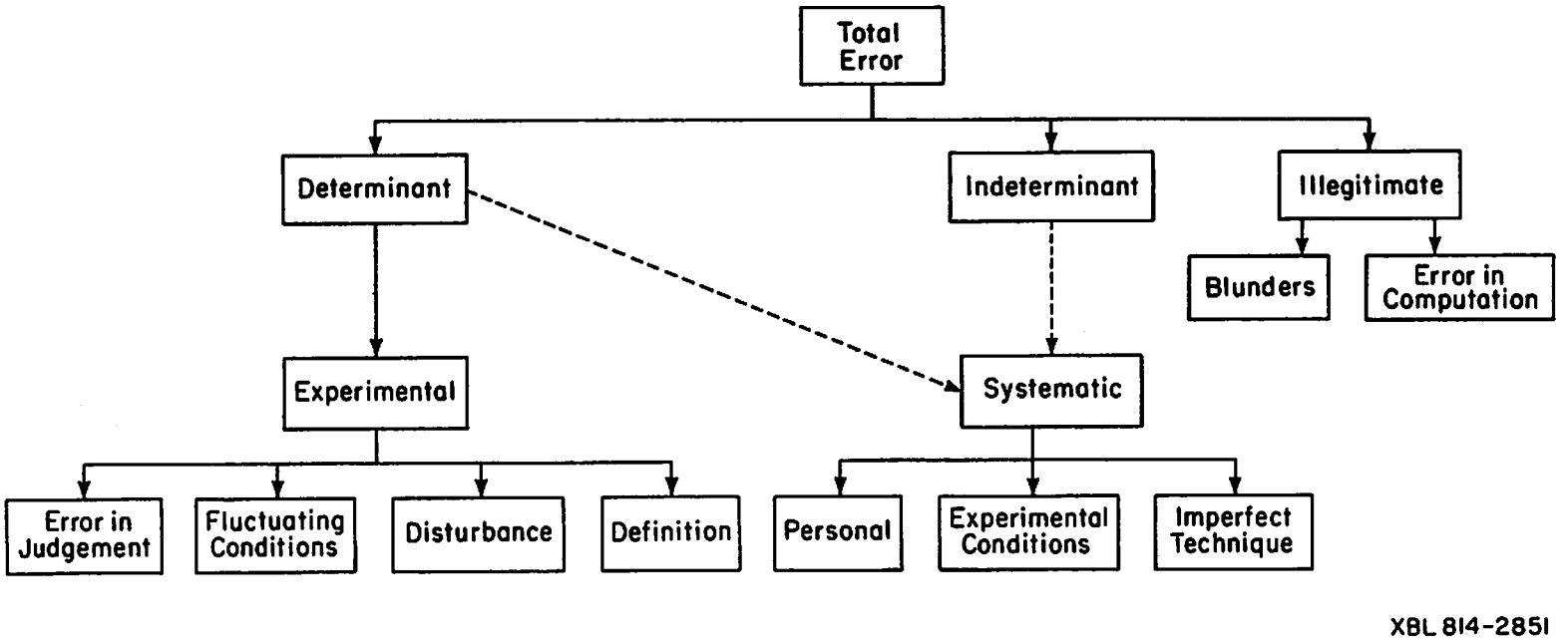

Fig. 27. Types of errors occurring in experiments.

5.1.2 Principles of Experimental Error Analysis

Experimental error results from deviations in measurement that occur due to random, irregular fluctuations in instrument and reader accuracy. An example is illustrated in Fig. 28, which shows the fluctuations that typically occur in repeated measurements of the same parameter with a constant true value of μ. The theoretical basis for determining experimental error will be presented in this section.

5.1.2.1 Use of the Gaussian Error Curve for Experimental Error. The The probability (Pr) of a measured quantity x being in the range $a < x < b$ is represented by the Gaussian (normal) error curve for experimental error as:

$$\Pr(a < x < b) = \int_a^b \frac{1}{\sqrt{2\pi\sigma}} \exp\left(-\frac{(t-\mu)^2}{2\sigma^2}\right) dt = \int_a^b p(t)dt ,$$

where μ = true value,

σ^2 = variance,

$p(t)$ = normal density function.

For further information on the use of the Gaussian error curve, the reader is referred to Topping (1962).

The field measurements made for the Macropermeability Experiment are all of the type for which Gaussian error distributions have been found to apply; that is, they are all measurements of parameters for which a "true value" is assumed to exist at the particular time and place of measurement. If the measurements are unbiased, then it is also reasonable to assume that if a sufficient number of measurements could be made during the short time that the "true value" is stable, the errors would be normally distributed. In view of this reasoning and of the successes generally reported for

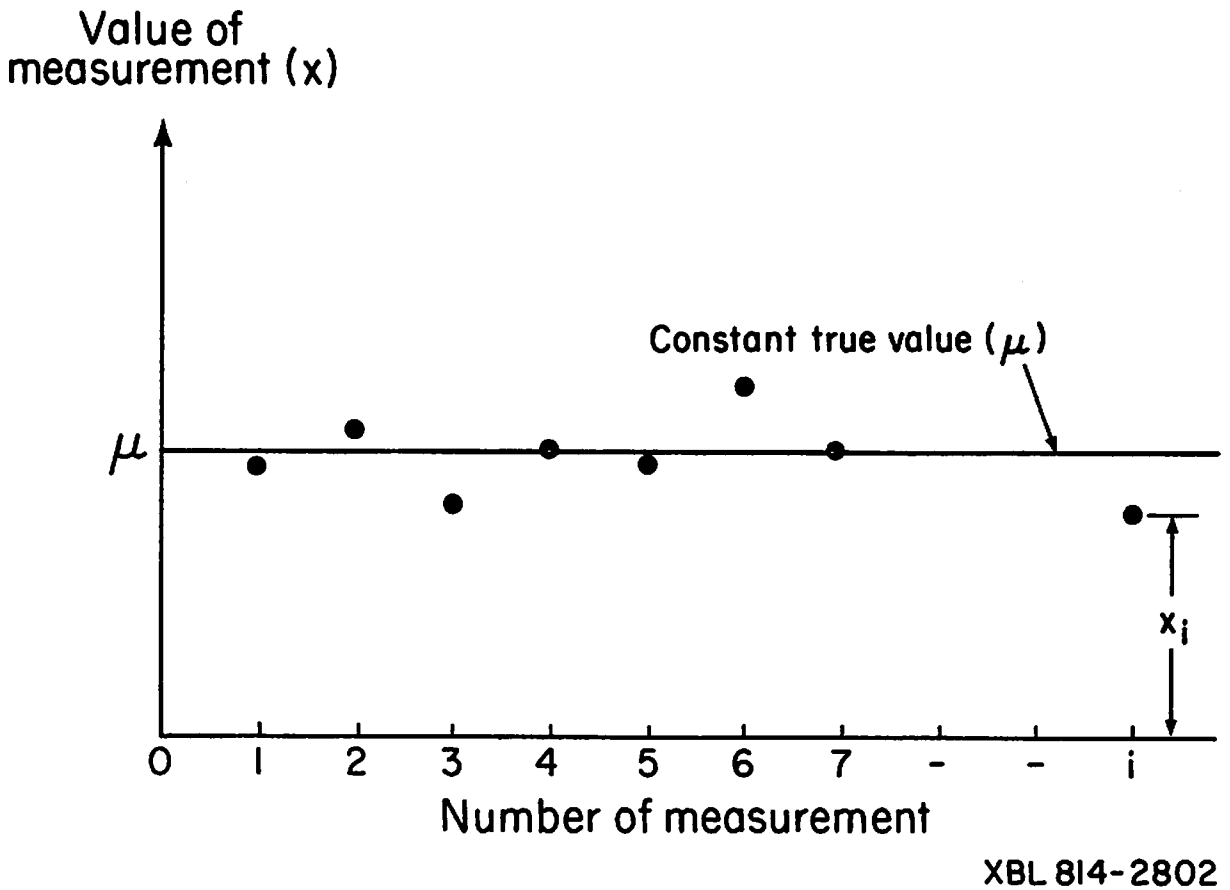

Fig. 28. Hypothetical results of repeated measurements of a constant parameter.

treatment of experimental error by Gaussian techniques, it was decided to base experimental error analysis on the Gaussian error curve.

5.1.2.2 Properties of the Gaussian Error Curve. The normal density function, based on an infinite number of observations, is a symmetric curve about the true value, μ. This curve is completely characterized by the parameters of true value (μ) and variance (σ^2). The value of μ identifies the center of mass of the distribution, and the value of σ^2 indicates the amount of dispersion of the distribution about μ. As σ^2 increases, the error curve flattens and spreads out, as shown in Fig. 29.

The area under the error curve between any two given values of λ represents the probability of observing a value of λ which lies between those two values. Thus the total area under the Gaussian error curve is 1. The area between $\mu - \sigma$ and $\mu + \sigma$ is 0.6826. Therefore any value of λ has a probability of 0.6826 of falling between $\pm\ \sigma$ of the true value, as illustrated in Fig. 30. The standard error is defined as the value of σ, thus the probability of a measurement falling within one standard error of the mean or "true" value is also 0.6826. The terms standard error and experimental error will be used synonymously in this report.

5.1.2.3 Estimates of Variance and True Value. The Gaussian error curve is theoretically based on a population consisting of an infinite number of measurements of a given constant parameter. Since one cannot obtain an infinite number of measurements, one will have to estimate the true value (μ) and variance (σ^2) based on a finite sample. The true value will be assumed to equal its uniformly minimum variance unbiased estimate, which for a normal distribution is simply the arithmetic mean of the sample values:

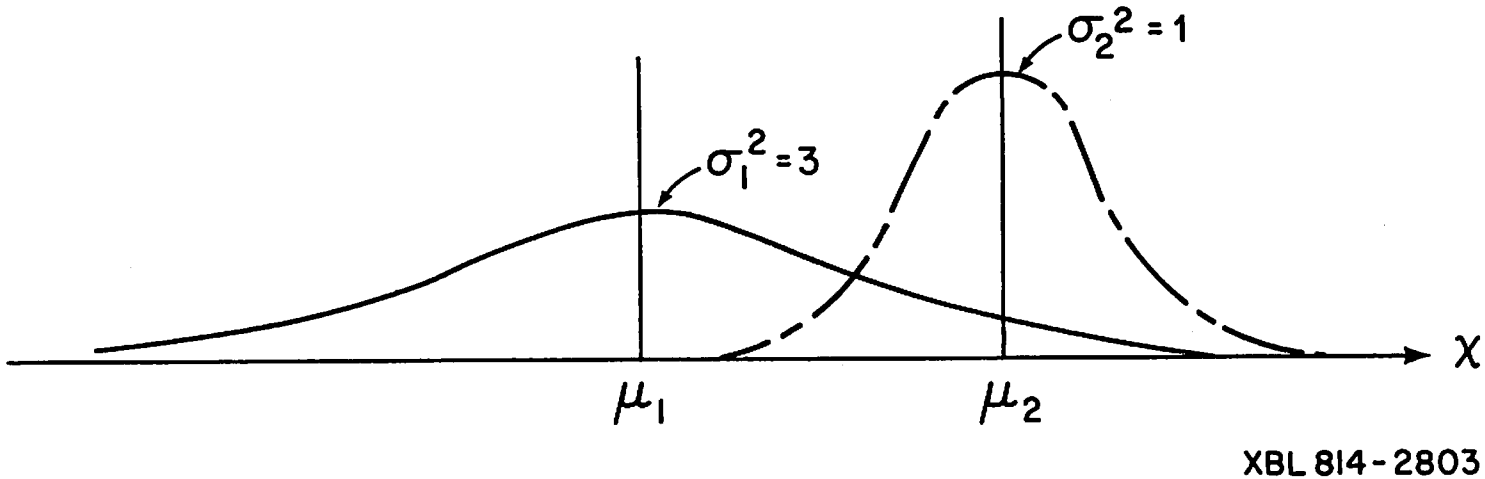

Fig. 29. Examples of two Gaussian error curves with different values of mean (μ) and variance (σ^2).

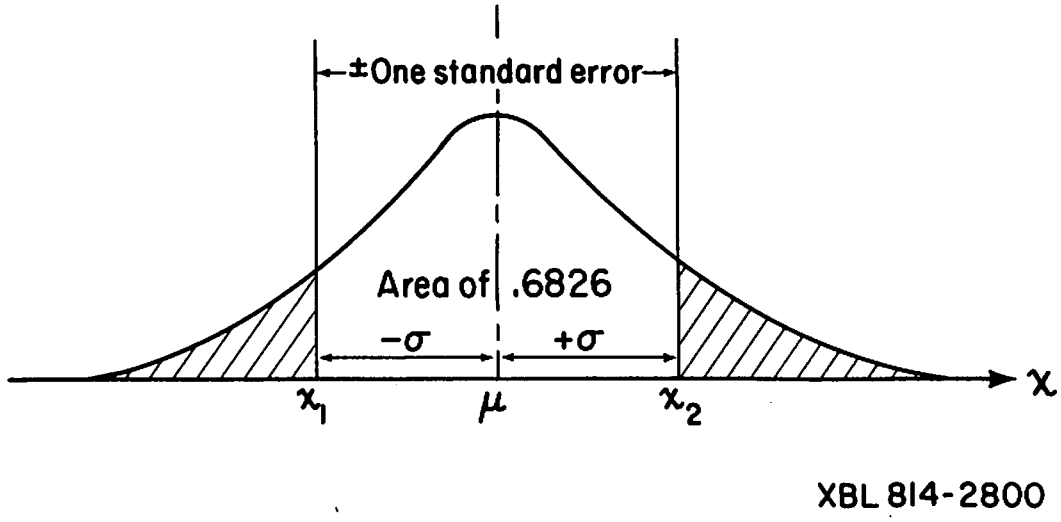

Fig. 30. Illustration of standard error.

$$\bar{x} = \frac{\Sigma x_i}{n} \quad ,$$

where the x_i are the individual observations. The uniformly minimum variance unbiased estimate of the variance is:

$$\hat{\sigma}^2 = \frac{1}{n-1} \Sigma (x_i - \bar{x})^2 \quad .$$

This estimate of σ is defined as the standard deviation S. Thus:

$$S = \sqrt{\hat{s}^2} = \sqrt{\frac{1}{n-1} S(x_i - \bar{x})^2} \quad .$$

It can be shown that as n increases, both S and $\bar{x}$ become better estimates of σ and μ respectively.

5.1.2.4 Experimental Error in Functions of Observed Measurements. The experimental error (Δx) resulting from the measurement of x represents the probability of approximately 0.68 that any observation will fall within $\pm\Delta x$ of the true value. If a quantity Z is a function of $x_1, x_2, \ldots, x_n$ measured variables (i.e. $Z = f(x_1, x_2, \ldots, x_n)$, each with an experimental error $\Delta x_1, \Delta x_2, \ldots, \Delta x_n$ respectively, it can be shown (Beers, 1957) that the experimental error in Z is:

$$\Delta Z = \sqrt{\left(\frac{\partial f}{\partial x_1} \Delta x_1\right)^2 + \left(\frac{\partial f}{\partial x_2} \Delta x_2\right)^2 + \ldots + \left(\frac{\partial f}{\partial x_n} \Delta x_n\right)^2} \quad . \qquad (12)$$

This principle will be illustrated for four mathematical operations.

1) Let $Z = x_1 + x_2$. Then $\Delta Z = \sqrt{(\Delta x_1)^2 + (\Delta x_2)^2}$
2) Let $Z = Kx_1 - x_2$. Then $\Delta Z = \sqrt{(K\Delta x_1)^2 + (\Delta x_2)^2}$
3) Let $Z = ax^b$. Then $\Delta Z = abx^{b-1}\,\Delta x$
4) Let $Z = x_1 x_2$. Then $\Delta Z = \sqrt{(x_2\,\Delta x_1)^2 + (x_1\,\Delta x_2)^2}$

5.1.3 Application of Error Theory to Macropermeability Experiment Data

As an example of the application of Gaussian error analysis to the Stripa data, the experimental error in the determination of the density of dry air will be presented. This parameter is necessary in the computation of the net moisture pickup.

The density of dry air, $\rho_{m(app)}$, is calculated as:

$$\rho_{m(app)} = \frac{1}{R_a} \frac{P - e}{t_d} ,$$

where P = pressure,

e = vapor pressure of water,

t_d = dry bulb temperature,

R_a = gas constant for air.

To calculate the experimental error in $\rho_{m(app)}$, $\Delta\rho_{m(app)}$, the following partial derivatives must be evaluated: (1) $\frac{\partial\rho_{m(app)}}{\partial p}$, (2) $\frac{\partial\rho_{m(app)}}{\partial e}$, and (3) $\frac{\partial\rho_{m(app)}}{\partial t_d}$

Now:

$$\frac{\partial\rho_{m(app)}}{\partial p} = \frac{1}{R_a t_d} ,$$

$$\frac{\partial\rho_{m(app)}}{\partial e} = - \frac{1}{R_a t_d} ,$$

$$\frac{\partial\rho_{m(app)}}{\partial t_d} = - \frac{(P - e)}{R_a t_d^2} .$$

Therefore

$$\Delta\rho_{m(app)} = \frac{1}{R_a t_d}\sqrt{\Delta P^2 + \Delta e^2 + \left(\frac{(P-e)}{t_d}\right)^2 \Delta t_d^{\,2}} \quad .$$

Thus, the experimental error resulting from the determination of the density of dry air can be ascertained for a specific condition (P, e, t_d) if the experimental errors for the individual measurements of P, e, and t_d are known.

The experimental error for individual measurements made during the course of the Macropermeability Experiment is generally based on the manufacturer's specifications for instrument accuracy (Table 3). The major exception is the air flow monitoring system, which was calibrated in the field without reference to the manufacturer's specifications.

5.2 Error Analysis of Net Moisture Pickup Data

The experimental error in net moisture pickup data will be determined using the Gaussian error analysis methodology set forth in Section 5.1. Experimental error is computed following the same stepwise procedure used in Section 4.3 and Appendix A. The application of this procedure is illustrated graphically in Fig. 31. From this figure it is evident that experimental error in net moisture pickup originates from errors in measuring the fundamental input parameters: (1) wet bulb temperatures, (2) dry bulb temperatures, (3) air pressures, and (4) air flow rate.

The experimental error Δf for a function f of x, y, z (i.e., f(x,y,z)) with experimental errors for x, y and z of Δx, Δy, and Δz, respectively, is given by Eq. (12) [Section 5.1.2.4] as:

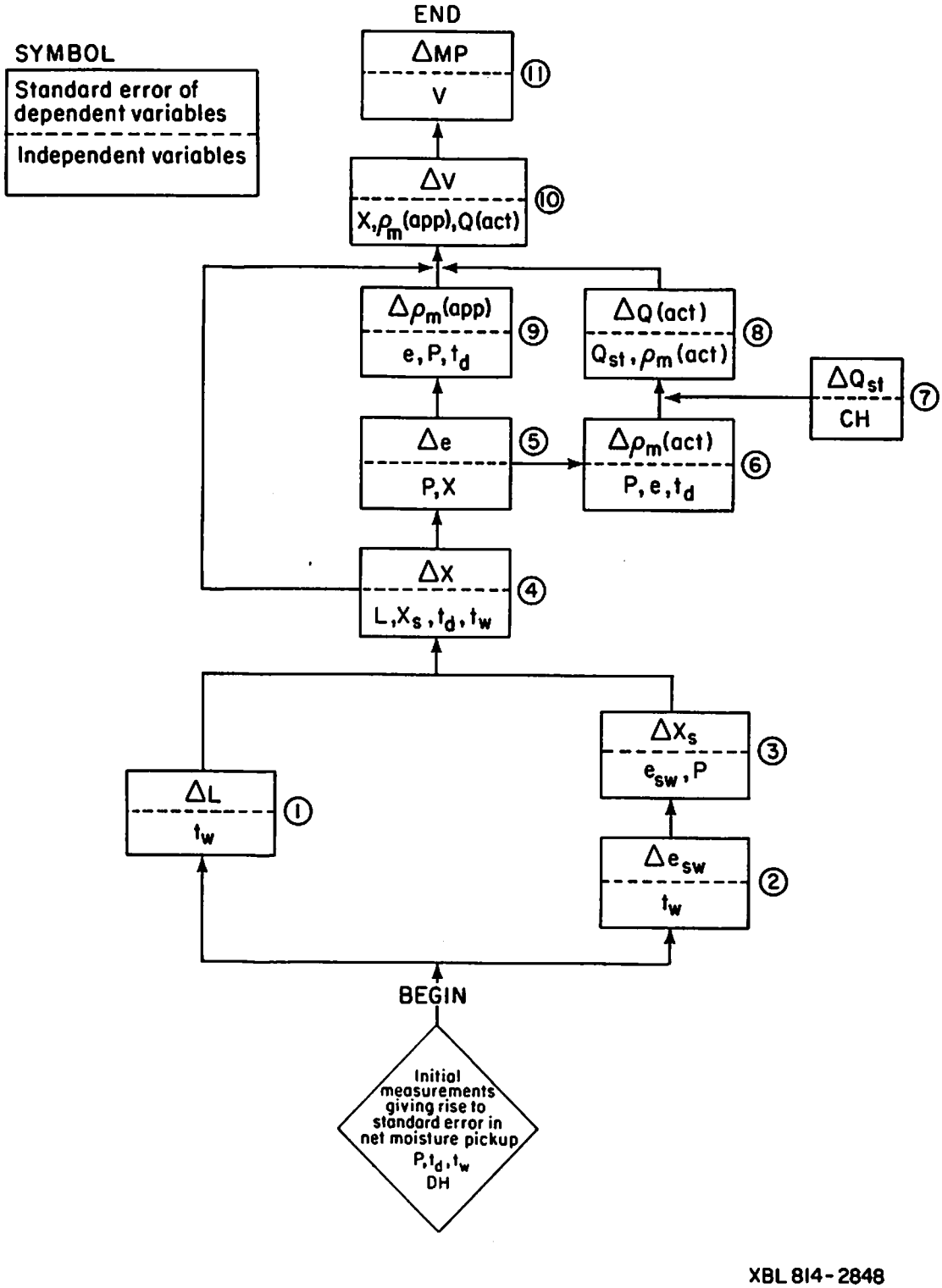

Fig. 31. Flow chart for determination of experimental error in net moisture pickup.

$$\Delta f = \sqrt{\frac{\partial f}{\partial x}\Delta x^2 + \frac{\partial f}{\partial y}\Delta y^2 + \frac{\partial f}{\partial z}\Delta z^2} \quad .$$

The experimental error at all steps of Fig. 31 can be determined from Eq. (12) except for Step 7, computation of standard air flow rate. Experimental error in the standard air flow (Q_{st}) is a special case because it is related to the goodness of fit of the regression curve of Q_{st} vs. the chart reading (CH). The methods used to evaluate experimental error for the net moisture pickup data are described below.

5.2.1 Experimental Error in Regression Analysis For Air Flow Rate

The air flow calibration curves for the test periods August 1979 to 22 April 1980 (pre-experimental and initial 20°C test) and 2 August 1980 to 22 September 1980 (20°C cooldown test) are linear (Figs. A1 and A4 respectively). The regression curves for the test periods 14 May 1980 to 27 May 1980 and 28 May 1980 to 29 July 1980 (30°C and 45°C tests; Figs. A2 and A3, respectively) are nonlinear. An estimate of the experimental error (S_{yo}) for any particular value of the chart reading (CH_o) for the linear models is given by (Huntsberger and Billingsley, 1977, p. 275):

$$S_{yo} = S_{y/x}\sqrt{1 + \frac{1}{n} + \frac{(CH_o - \overline{CH})^2}{\sum_i^n (CH_i - \overline{CH})^2}} \quad , \tag{13}$$

where $S_{y/x} = \sqrt{\frac{1}{n-2}\sum_i^n (Yi - \hat{Y}i)^2}$,

Yi = the ith actual measurement of the standard air flow during the calibration test,

$\hat{Y}i$ = regression estimate of the ith measurement,

n = number of measurements,

$\overline{CH} = \frac{\Sigma CH_i}{n} \equiv$ mean value of all chart readings made during the calibration test.

According to Eq. (13), the experimental error increases as the chart reading (CH_0) deviates farther from the mean chart reading ($\overline{CH}$). For the test period August 1979 to 22 April 1980 experimental error is given by:

$$S_{yo} = 0.00760 \sqrt{1 + \frac{1}{7} + \frac{(CH_0 - 49.11)^2}{4346.47}} \quad .$$

Similarly, for the test period 4 August 1980 to 22 September 1980, experimental error is given by:

$$S_{yo} = 0.00426 \sqrt{1 + \frac{1}{11} + \frac{(CH_0 - 35.41)^2}{3425.91}} \quad .$$

Regression error for the nonlinear curves will be assumed to equal the maximum error obtained from Eq. (13) for the range encompassing at least 70% of all standard air flows measured during the particular test period. For example, during the test period 28 May 1980 to 29 July 1980 over 70% of the standard air flows fell within the range of CH = 70 to CH = 80. Using the data from the calibration test, the experimental error is estimated to be:

$$S_{yo} = 0.00256 \sqrt{1 + \frac{1}{10} + \frac{(80-68.6)^2}{5990.40}} = 0.00271 \ m^3/s \quad .$$

For the test period 4 May 1980 to 27 May 1980, S_{yo} was estimated to be 0.00237 m^3/s.

5.2.2 Experimental Error in Air Temperature and Pressure Data

The experimental errors for the input parameters of air temperature and air pressure were taken from the manufacturer's specifications for the measurement instruments. The specified accuracy of each instrument, as listed in Table 3, was assumed to be equal to the standard error of measurement. In general, these errors are assumed to be similar in magnitude to the precision of the instruments. These errors are as follows:

Standard error in barometric pressure: ± 0.80 mb

Standard error in differential pressure head: ± 0.1 inch of water

Standard error in wet or dry bulb temperature: ± 0.056°C

5.2.3 Illustration of the Process of Determining Experimental Error in Net Moisture Pickup Data

Step 5 in the flow chart of Fig. 31 will be calculated using inlet duct data taken on 6 June 1980 during the 30°C test.

Step 5: Experimental error in the vapor pressure of water (e), at the inlet duct. The vapor pressure of water is defined as (see Section A.7):

$$e_I = \frac{P_I X_I}{X_I + \frac{R_a}{R_v}} \quad .$$

The experimental error in e_I (Δe_I) arises due to errors in P_I and X_I.

$$\frac{\partial e_I}{\partial P_I} = \frac{X_I}{X_I + \frac{R_a}{R_v}}$$

and

$$\frac{\partial e_I}{\partial X_I} = \frac{P_I\left(X + \frac{R_a}{R_v}\right) - X_I P_I}{\left(X_I + \frac{R_a}{R_v}\right)^2} = \frac{P_I\left(\frac{R_a}{R_v}\right)}{\left(X_I + \frac{R_a}{R_v}\right)^2} \quad .$$

So using Eq. (11):

$$\Delta e_I = \sqrt{\left(\frac{X_I}{X_I + \frac{R_a}{R_v}}\right)^2 \Delta P_I^{\,2} + \left[\frac{P_I \frac{R_a}{R_v}}{\left(X_I + \frac{R_a}{R_v}\right)^2}\right]^2 \Delta X_I^{\,2}} \quad ,$$

where ΔP_I ≡ standard error in the barometric pressure at the exhaust = 80 P_a,.

ΔX_I ≡ standard error in $X_I = 4.45 \times 10^{-5}$ (calculated in step 4).

Substituting the results from Section A.7 for 6 June 1980:

$$\Delta e_I = \sqrt{\left(\frac{0.00633}{0.00633 + \frac{287.15}{461.7}}\right)^2 (80)^2 + \frac{104250.0 \quad \frac{287.15}{461.7}}{\left(0.00633 + \frac{287.15}{461.7}\right)^2}^{\,2} \quad (4.45 \times 10^{-5})^2}$$

$$\Delta e_I = 7.35 \ P_a$$

5.2.4 Experimental Error in Net Moisture Pickup Data

The experimental error in net moisture pickup data is presented graphically on Fig. 32 and in tabular form in Table 5. The absolute magnitude of net moisture pickup fluctuated considerably during the period from November 1979 to January 1980, when equipment installation was being completed and standing water in the room pumped out. The progressive increases in net moisture pickup observed in December and January are attributed to a buildup of water pressure in the rock after sealing the R and HG holes. Net moisture

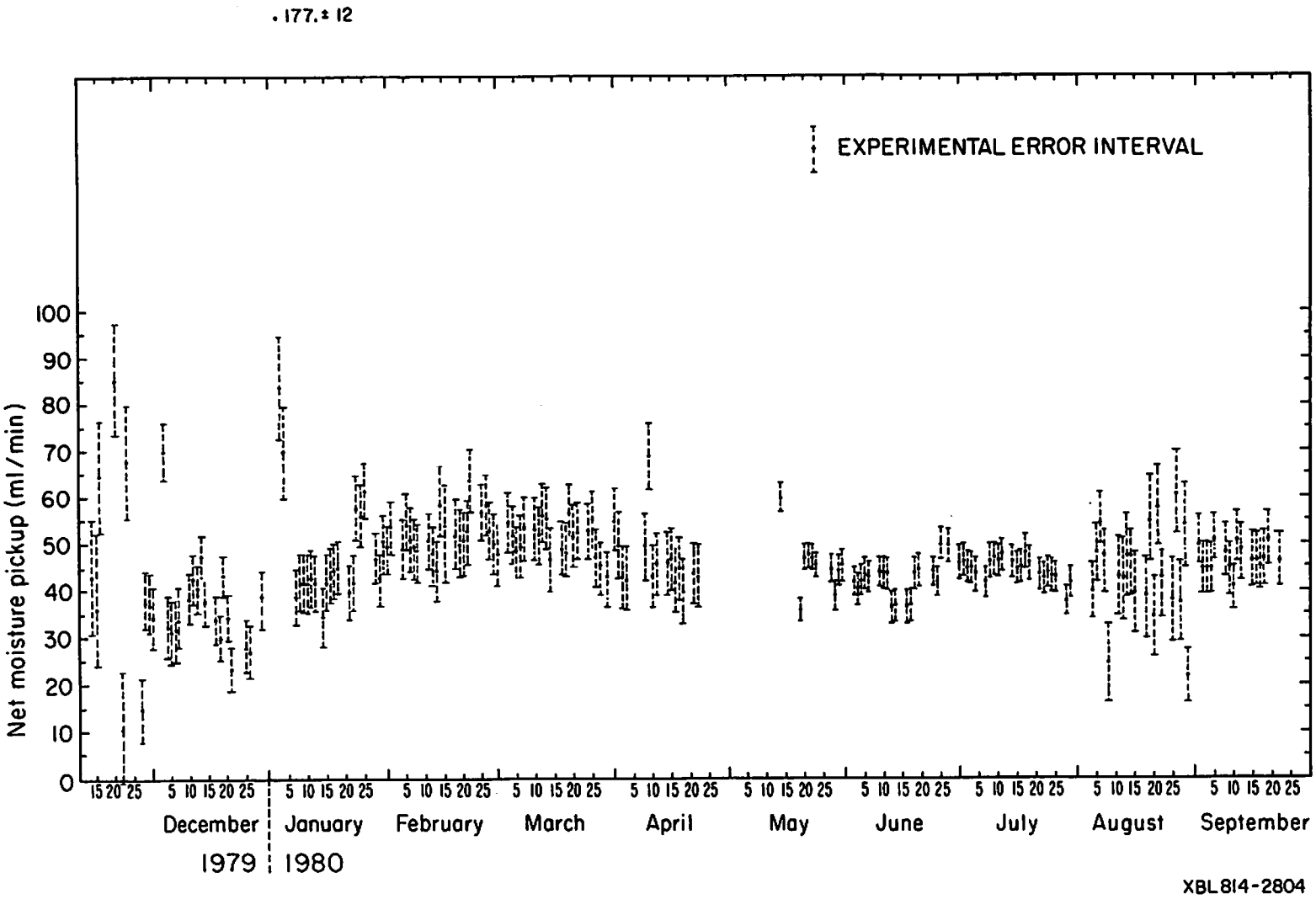

Fig. 32. Experimental error bars for net moisture pickup data.

pickup leveled off at about 50 ml/min during February and March, when the initial 20°C test was conducted. During this test, the experimental error averaged about 6.5 ml/min, about 13% of the measured value and within the same order of magnitude as the range of fluctuations observed in the data.

Net moisture pickup declined to about 42 ml/min during the 30°C and 45°C tests. Experimental error also declined during these tests to about 3.4 ml/min, about 8% of the measured value. Pickup increased as the room was cooled back to 20°C following the 45°C test, but the error also increased because a higher fan speed was required.

5.3 Sensitivity Analysis of Net Moisture Pickup

The sensitivity of the net moisture pickup is a function of the following measurements (seven variables in all): (1) the wet bulb temperature of the inlet and exhaust ducts (t_{wI} and t_{wE}); (2) the dry bulb temperature of the inlet and exhaust ducts (t_{dI} and t_{dE}); (3) the barometric pressures at the inlet and exhaust ducts (P_I and P_E); (4) the air flow chart reading (CH). The sensitivity analysis will examine the change in the net moisture pickup (MP) with respect to the change in each of the initial measurements. As examples, the sensitivity of the input data will be established for two days: 21 March 1980 (the 20°C test period, when a higher sensitivity to temperature is expected), and 25 July 1980 (the 45°C test period, when a lower sensitivity is expected).

5.3.1 Determining the Sensitivity of Net Moisture Pickup to Input Variables

As an example, the first few steps in the procedure for determining the sensitivity of net moisture pickup to the wet bulb temperature at the

exhaust duct (t_{wE}) will be demonstrated. The computational procedure is the same as the determination of net moisture pickup (see equations in Appendix A), except that instead of determining the dependent variable at each step, the partial derivative of the dependent variable with respect to the input variable (i.e., t_{wE}) is evaluated.

Step 1: Determination of $(\partial L_E)/(\partial t_{wE})$

$$L_E = 3152.15 - 2.3772\ t_{wE}$$

so:

$$\frac{\partial L_E}{\partial t_{wE}} = \frac{dL_E}{dt_{wE}} = -2.3772 \quad .$$

Step 2: Determination of $(\partial e_{swE})/(\partial t_{wE})$

$$e^{swE} = 610.6 \exp\left(\frac{17.27\ t_{wE}}{237.3 + t_{wE}}\right)$$

so:

$$\frac{\partial e_{swE}}{\partial t_{wE}} = \frac{de_{swE}}{dt_{wE}} = e_{swE}\left(\frac{17.27(237.3 + t_{wE}) - 17.27\ t_{wE}}{(237.3 + t_{wE})2}\right)$$

$$= \left(\frac{17.27(237.3)}{(237.3 + t_{wE})^2}\right) e_{swE} \quad . \tag{14}$$

Step 3: Determination of $(\partial X_{sE})/(\partial t_{wE})$

$$X_{sE} = \left(\frac{R_a}{R_v}\right) \frac{e_{swE}}{P_E - e_{swE}} \quad . \tag{15}$$

In the equation above, only e_{swE} is a function of t_{wE}. So by the chain rule for partial derivatives:

$$\frac{\partial X_{sE}}{\partial t_{wE}} = \frac{\partial X_{sE}}{\partial e_{swE}} \frac{\partial e_{swE}}{\partial t_{wE}} \quad . \tag{16}$$

From Eq. (14):

$$\frac{\partial X_{sE}}{\partial e_{swE}} = \left(\frac{R_a}{R_v}\right) \frac{P - e_{swE} + e_{swE}}{(P_E - e_{swE})^2} = \left(\frac{R_a}{R_v}\right) \frac{P_E}{(P_E - e_{swE})^2} \tag{17}$$

Substituting the results of Eqs. (14) and (15) into Eq. (16) leads to:

$$\frac{\partial X_{sE}}{\partial t_{wE}} = \left(\frac{R_a}{R_v} \frac{P_E}{(P_E - e_{swE})^2}\right) \left(\frac{17.27\ (237.3)}{(237.3 + t_{wE})^2}\ e_{swE}\right) .$$

If this procedure for determining the partial derivative of each dependent variable with respect to the wet bulb temperature at the exhaust is continued for steps 4 through 11 as illustrated in Fig. 15, the sensitivity of net moisture pickup to the wet bulb temperature of the exhaust can be calculated. The same general procedure will yield similar results for the other six input variables. The necessary equations are presented in Appendix B.

5.3.2 Example Sensitivity Analysis Results for 21 March 1980 and 25 July 1980

Using the procedure described above, we determined the sensitivity of the net moisture pickup to each of the seven input variables for the dates 21 March 1980 and 25 July 1980. These dates were selected because they represent the range of conditions experienced in the sealed drift during the experiment. The data of 21 March 1980 represent conditions at the end of the initial 20°C test, while the data of 25 July 1980 represent conditions at the end of the 45°C test.

The results of these sample sensitivity calculations are presented in Table 7. The net moisture pickup was most sensitive to the wet bulb temperature in the inlet and exhaust ducts, for which absolute sensitivity values were -33.7 ml/min/°C for the inlet duct and 37.7 ml/min/°C for the exhaust duct, using the 20°C test data. Since our temperature measurements were made to ±0.1°C, the experimental sensitivity was 3.37 ml/min/0.1°C and 3.77 ml/min/0.1°C, respectively. These sensitivity values are each about 7% of the net moisture pickup measured on the example day. As discussed earlier, this relatively high sensitivity was anticipated, and was reduced significantly by increasing the room temperature in subsequent tests. Wet bulb temperatures remained the most critical input data in the 45°C test, but the magnitude of the absolute sensitivity values dropped on our example date to 4.6 ml/min/°C for the inlet duct and 8.1 ml/min/°C for the exhaust duct. The corresponding experimental sensitivities of 0.46 ml/min/0.1°C and 0.81 ml/min/0.1°C represent only about 1% to 2% of the net moisture pickup measured on the example day.

After the wet bulb temperatures, the next most sensitive input data are the dry bulb temperatures, but net moisture pickup is less than half as sensitive to dry bulb temperature as it is to wet bulb temperature. Compared with its sensitivity to the temperature measurements, moisture pickup is relatively insensitive to the remaining input parameters of air pressure and air flow rate.

5.4 Error Resulting From Use of Simplified Head

The relationship between the actual hydraulic head, h, and simplified hydraulic head, h_s, is:

Table 7. Sensitivity of net moisture pickup to input parameters: examples for data of 20°C and 45°C tests.

Parameter	20°C Test (data of 21 March 1980)	45°C Test (data of 25 July 1980)
Inlet Conditions		
t_{wI} (°C)	8.7	11.6
t_{dI} (°C)	13.2	15.9
ρ_{wI} (Kg/m^3)	999.35	998.96
Exhaust Conditions		
t_{wE} (°C)	12.4	27.7
t_{dE} (°C)	18.2	44.2
ρ_{wE} (Kg/m^3)	998.56	990.58
Other Variables		
CH (chart divisions)	31.6	76.5
DH (inches water)	0.46	0.08
P_I (mb)	1036.6	1044.0
Computed Values		
Q_{st} (m^3/s)	0.53	0.067
MP (ml/min)	52.0	42.5
Sensitivity Data		
$\partial MP/\partial t_{dE}$ (ml/min/°C)	-16.2	-2.1
$\partial MP/\partial t_{dI}$ (ml/min/°C)	16.3	2.0
$\partial MP/\partial t_{wE}$ (ml/min/°C)	37.7	8.1
$\partial MP/\partial t_{wI}$ (ml/min/°C)	-33.7	-4.6
$\partial MP/\partial p_E$ (ml/min/P_a)	-0.55	-0.17
$\partial MP/\partial P_I$ (ml/min/P_a)	0.43	0.07
$\partial MP/\partial CH$ (ml/min/CH)	1.2	0.5

$$h = h_s + C_h \tag{18}$$

where C_h is a correction for the simplifying assumption that γ_w is constant. For this example, γ_w will be taken as 9802.10 N/m^3, the specific weight of water at 12°C. This is approximately the average rock temperature around the drift during the experiment.

To determine the maximum magnitude of the correction C_h, the hydraulic head and simplified hydraulic head were calculated for selected zones using the data of 25 July 1980, the last day of the 45°C test. The average temperature in the ventilation drift was highest during this test, and consequently, the temperature gradient in the surrounding rock was the largest. Since the specific weight of water is a function of temperature, the greatest violation of the constant specific weight assumption also occurred during this period, and this implies that the correction reached its maximum magnitude.

The magnitude of the correction C_h and the error involved in using the simplified hydraulic head (h_s) as opposed to the actual head are shown in Table 6 for a number of selected boreholes and zones. The boreholes were selected to provide one sample from each group of R holes, one sample from the HG holes, and one sample from DBH-2. These zones represent conditions at various distances into the rock and demonstrate the way in which the error decreases with distance into the rock. The maximum error in Table 6 is less than 0.3%. The greatest error was consistently observed in the zone 1 data, where rock temperature deviated most significantly from the simplifying assumption of a constant 12°C. The error in hydraulic head computation dropped rapidly with increasing distance from the drift wall, and in some cases was essentially reduced to zero.

Computational effort can be significantly reduced when using the simplified head (h_s) in place of the actual head (h). To demonstrate this point, an example calculation of the actual head for zone 3 of borehole R04 is presented.

5.4.1 Example Calculation of Hydraulic Head for R04 zone 3 on 25 July 1980

The geometric information necessary to compute hydraulic head for any zone in any borehole is available from Figs. 17 through 24 and Microfiche file 11. An example of the application of these data is provided below for zone 3 of R04, a vertical borehole extending downward from the floor of the ventilation drift. The geometric information pertinent to computing hydraulic head for this zone is summarized on Fig. 33.

5.4.1.1 Actual Hydraulic Head. To determine the actual hydraulic head, h, the integral in Eq. (11) must be evaluated. The following assumption is used: in each incremental length of pressure tube between the monitored zone and the pressure gauge, the specific weight of water is a constant, equal to the value of γ_w and corresponding to the average ambient temperature along the incremental length. On the basis of this assumption, the following steps are used to determine the specific weight of water at the zone midpoint:

1. Identify the incremental lengths into which the pressure tubing will be divided.

2. From temperature data such as that shown in Fig. 34 (a composite plot of temperature versus distance from drift wall for R04 and TG-1), determine the average temperature appropriate for each incremental length.

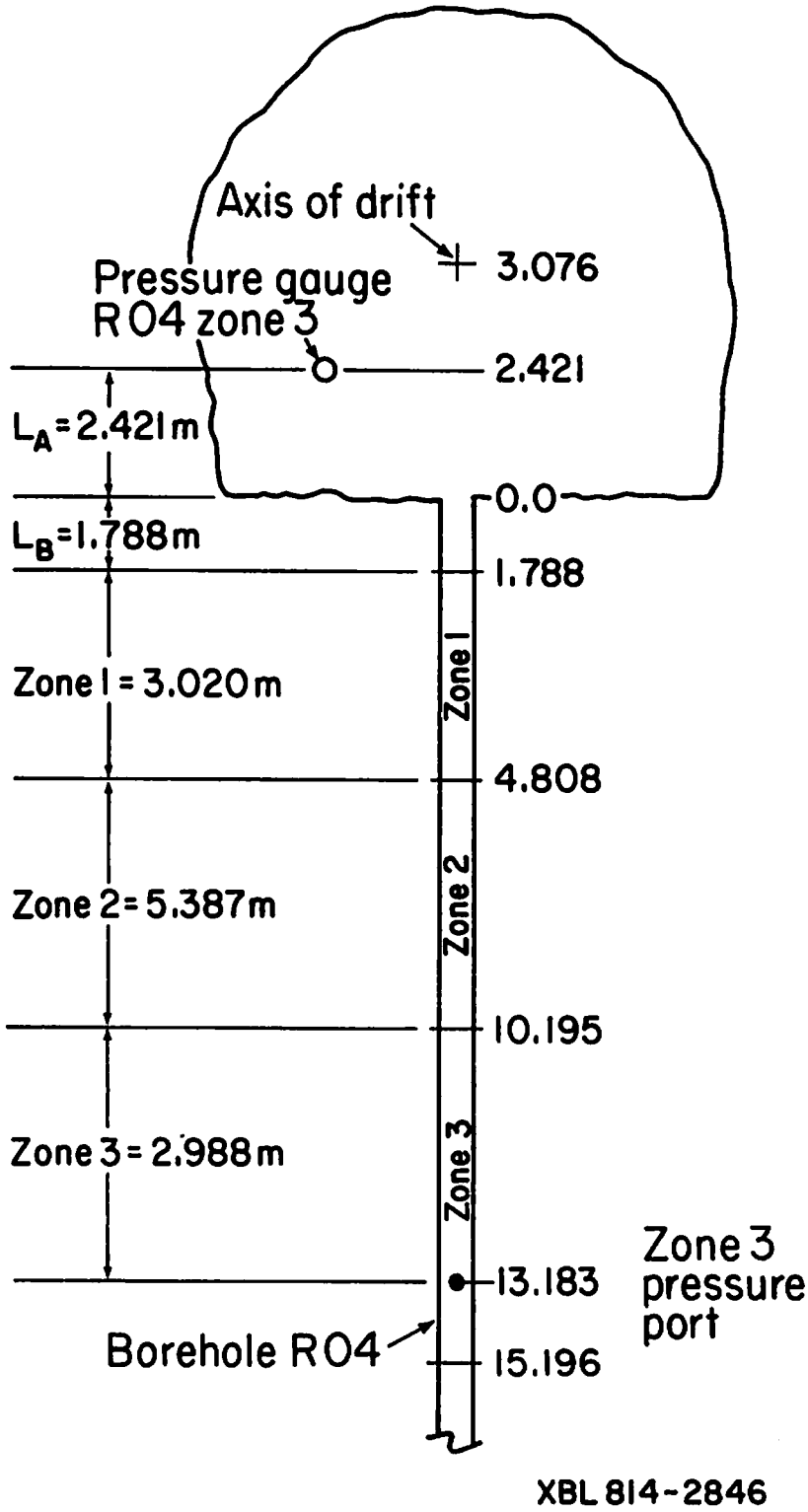

Fig. 33. Geometric information for computing hydraulic head in R04 zone 3.

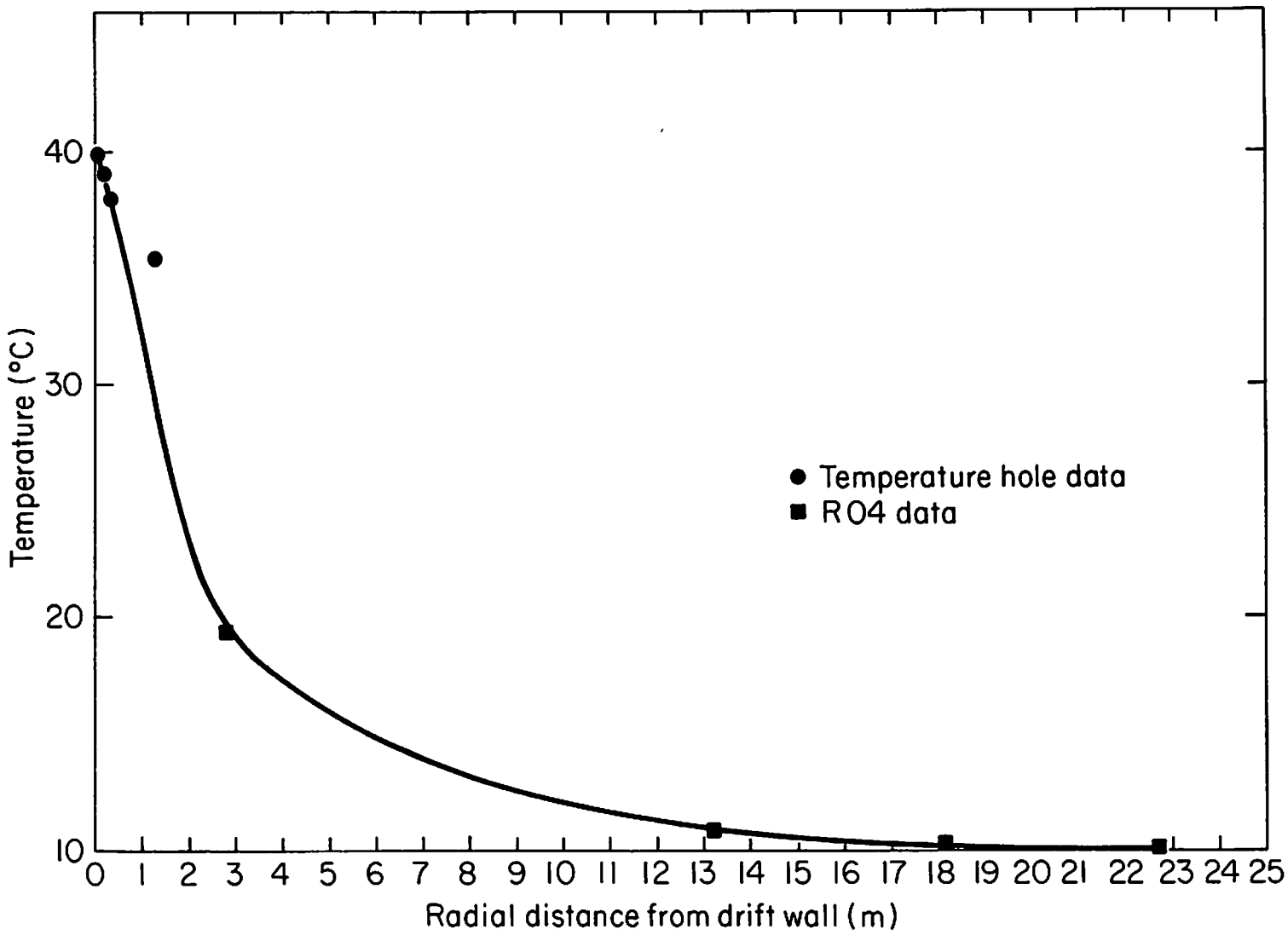

XBL 814-2839

Fig. 34. Temperature variation with distance from drift wall for R04 and temperature hole on 25 July 1980.

3. Using a table giving the density of water (ρ_w) for various temperatures, determine the effective specific weight of water ($\gamma_w = \rho_w g$) for each incremental length. See, for example, Dean, 1973, Table 10.56.

With the specific weight in each length known, the integral in Eq. (11) may be evaluated. An example using four incremental lengths to determine the actual head in zone 3 of borehole R04 follows:

$$\int_{Z_G}^{Z_p} \gamma_w(z)dz = \underbrace{(L_{zA})(\gamma_{zA})}_{\text{pressure increase from gauge 3 to collar of R04}} + \underbrace{(L_{zB})(\gamma_{zB})}_{\text{pressure increase from collar of R04 to beginning of zone 1}} + \underbrace{(L_{z1})(\gamma_{z1}) + (L_{z2})(\gamma_{z2})}_{\text{pressure increases in zones 1 and 2}} + \underbrace{(L_{z3})(\gamma_{z3})}_{\text{pressure increase from beginning of zone 3 to pressure port}} \tag{19}$$

where γ_{zi} = specific weight of water in length i,

L_{zi} = elevation change in length i.

Using the steps outlined above, we determine γ_w for each incremental length as:

Incremental Length	Average Temperature (°C)	ρ_w (Kg/m^3)	γ_w (N/m^3)	Distance from drift wall (m)
zA	44.0	990.63	9715.14	(in drift)
zB	33.0	994.70	9755.02	0.89
z1	18.4	998.52	9792.49	3.25
z2	13.6	999.93	9806.31	7.50
z3	11 0	999.61	9803.18	12.70

Substituting γ_w and the vertical elevation change in each length (see Fig. 33) into Eq. (19) leads to:

$$\int_{Z_G}^{Z_p} \gamma_w(z)dz = (2.421)(9715.14) + (9755.02)(1.788) + (9792.49)(4.808-1.788) +$$

$$9806.31(10.195-4.808) + (9803.18)(13.183-10.195)$$

$$= 152654.14 \text{ N/m}^2 \quad .$$

The pressure at gauge 3 for R04 was 154.5 psi (1065277.50 N/m^2) on 25 July 1980. Thus carrying through all digits and rounding at the end, we find the hydraulic head is:

$$h = \frac{1065277.50 + 152654.14}{9803.18} - (13.183 + 2.421 + 0.655)$$

or

$$h = 107.98 \text{ m}$$

5.4.1.2 Simplified Hydraulic Head.

$$h_s = \frac{P_G}{\gamma_w} + Z_D - Z_G$$

The simplified hydraulic head is

$$h_s = \frac{1065277.50}{9802.10} - 0.655 = 108.02 \text{ m}$$

A very simple calculation, with an error of -0.04%.

5.4.2 Experimental Error in Hydraulic Head

The sources of experimental error in hydraulic head are shown in Fig. 35. These consist of errors in pressure measurement, errors in solving the integral in Eq. (11), and errors in surveyed elevations within the drift and boreholes.

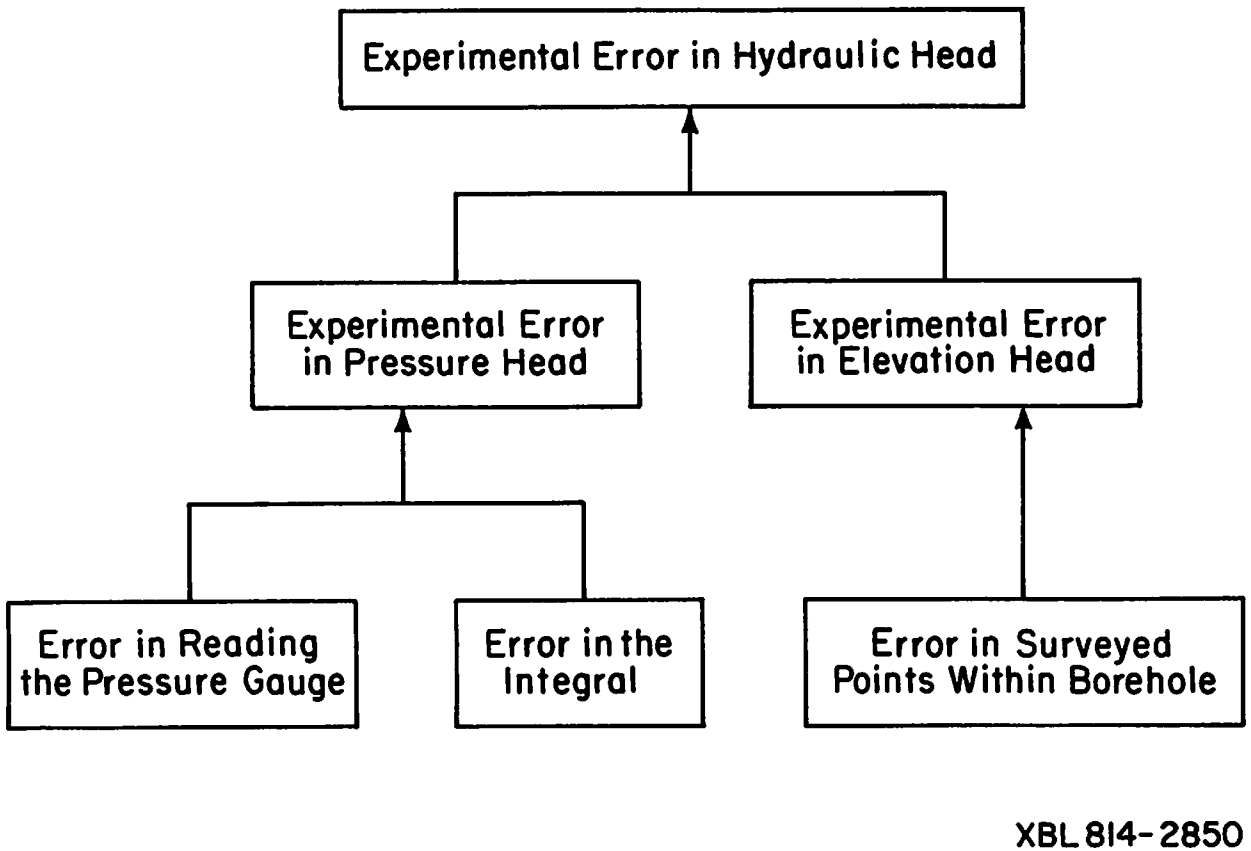

Fig. 35. Sources of error in the hydraulic head.

5.4.2.1 Experimental Error in Elevation Head The elevation head as defined in Eq. (10) is:

$$Z_H = Z_D - Z_P$$

By Eq. (12) (Section 5.1.2.4), the experimental error in the elevation head (ΔZ_H) is:

$$\Delta Z_H = \sqrt{\Delta Z_D^{\,2} + \Delta Z_P^{\,2}}$$

where

ΔZ_D = experimental error in the Z coordinate of the gauge

= 0.005 m (see Kurfurst et al., 1978, p. 28),

ΔZ_P = standard error in the Z coordinate of the pressure port

= 0.0073 m, the standard deviation in the length of a borehole (see Kurfurst, et al., 1978, p. 32).

Thus, $\Delta Z_H = 0.0088$ m

5.4.2.2 Experimental Error in Pressure Head. The experimental error from reading the gauge is determined as follows. The first term in Eq. (11) represents the pressure head due to the gauge pressure:

$$h_G = \frac{P_G}{\gamma_{wz}} \quad .$$

The experimental error in h_G is

$$\Delta h_G = \frac{1}{\gamma_{wz}} \quad \Delta P_G$$

where ΔP_G = experimental error in the pressure measured at the gauge

= 0.75 psi = 5171.25 Pa (see Table 3).

If the fluctuation in γ_W due to the temperature range experienced in the ventilation drift and boreholes is considered negligible, the experimental error in Δh_G may be determined using an approximate average temperature of 12°C for the rock around the drift. In this case, γ_{WZ} = 9802.10 N/m^3 and:

$$\Delta h_G = \frac{1}{9802.10} \ (5171.25) = 0.528 \text{ m} \quad .$$

5.4.2.3 Experimental Error from the Integral Term. If the fluctuation in γ_W due to variations in temperature is considered, the experimental error in the integral term in Eq. (11) must be evaluated. An example of this calculation is presented below.

$$\frac{\int_{Z_G}^{Z_p} \gamma_W(z)dz}{\gamma_{Zk}} = I = \frac{g\ \rho_{ZA}(Z_G-Z_{AB}) + g\ \rho_{ZB}\ (Z_{AB}-Z_{B1}) + \ldots + g\ \rho_{Zn}(Z_{k-1,k}-Z_p)}{\gamma_{Zk}}$$

where $Z_{i,i+1}$ = Z coordinate of boundary between lengths i and i+1,

ρ_{Zi} = average density of water in length i,

k = zone where pressure head is evaluated.

To determine the experimented error in I (ΔI) the partial derivatives of I with respect to Z_G, $Z_{A,B}$,...,Z_p must be evaluated:

$$\frac{\partial I}{\partial Z_G} = \frac{g\rho_{ZA}}{\gamma_{Zk}} \quad ,$$

$$\frac{\partial I}{\partial Z_{AB}} = \frac{g(\rho_{ZB}-\rho_{ZA})}{\gamma_{Zk}}$$

$$\vdots$$

$$\frac{\partial I}{\partial Z_p} = \frac{g\rho_{Zk}}{\gamma_{Zk}} \quad ,$$

$$\Delta I = \frac{g}{\gamma_{Zk}} \sqrt{\left[(\rho_{ZA})^2 + (\rho_{ZB}-\rho_{ZA})^2 + \ldots + (\rho_{Zk})^2\right] \Delta Z_H^2} \quad .$$

To provide an idea of the possible magnitude of this error, we will substitute the value 4.07 kg/m^3 for the density difference between adjacent zones (this is the maximum observed value in calculations for R04, zone 3) and compute water density based upon the lowest water temperature (10°C) observed in the boreholes. Thus an estimate of the maximum error in evaluating the integral is:

$$\Delta I \cong \frac{9.807}{9804.05} \sqrt{\left[(k+1)(4.07)^2 + 2(999.70)^2\right] \; (0.0088)^2} \qquad (20)$$

where k is the number of the zone where pressure head is evaluated.

5.4.2.4 Total Experimental Error in Hydraulic Head. Combining the components of experimental error for surveyed elevations, integral evaluation, and gauge readings, the total experimental error in the hydraulic head for zone k is:

$$\Delta h = \sqrt{\Delta Z_H{}^2 + \Delta h_G{}^2 + \Delta I^2}$$

$$= \sqrt{(0.0088)^2 + (0.528)^2 + \left(\frac{9.807}{9804.05}\right)^2 \left[(k+1)(4.07)^2 + 2(999.70)^2\right](0.0088)^2}$$

This error is maximized for zone 6, where k = 6 and:

$\Delta I = 0.012$

and $\Delta h = 0.528$ m .

This calculation shows that the experimental error in the hydraulic head calculation is almost totally due to errors in pressure measurement at the

gauge and that errors due to elevation head and the integral evaluation are negligible. In view of this, the error in hydraulic head can be taken as a constant equal to 0.53 m for all zones. Thus the hydraulic head may be computed as:

$$h = h_s + C_h \pm 0.53 \quad . \tag{21}$$

Substituting the maximum and minimum correction (C) from Table 7 into Eq. (21) leads to:

$$h = h_s + 0.18 \pm 0.53 \text{ (for maximum } C_h)$$

and

$$h = h_s \pm 0.53 \text{ (for minimum } C_h) \quad .$$

As observed earlier, the correction (C_h) due to temperature variations in the drift and boreholes introduces an error of less than 0.3% of total head, and is less in absolute magnitude than the experimental error. The magnitude of the correction (C_h) has not been determined for all zones in all boreholes because of its relative insignificance. The data necessary to compute this correction for any zone are available in this report.

The experimental error in hydraulic head is itself quite small, being less than 0.9% for all valid pressure measurements made during the experiment. Maximum error is expected to increase to about 1.2% when the correction for temperature variations is included. These values are up to an order of magnitude less than the errors observed in net moisture pickup computation.

5.5 Error in Temperature Data

The manufacturer's specifications for the temperature transducers identifies the absolute error when the calibration error is set to zero at 25°C. The

absolute error is the maximum difference between the actual and measured temperature for the temperature range -55°C to 150°C with the difference between the actual and indicated temperature at 25°C trimmed to zero. The transducers for each of the three sets of temperature measurements employed in the ventilation drift were calibrated before actual operation of the instruments. This field calibration was similar to the way the manufacturer established the absolute error. Thus, the experimental error for each transducer model will be defined as the absolute error for the particular model.

For the R and HG holes, the experimental error in the actual temperature (Δt) is:

$$\Delta t = \sqrt{\Delta t_r^{\,2} + \Delta C_t^2}$$

where

Δt_r = experimental error in the measured temperature

= 1.6°K (according to manufacturer's specifications for model L),

ΔC_t = experimental error in temperature correction

= experimental error in time scale thermocouples

= 0.5°K (as obtained from thermocouple calibrations).

Thus

$$\Delta t = \sqrt{(1.6)^2 + (0.5)^2} = 1.7°K$$

For the drift wall measurements the experimental error is 1.6°K. For the temperature hole measurements, transducer model K was used with an experimental error of 2 K.

6.0 PRESENTATION OF DATA

6.1 Organization

All the data recorded or charted to meet the principal objectives of the Macropermeability Experiment are described in this report. Because these data are voluminous, most are on microfiches that are available on request from the Earth Sciences Division at LBL. These data are grouped by type, and are organized as shown in Table 8.

Other data that are not voluminous are included in this report in standard tabular form. These include: (1) lengths of tubing between boreholes and pressure gauges; and (2) examples of tracer test data (Tables 15, 16, 21, 22, 23, and 24).

6.2 Water Pressure Data

Water pressure data are presented on microfiche file 1. A sample is given in Table 9. Pressure readings were made once each working day, and each table contains one day's gauge readings in units of pounds per square inch. Dashed lines in the place of data indicate no reading was made, either because the monitoring system had not yet been installed or was removed for repair.

Early water pressure data taken before the standard data sheets were introduced were entered directly into the daily log. These data are listed by borehole and included in the microfiche files with the balance of the pressure data. Table 10 shows an example of these data sheets.

Table 8. Organization of microfiche data files.

File No.	Type of Data	Microfiche No.
1.	Water Pressure	001-005
2.	Water Temperature in Boreholes	006-009
3.	Ventilation System	010
4.	Shunting Tests	011
5.	Rock Temperature in Temperature Hole	012
6.	Rock Temperature in Drift Walls	013
7.	Exhaust Duct Temperature	014
8.	Differential Duct Temperature	015
9.	Room Air Temperature	016
10.	Air Flow Measurements	017
11.	Location of Water Temperature Monitoring Zones in R & HG Boreholes	018

Table 9. Sample water pressure data.

Borehole Pressure Measurements in PSI

Date: 800609 Time: 8:09

Zone	R01	Zone	R02	R03	R04	R05
3	196.5	1	153.0	133.0	140.0	144.0
4	208.0	2	171.0	180.0	148.5	139.0
5	209.0	3	107.0	181.0	152.0	132.0
6	210.5	4	213.0	182.5	154.0	244.0
7	235.0	5	220.0	186.5	153.0	178.0
8	246.5	6	228.5	200.0	156.0	133.0

Date: 800609 Time: 8:00

Zone	R06	Zone	R07	R08	R09	R10
3	171.0	1	102.0	94.0	110.5	254.0
4	201.0	2	102.0	113.0	125.5	183.0
5	205.5	3	5.5	133.0	149.0	159.5
6	206.5	4	159.0	172.0	138.0	13.0
7	216.0	5	174.0	161.0	156.0	206.0
8	240.5	6	176.0	161.0	144.5	186.0

Date: 800609 Time: 8:20

Zone	DBH2	Zone	HG1	HG2	HG3	HG4	HG5
1	198.0	1	109.0	184.0	115.5	121.0	103.0
2	209.0	2	204.0	188.0	174.0	161.5	166.0
3	130.0	3	195.0	194.0	78.0	10.0	214.0
4	48.0	4	216.0	205.0	195.0	25.0	214.0
5	231.5	5	204.5	211.0	229.0	214.5	214.5
		6	208.0	216.0	231.5	216.5	214.0

Table 10. Sample early time water pressure data.

EARLY TIME WATER PRESSURE MEASUREMENTS IN PSI
AT INDICATED DATES AND TIMES
BOREHOLE R03

Commence pressure buildup.

Zone	790906 7:50	790906 7:55	790906 8:15	790906 8:45	790906 10:40
1	1.5	2.0	5.0	9.0	22.0
2	7.0	12.0	61.0	79.5	83.5
3	25.0	73.0	83.0	85.0	87.5
4	15.0	73.5	85.0	87.0	89.5
5	5.0	60.0	87.0	91.0	99.0
6	1.0	2.0	14.0	35.5	110.0

Zone	790906 14:30	790907 --	790910 6:50	790911 6:35	790912 6:48
1	49.0	61.0	64.0	64.5	64.5
2	85.0	89.0	92.5	93.0	93.5
3	89.5	88.0	96.5	96.5	97.0
4	91.5	95.0	98.5	99.0	99.0
5	105.0	114.0	122.0	122.5	123.0
6	127.0	123.5	132.0	132.0	132.0

Zone	790913 14:05	790914 8:50	790917 7:12	790918 6:40	790919 7:00
1	65.5	66.0	70.0	71.0	70.0
2	94.0	95.0	104.0	105.0	103.0
3	98.0	98.5	107.0	109.0	106.5
4	100.0	100.5	108.0	109.5	108.0
5	123.5	124.0	128.0	129.0	129.5
6	132.5	132.5	135.0	136.5	187.0

6.3 Borehole Water Temperature Data

Water temperature data from the R and HG boreholes are presented on microfiche file 2. A sample is presented in Table 11. Temperature readings were generally made once each working day, and each table presents one day's readings in K. These data were corrected for the 0.8 K bias discussed in Section 4.5.1 and thus represent actual temperatures. Dashed lines indicate no readings were made, either because equipment had not yet been installed or because the data collection schedule was changed. Asterisks indicate unstable data or a malfunctioning sensor.

6.4 Ventilation System Data

Ventilation system data are presented on microfiche file 3. A sample is given in Table 12. The data are entered in 17 columns. The meaning of each column is as follows:

1. Date data were taken, presented as a six-digit entry for year-month-day.

2. Time data were taken, presented in 24-hour clock.

3. Inlet duct wet bulb temperature, a spot measurement in °C taken with an Assman psychrometer.

4. Inlet duct dry bulb temperature, a spot measurement in °C taken with an Assman psychrometer.

5. Barometric pressure in control area, representative of inlet conditions, in millibars.

6. Differential wet bulb temperature, equals exhaust duct temperature minus inlet duct temperature, taken as spot reading from continuous circular chart in °C (see Section 5.9).

7. Differential dry bulb temperature, equals exhaust duct temperature minus inlet duct temperature, taken as spot reading from continuous circular chart in °C (see Section 5.9).

8. Exhaust duct wet bulb temperature, a spot measurement in °C taken with an Assman psychrometer.

Table 11. Sample borehole water temperature data.

Borehole Temperature Measurements in Degrees Kelvin

Date: 800704 Time: 8:28

Zone	R01	Zone	R02	R03	R04	R05
3	319.2	1	292.0	* *	289.3	290.0
4	* *	2	285.1	284.7	* *	* *
5	* *	3	283.7	283.5	283.5	* *
6	283.4	4	283.2	283.4	283.4	283.3
7	283.4	5	283.4	283.3	283.2	* *
8	283.3	6	283.3	* *	* *	* *

Date: 800704 Time: 7:58

Zone	R06	Zone	R07	R08	R09	R10
3	283.7	1	289.9	291.5	283.0	* *
4	283.5	2	285.1	284.4	285.4	* *
5	283.4	3	284.0	283.7	284.1	* *
6	283.4	4	283.5	283.4	* *	* *
7	283.3	5	283.3	283.4	283.5	* *
8	283.2	6	283.4	283.7	283.3	* *

Date: 800704 Time: 8:38

Zone	DBH2	Zone	HG1	HG2	hG3	HG4	HG5
1	- -	1	289.0	287.2	288.4	288.5	288.8
2	- -	2	284.2	284.1	284.1	283.9	283.7
3	- -	3	293.4	283.3	283.4	283.4	283.3
4	- -	4	283.2	283.3	283.3	* *	283.2
5	- -	5	283.3	283.4	283.5	* *	283.1
		6	283.2	283.2	283.2	* *	283.3

- - No Data Entered.
* * Bad Data. Readings highly erratic.

Table 12. Sample ventilation system data.

Ventilation Data

		Inlet Duct					Exhaust Duct								
		Assman Reads		Barometric	Chart Record1		Assman Reads		Press.	Chart Recorder			Heater Contr	Cum.	Mine Air Temperature
Date	Time	tw (oC)	td (oC)	Pressure (mb)	~tw (oC)	~td (oC)	tw (oC)	td (oC)	across blkhd2	tw (oC)	td (oC)	Air Flow3	Room Temp (oC)	Energy use (wt-hr)	Elec (oK)	Merc (oC)
800811	07:27	11.8	15.9	1034.3	4.4	6.0	15.0	22.1	1.200	20.5	22.0	58.5	24.2	822236	289.3	16.5
800812	07:30	11.8	16.0	1032.5	4.8	6.4	15.1	22.5	1.000	21.0	22.4	59.5	24.0	822716	289.3	16.5
800813	07:24	11.7	15.9	1032.0	4.7	6.0	15.0	22.2	1.000	20.7	22.0	60.0	23.9	823195	289.3	16.5
800814	07:27	11.6	15.9	1039.7	4.6	5.9	14.8	21.9	1.000	20.5	21.8	60.0	23.1	823676	289.3	16.5
800815	07:37	12.0	16.5	1045.0	4.5	5.5	14.7	21.6	1.000	20.4	21.5	60.0	23.0	824163	289.7	16.5
800816	07:24	11.6	15.7	1046.8	4.4	5.0	14.3	20.8	1.000	20.0	20.8	63.0	22.0	825629	289.2	16.3
800819	07:31	12.0	15.9	1043.9	4.1	4.6	14.8	20.7	1.000	19.9	20.6	61.0	21.8	826112	289.4	16.4
800820	07:32	11.5	15.5	1028.1	4.5	4.9	14.1	20.5	1.000	19.5	20.5	61.0	21.6	826598	288.8	16.0
800821	07:28	11.6	15.5	1007.3	4.3	4.6	14.4	20.2	1.000	19.6	20.0	61.0	21.2	827077	288.7	16.0
800822	07:28	11.5	15.5	1005.6	2.7	4.5	14.0	20.0	1.000	19.5	19.9	61.0	21.0	827633	288.8	16.0
800825	07:31	12.7	17.4	1033.9	1.2	2.7	14.4	20.2	1.000	19.0	20.0	61.0	21.0	829459	291.0	18.0
800826	07:28	12.1	16.4	1038.0	0.5	3.1	14.5	20.0	1.000	18.5	20.0	61.0	21.0	830808	289.9	17.1
800827	07:28	12.0	15.9	1043.3	0.9	3.5	14.1	19.6	1.000	17.6	19.5	61.5	20.5	830716	289.3	16.5
800828	07:25	11.9	15.8	1035.6	1.0	3.8	14.4	19.9	1.050	17.6	19.6	61.5	20.8	831747	289.2	16.5
800829	07:23	12.1	15.1	1027.0	4.2	3.8	14.6	19.8	0.350	17.3	19.6	29.5	20.8	832411	289.3	16.5
800901	07:28	11.6	15.7	1044.0	4.4	4.3	14.8	20.2	0.370	17.3	20.0	30.0	21.2	835796	289.1	16.4
800902	07:17	11.8	15.8	1044.0	4.3	4.3	14.8	20.2	0.370	17.1	20.0	30.0	21.3	836937	289.1	16.4
800903	07:28	11.7	15.8	1036.0	4.3	4.3	14.7	20.2	0.370	17.0	20.0	30.0	21.5	838092	289.2	16.4

Footnotes:
1. Positive Number indicates higher temperature in exhaust duct.
2. Positive Number indicates higher pressure outside room. Pressure in inches o f water.
3. Air Flow in Chart Divisions, except for period 14 to 27 May 1980 which is in mm o f water.

9. Exhaust duct dry bulb temperature, a spot measurement in °C taken with an Assman psychrometer.

10. Differential pressure across bulkhead in inches of water. Equals pressure in control area minus pressure inside sealed part of drift.

11. Exhaust duct wet bulb temperature, taken as spot reading from continuous circular chart in °C (see Section 5.8).

12. Exhaust duct dry bulb temperature, taken as spot reading from continuous circular chart in °C (see Section 5.8).

13. Air flow in chart divisions, taken as spot reading from continuous circular chart (see Section 5.19). These data were transferred to engineering units using the calibration curves in Appendix A.

14. Room air temperature as indicated by the air temperature sensor linked with the heater controls. Data taken as spot reading in °C from circular chart (see Section 5.9).

15. Cumulated energy use within sealed portion of ventilation drift, in watt-hours.

16. Air temperature in control room area outside bulkhead, using electronic temperature transducer of the same type as used in R and HG boreholes, in °K.

17. Air temperature in control room area outside bulkhead, using mercury thermometer, in °C.

6.5 Shunting Test Data

Shunting test data are presented on microfiche file 4. Samples are given in Table 13 for the two-zone tests and in Table 14 for the three-zone tests. These data sheets indicate the flow patterns for which the flow metering equipment was assembled (e.g., to monitor flow from zone A to zone B), the date and time of measurement, the water pressure as indicated by the gauge for each zone in the borehole being tested, and the flow rate measured. The other data required for test interpretation is the resistance to flow provided by the tubing interconnecting the two zones. Tubing lengths and inside diameters are given in Table 15 for the portion between

Table 13. Sample data from two-zone shunting tests.

Hole	Flow Pattern from zone	Flow Pattern to zone	Date	Time	Pressure Data by Zone (psi) 3	4	5	6	7	8	Panel No.	Flow Rate % of scale	Flow Rate ml/min
R01	7	6	22	8:00	199.5	210.0	209.0	206.5	238.0	245.0	1	0	0
	START TEST			8:40	199.5	210.0	209.0	16.0	20.0	245.0	1	>100	>29
				8:45	--	--	--	22.0	30.0	--	1	32	9.3
				8:50	199.5	210.0	209.0	30.0	31.0	245.0	1	5	1.4
				11:15	199.5	210.0	209.0	40.0	43.5	245.0	1	0	0
				11:45	119.5	210.0	209.0	45.5	45.0	245.0	1	0	0
				12:00	--	--	--	45.5	46.0	--	1	0	0
				13:15	199.0	210.0	209.0	51.0	56.0	245.0	1	0+	0
			23	7:30	199.5	210.0	209.0	66.0	116.0	245.0	1	10	2.9
				13:40	199.5	209.5	209.0	70.5	124.0	245.0	1	10	2.9
			24	7:30	199.5	210.0	209.0	129.0	143.5	245.0	1	10	2.9

Notes:

. Month and year September 1980

. Full scale flow rate = 29 ml/min.

. Zone 6 was full of gas at start of test.

Table 14. Sample data from three-zone shunting tests.

Hole	Flow Pattern from zone	to zone	to zone	Date	Time	Pressure Data by Zone (psi) 1	2	3	4	5	6	Panel No.	Flow Rate Zone 4[1] % of Scale[2]	ml/min	Zone 5[3] % of Scale[2]	ml/min	Zone 6 % of Scale	ml/min
R02	no shunt steady state 6	5	4	22	800	155.5	173.0	111.5	216.5	221.5	230.0	2						
START TEST				24	1230	155.5	173.0	114.0	136.5	136.0	135.5	2	0	0	0	0	0	0
				24	1350				148.5	147.0	149.0	2	0	0	0	0	34	9.9
				24	1430	155.5	173.0	115.0	194.5	193.0	195.0	2	2	0.6	0	0	15	4.4
				25	10:14	155.5	173.0	117.0	227.5	220.5	228.5	2	0	0	0	0	0	0
				26	10:10	155.5	173.0	119.0	227.0	221.0	229.0	2	0	0	0	0	4	1.2
				29	12:02	155.5	173.0	124.0	228.00	222.5	230.0	2	0	0	0	0	3	0.9

Notes:

. Month and Year September 1980

. Full scale for all gage's = 29 ml/min

Table 15. Tubing lengths between monitored zones and pressure gauges.

Borehole	Distance from gauge to collar (m) (0.15-inch ID tubing)		Distance from collar to each port (m) (0.11-inch ID tubing) by zone					
	outside room	inside room	1	2	3	4	5	6
R01 *	3	32.6	11.9	17.3	22.7	27.9	32.6	40.1
R02	3	37.2	2.5	7.6	12.4	17.9	22.1	29.0
R03	3	37.2	2.2	7.1	16.7	17.9	20.4	23.7
R04	3	34.8	2.8	8.1	13.2	18.1	22.8	26.5
R05	3	32.6	1.9	7.0	11.6	16.8	22.7	26.5
R06 *	2	12.6	12.7	18.5	22.4	27.8	32.6	40.0
R07	2	17.2	3.0	8.0	12.5	17.1	23.5	29.8
R08	2	17.2	2.3	7.7	13.2	17.5	22.3	26.1
R09	2	14.8	2.9	7.9	12.6	17.4	22.9	26.7
R010	2	12.6	2.0	7.0	14.5	16.8	22.2	27.3
HG1	4	35.1	3.0	8.3	13.0	17.9	22.9	29.9
HG2	4	38	3.6	8.0	12.8	18.0	23.3	29.3
HG3	4	38	2.9	8.0	12.9	18.0	23.2	26.6
HG4	4	36	3.0	8.4	13.0	18.0	23.2	26.4
HG5	4	34.3	3.0	8.0	13.0	18.0	23.0	26.6
DBH2 †	2	--	48.4	58.2	68.1	78.2	88.1	--

* The zone numbers for these holes (R01 & R06) are 3,4,5,6,7,8.

† Tubing inside borehole DBH2 is 0.078 inches ID.

the boreholes and the gauges, and in Table 16 for the portion passing through the flow meters interconnecting the gauges.

6.6 Rock Temperature Data from Temperature Hole

Rock temperature data from the temperature hole are presented on Microfiche file 5. A sample is shown on Table 17. Eight sensors were used at logarithmically spaced depths as indicated on the table. Dashes are entered in place of data when no measurement was made. The lack of a measurement generally indicates failure of the sensor. Asterisks following data entries indicate unstable sensor output.

6.7 Rock Temperature Data from Drift Walls

Rock temperature data from the drift walls are presented on microfiche file 6. A sample is shown on Table 18. Seven sensors monitored wall temperature, and were affixed to the walls near the collars of the boreholes indicated on the table. Dashes indicate when no data were available.

6.8 Exhaust Duct Temperature Data

Wet and dry bulb exahust duct temperatures in °C were recorded on circular charts, which are on microfiche file 7. The original chart data were color coded, with red indicating dry bulb temperature and violet indicating wet bulb temperature. These can be distinguished on the microfiche charts because wet bulb temperature was always less than dry bulb temperature. These data were used as backup for the primary measurements made with the Assman psychrometer, which are presented as part of the ventilation system data discussed in Section 6.4 (microfiche file 3). An example of the exhaust duct temperature data is presented in Fig. 36.

Table 16. Tubing lengths between gauges and common for shunting tests.

a. Two-Zone Tests

Borehole	Flow path from indicated gauge to common	Length of flow path (m)	
		0.150 inch ID tubing	0.125 inch ID tubing
R01	6	2.5	0.5
	7	3.8	1.0
R02	5	2.5	0.5
	6	3.8	1.0
R06	7	2.5	0.5
	8	3.3	1.5
R07	4	2.5	0.5
	5	3.3	1.5
R09	4	2.5	0.5
	5	3.3	1.5

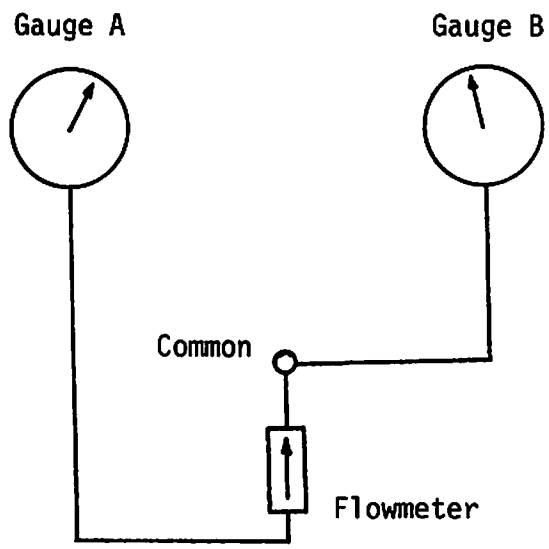

Table 16 (continued). Tubing lengths between gauges and common for shunting tests

b. Three-Zone Tests

Borehole	Flow path from indicated gauge to common	Length of flow path (m) 0.150 inch ID tubing	0.125 inch ID tubing
	6	3.8	1.0
R01	7	3.3	1.5
	8	2.8	1.5
	4	3.8	1.0
R02	5	3.3	1.5
	6	2.8	1.5
	6	3.3	1.5
R06	7	3.3	1.5
	8	3.4	1.0
	4	3.3	1.5
R09	5	3.3	1.5
	6	3.4	1.0

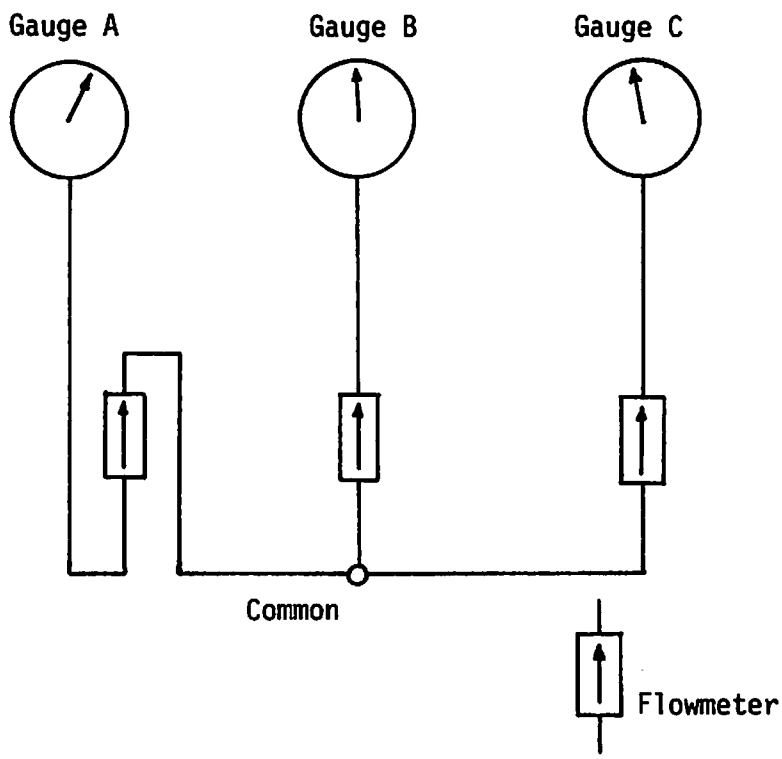

Table 17. Sample data for rock temperature from temperature hole.

Temperature Hole Data in Degrees Kelvin

Date	Time	Sensor Depth (m)							
		0.07	0.15	0.30	0.60	1.25	2.5	5.0	10.0
791009	06:45	284.4	284.3	284.2	284.5	284.4	284.4	283.6	283.2
791016	08:05	284.6	284.4	284.4	284.5	284.5	284.3	283.6	283.2
791022	07:00	284.5	284.4	284.3	284.5	284.5	284.5	283.6	283.2
791030	08:18	284.3	284.1	284.1	284.4	284.4	284.7	283.5	283.2
791106	13:25	284.6	284.4	284.3	284.5	284.5	284.3	283.6	283.2
791113	11:16	284.3	284.2	284.1	284.4	284.5	284.3	283.6	283.2
791114	13:03	284.3	284.2	284.1	284.4	284.5	284.4	283.6	283.2
791115	11:03	284.4	284.2	284.2	284.4	284.5	284.3	283.6	283.2
791116	11:44	284.3	284.1	284.1	284.4	284.5	284.3	283.6	283.2
791119	11:00	284.3	284.1	284.1	284.4	284.4	284.4	283.6	283.2
791120	12:46	284.3	284.1	284.1	284.4	284.4	284.4	283.6	283.2
791121	12:23	284.3	284.1	284.1	284.4	284.4	285.6	283.6	283.2
791122	10:56	284.3	284.1	284.1	284.4	284.4	284.3	283.6	283.2
791123	11:05	284.5	284.3	284.2	284.4	284.4	294.4	283.6	283.2
791126	11:05	284.5	284.3	284.3	284.5	284.5	284.5	283.6	283.2
791127	10:42	284.5	284.3	284.3	284.5	284.5	284.4	283.6	283.2
791128	11:17	284.5	284.3	284.3	284.5	284.5	284.4	283.6	283.2
791129	10:42	284.4	284.3	284.3	284.5	284.5	294.3	283.6	283.2

Table 18. Sample data for rock temperature from drift walls.

Wall Temperature at Borehole in Degrees Kelvin

Date	Time	R1	R2	R4	R5	R7	R9	Temp Hole (TG-1)
791113	11:18	285.4	285.1	285.4	285.4	285.2	284.8	285.3
791114	12:38	285.5	285.2	285.5	285.4	285.2	284.9	285.3
791115	13:57	285.4	285.0	285.4	285.4	285.2	284.8	285.3
791116	11:42	285.5	285.2	285.5	285.3	285.2	284.9	285.3
791119	13:55	285.5	285.1	285.5	285.3	285.2	284.9	285.3
791120	12:44	285.5	285.2	285.6	285.3	285.2	285.0	285.3
791121	12:19	285.6	285.2	285.6	285.3	285.2	285.0	285.3
791122	10:50	285.6	285.2	285.6	285.4	285.2	285.0	285.3
791123	11:02	285.6	285.2	285.3	285.2	285.1	285.0	285.4
791126	11:00	285.4	284.8	285.1	285.1	285.0	284.9	285.3
791127	11:30	285.2	284.8	285.1	285.1	285.0	284.9	285.2
791128	11:06	285.1	284.7	285.0	285.1	285.0	284.9	285.2
791129	13:40	285.2	284.7	284.9	285.0	284.9	284.8	285.2
791130	10:46	285.2	284.7	284.9	285.0	284.9	284.8	285.2
791203	12:15	285.2	284.7	284.9	285.0	284.9	284.8	285.2
791204	08:58	285.0	284.7	284.8	285.0	284.9	284.8	285.2
791205	11:03	285.0	284.6	284.8	285.0	284.9	284.7	285.1
791206	10:46	284.9	284.6	284.9	285.0	284.9	284.7	285.1
791207	11:00	285.2	284.6	285.0	284.9	284.8	284.7	285.1
791210	11:20	285.0	284.4	284.7	284.8	284.7	284.6	284.9
791211	12:37	285.0	284.4	284.7	284.8	284.7	284.6	285.0

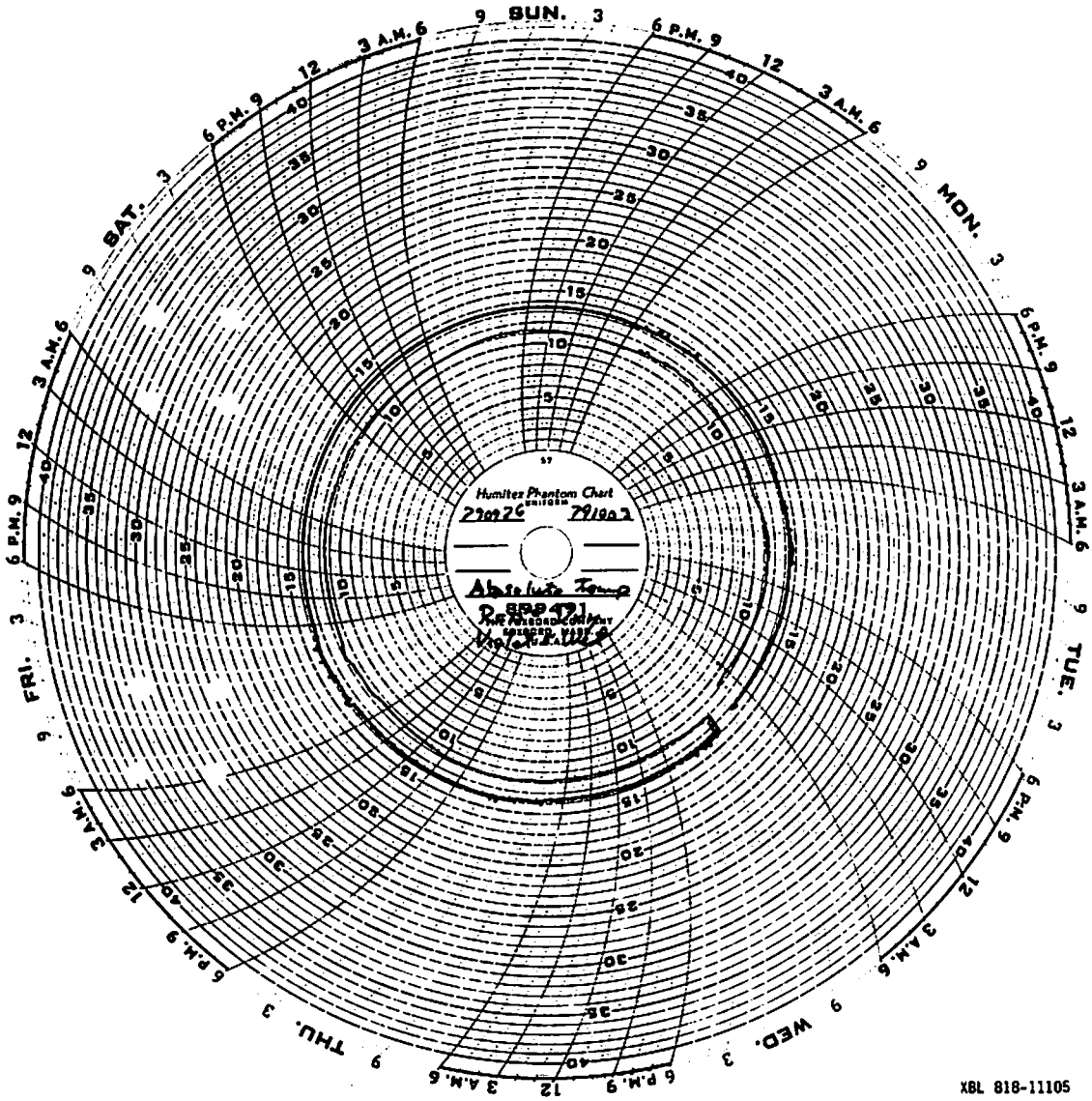

Fig. 36. Example of exhaust duct circular chart temperature data.

6.9 Differential Duct Temperature Data

Wet and dry bulb differential duct temperatures in °C were recorded on circular charts, which are presented on microfiche file 8. The original chart data were color coded, with red indicating wet bulb temperature and violet indicating dry bulb temperature. The wet and/or dry bulb lines are indicated on each chart. The sign convention for the differential temperature recorder was changed several times during the experiment in an effort to maintain positive chart readings. The dates of these changes and the sign conventions are indicated on Table 19. The spot readings of the differential temperature data presented with the ventilation system data in Section 6.4 have been corrected to yield a consistent sign convention wherein $\Delta t = t_E - t_I$ for both wet and dry bulb measurements.

Table 19. Sign conventions for differential duct temperature records on circular charts.

Time Period*	Wet Bulb	Dry Bulb
791114 to 791203	$\Delta t_w = t_{wI} - t_{wE}$	$\Delta t_d = t_{dI} - t_{dE}$
791204 to 800222	$\Delta t_w = t_{wE} - t_{wI}$	$\Delta t_d = t_{dI} - t_{dE}$
800223 to 800922	$\Delta t_w = t_{wE} - t_{wI}$	$\Delta t_d = t_{dE} - t_{dI}$

* The digits indicate year, month, and day. E.g. 791114 is 14 November 1979.

The differential temperature chart records were used as backup for the primary measurements made with the Assman psychrometer. An example of the differential duct temperature data is presented in Fig. 37.

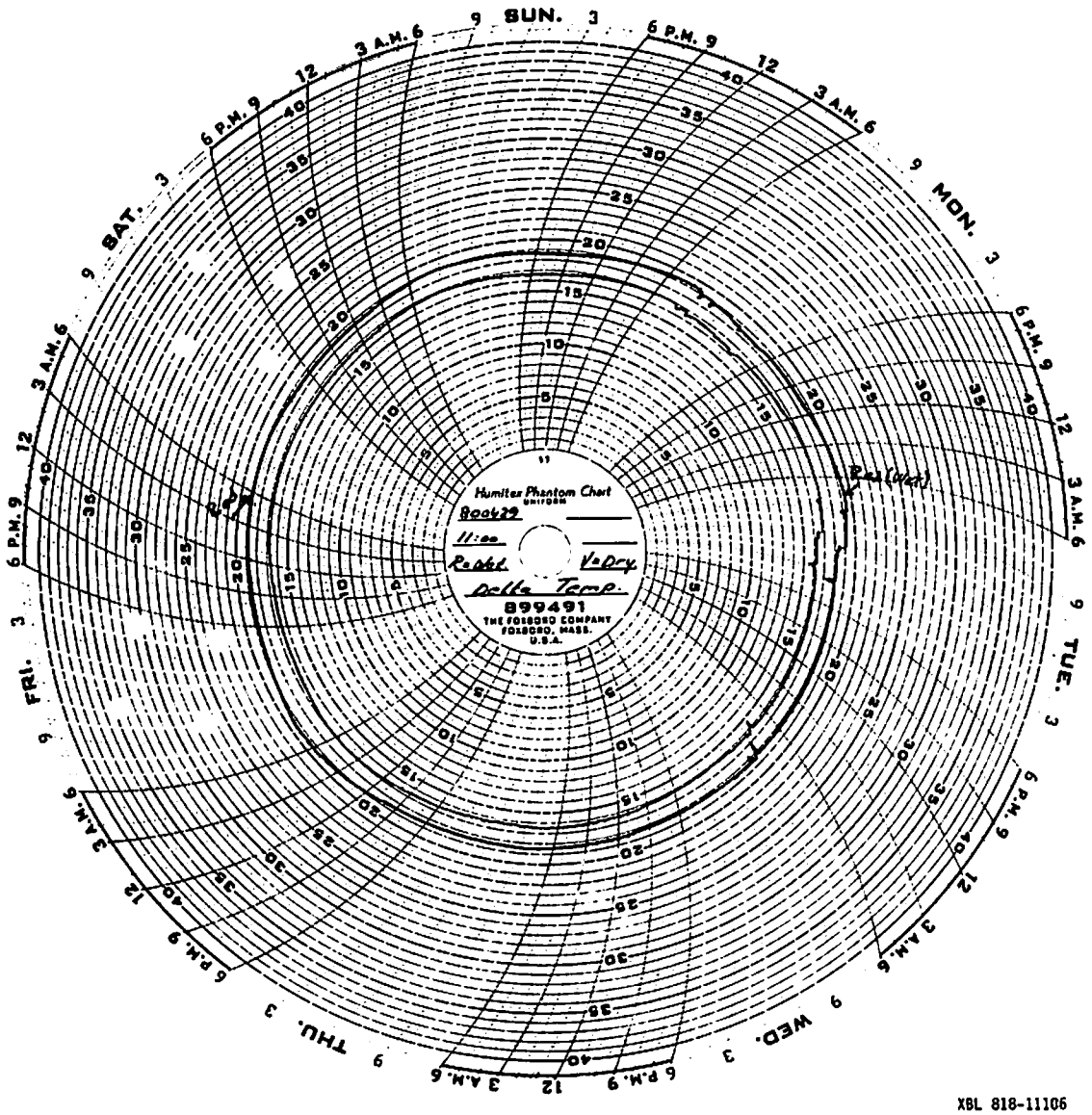

XBL 818-11106

Fig. 37. Example of differential duct circular chart temperature data.

6.10 Room Air Temperature Data

Air temperature in °C within the sealed portion of the drift was continuously recorded on circular charts for three locations as shown on Fig. 3. These data are presented on microfiche file 9. The original chart data were color coded, with green indicating the sensor nearest the bulkhead, red indicating the control sensor, and violet indicating the sensor nearest the face of the drift. The central sensor (red) was also connected with the automatic heater control unit, although automatic control was rarely used during the experiment. Spot readings of the central sensor output are presented on the ventilation system data sheets discussed in Section 6.4. An example of the room air temperature data is presented in Fig. 38.

6.11 Air flow Data

Air flow rate in the exhaust duct was continuously recorded on circular charts and are presented in microfiche file 10. These data are in chart divisions, and can be reduced to engineering units using the calibration charts in Appendix A. Spot readings of air flow are given on the ventilation system data sheets discussed in Section 6.4. An example is presented in Fig. 39.

6.12 Geometric Data

Geometric data are required for conversion of water pressure measurements to hydraulic head. These data are presented as follows:

1. Borehole locations and orientations: Figs. 23 and 30.
2. Borehole installed equipment: Figs. 6, 23, 24, 25, 27, 30, 31, and microfiche file 11. (An example data sheet from microfiche file 11 is shown as Table 20.)
3. Pressure gauge layouts: Figs. 29 and 31.

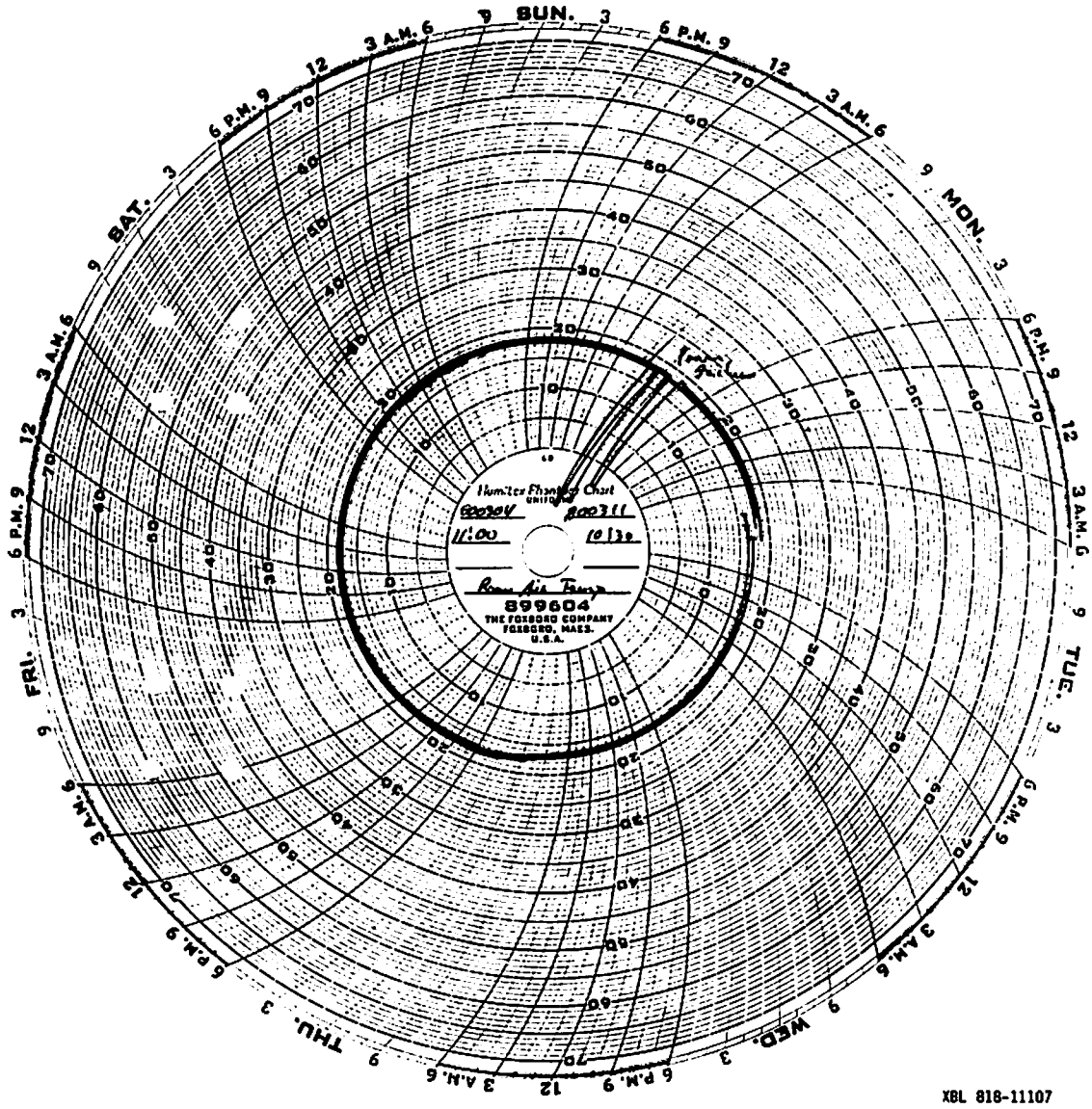

Fig. 38. Example of room air temperature circular chart data.

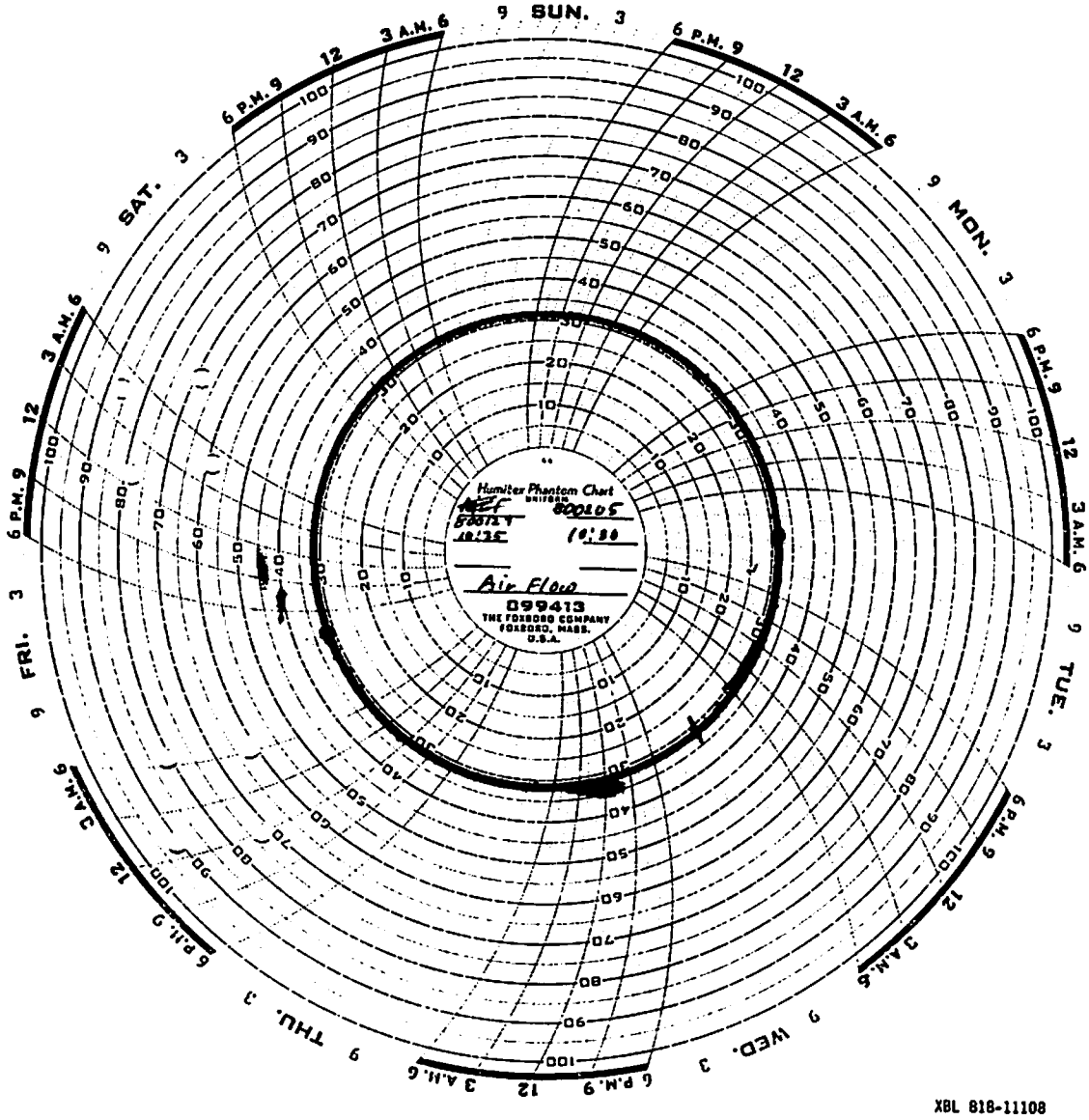

XBL 818-11108

Fig. 39. Example of air flow rate circular chart data.

Table 20. Sample data for zone ends and pressure port locations in R and HG holes.

Zone End, Pressure Port Locations for R02

Zone No.	I = Inner End P = Pressure Port O = Outer End	Hole Length (m)	Zone Length (m)	Mine Coordinates (m) x	y	z
	I	1.584		384.078	979.556	331.934
1	P	2.497	2.815	384.071	980.142	331.235
	O	4.399		384.058	981.364	329.77
	I	4.593		384.056	981.489	329.628
2	P	7.641	4.960	384.035	983.447	327.293
	O	9.553		384.021	984.675	325.828
	I	9.747		384.020	984.800	325.679
3	P	12.395	4.567	384.001	986.501	323.650
	O	14.314		383.988	987.734	322.179
	I	14.508		383.986	987.858	322.031
4	P	17.901	5.320	383.962	990.038	319.430
	O	19.828		383.949	991.276	317.954
	I	20.022		383.947	991.401	317.805
5	P	22.058	3.941	383.933	992.709	316.245
	O	23.963		383.919	993.933	314.785
	I	24.157		383.918	994.057	314.636
6	P	29.018	5.197	383.883	997.180	910.911
	O	29.354		383.881	997.396	310.654
	I					
7	P					
	O					
	I					
8	P					
	O					
Beginning of Borehole		0		384.089	978.538	333.148

4. Ventilation drift dimensions: Fig. 3.

5. Experimental area dimensions: Figs. 3 and 4; Table 1.

6.13 Tracer Test Data

Electrical conductance of groundwater was monitored daily in all zones of the HG holes and in zone 4 of borehole R01 from 6 November 1979 through 22 September 1980. A 40,000 mg/l NaCl solution was introduced into zone 6 of borehole HG3 on 31 March 1980, as described in Section 2.2.3.3. Conductance was measured by comparing the voltage drop (E_i) across a reference resistor (R_{ref}) with the voltage drop (E_w) between two electrodes in the monitored zone. Since the electric current (I) responsible for these voltage drops is the same, we have:

$$I = \frac{E_w}{R_{zone}} = \frac{E_i}{R_{ref}} ,$$

and the zone conductance (C_{zone}) is given by:

$$C_{zone} = \frac{1}{R_{zone}} = \frac{E_i}{E_w} \frac{1}{R_{ref}} .$$

Conductance measurements taken on 31 March 1980 both before and after tracer injection are shown on Tables 21 and 22. Conductance measurements taken on 22 September 1980, the last day of the Macropermeability Experiment, are shown on Table 23. None of the monitored zones show a significant increase in conductance that could be attributed to tracer movement. The only indication that the tracer was in fact moving out of the injection zone was the zone's progressive but erratic decline in conductance after the tracer was injected. These conductance data are presented in Table 24.

Table 21. Conductance data for 31 March 1980 before tracer injection.

Zone 1	Borehole R01 Ei (mV)	Borehole R01 Ew (V)	Borehole R01 C_{zone} (mmho)	Borehole HG1 Ei (mV)	Borehole HG1 Ew (V)	Borehole HG1 C_{zone} (mmho)	Borehole HG2 Ei (mV)	Borehole HG2 Ew (V)	Borehole HG2 C_{zone} (mmho)
1	---	---	---	117.92	.2475	47.4	117.51	.2728	42.8
2	---	---	---	117.00	.3037	38.3	117.20	.2922	39.9
3	---	---	---	116.75	.3184	36.5	116.46	.3361	34.5
4	117.48	.2758	42.3	116.93	.3078	37.8	117.15	.2949	39.5
5	---	---	---	117.76	.2575	45.4	116.10	.3587	32.2
6	---	---	---	117.57	.2693	43.4	117.08	.2984	39.0

Zone 1	Borehole HG3 Ei (mV)	Borehole HG3 Ew (V)	Borehole HG3 C_{zone} (mmho)	Borehole HG4 Ei (mV)	Borehole HG4 Ew (V)	Borehole HG4 C_{zone} (mmho)	Borehole HG5 Ei (mV)	Borehole HG5 Ew (V)	Borehole HG5 C_{zone} (mmho)
1	117.29	.2868	40.7	116.38	.3434	33.7	117.71	.2621	44.7
2	115.99	.3672	31.4	117.08	.2994	38.9	117.21	.2921	39.9
3	116.69	.3221	36.0	116.89	.3122	37.3	116.02	.3645	31.7
4	116.70	.3228	36.0	116.98	.3060	38.0	116.98	.3061	38.0
5	117.23	.2901	40.2	116.63	.3271	35.5	117.12	.2976	39.2
6	116.60	.3293	35.2	117.22	.2908	40.1	117.76	.2588	45.3

R_{ref} = 10.05 ohms

Table 22. Conductance data for 31 March 1980 after tracer injection.

Zone 1	Borehole R01 Ei (mV)	Borehole R01 Ew (V)	Borehole R01 C_{zone} (mmho)	Borehole HG1 Ei (mV)	Borehole HG1 Ew (V)	Borehole HG1 C_{zone} (mmho)	Borehole HG2 Ei (mV)	Borehole HG2 Ew (V)	Borehole HG2 C_{zone} (mmho)
1	---	---	---	117.88	.2481	47.3	117.47	.2726	42.9
2	---	---	---	116.96	.3036	38.3	117.16	.2921	39.9
3	---	---	---	116.73	.3179	36.5	116.42	.3365	34.4
4	117.42	.2756	42.4	116.90	.3076	37.8	117.11	.2946	39.6
5	---	---	---	117.73	.2575	45.5	116.07	.3582	32.2
6	---	---	---	117.53	.2692	43.4	117.05	.2983	39.1

Zone 1	Borehole HG3 Ei (mV)	Borehole HG3 Ew (V)	Borehole HG3 C_{zone} (mmho)	Borehole HG4 Ei (mV)	Borehole HG4 Ew (V)	Borehole HG4 C_{zone} (mmho)	Borehole HG5 Ei (mV)	Borehole HG5 Ew (V)	Borehole HG5 C_{zone} (mmho)
1	117.27	.2858	40.8	116.34	.3426	33.8	117.65	.2618	44.7
2	115.97	.3656	31.6	117.03	.2994	38.9	117.16	.2918	39.9
3	116.67	.3211	36.2	116.84	.3317	37.3	115.99	.3636	31.7
4	116.67	.3223	36.0	116.94	.3057	38.1	116.93	.3066	38.0
5	117.19	.2899	40.2	116.59	.3266	35.5	117.07	.2973	39.2
6	121.49	.0299	404.2	117.18	.2907	40.1	117.71	.2587	45.3

R_{ref} = 10.05 ohms

Table 23. Conductance data for 22 September 1980.

Zone 1	Borehole R01 Ei (mV)	Borehole R01 Ew (V)	Borehole R01 C_{zone} (mmho)	Borehole HG1 Ei (mV)	Borehole HG1 Ew (V)	Borehole HG1 C_{zone} (mmho)	Borehole HG2 Ei (mV)	Borehole HG2 Ew (V)	Borehole HG2 C_{zone} (mmho)
1	---	---	---	5.96	7.039	.0835	117.84	.2502	46.4
2	---	---	---	117.27	.2841	40.7	117.14	.2930	39.4
3	---	---	---	116.81	.3126	36.9	116.43	.3364	34.1
4	117.25	.2833	40.8	116.68	.3203	35.9	116.95	.3039	38.0
5	---	---	---	117.72	.2572	45.1	116.48	.3332	34.5
6	---	---	---	117.50	.2705	42.8	117.28	.2840	40.7

Zone 1	Borehole HG3 Ei (mV)	Borehole HG3 Ew (V)	Borehole HG3 C_{zone} (mmho)	Borehole HG4 Ei (mV)	Borehole HG4 Ew (V)	Borehole HG4 C_{zone} (mmho)	Borehole HG5 Ei (mV)	Borehole HG5 Ew (V)	Borehole HG5 C_{zone} (mmho)
1	117.88	.2478	46.9	115.55	.3846	29.6	116.72	.3147	36.6
2	116.00	.3631	31.5	116.96	.3002	38.4	117.24	.2834	40.8
3	116.60	.3255	35.3	115.65	.3841	29.7	116.11	.3524	32.5
4	116.53	.3293	34.9	116.84	.3080	37.4	116.95	.3014	38.3
5	115.93	.3589	31.9	116.36	.3381	33.9	116.99	.2991	38.6
6	121.13	.0495	241.2	117.04	.2953	39.1	117.89	.2439	47.7

R_{ref} = 10.14 ohms

Table 24. Conductance data for zone 6 of borehole HG3 following tracer injection.

Date	Conductance (mmho)	Date	Conductance (mmho)	Date	Conductance (mmho)	Date	Conductance (mmho)
800331	404.2	800520	401.9	800707	387.8	800820	362.9
800401	408.6	800521	399.7	800708	385.6	800821	375.3
800402	408.0	800522	399.9	800709	385.2	800822	363.7
800403	405.5	800523	399.4	800710	387.1	800825	379.4
800408	403.8	800527	398.8	800711	385.8	800826	373.6
800409	403.5	800528	398.4	800714	384.8	800827	354.9
800410	403.4	800529	398.2	800715	385.3	800828	345.8
800411	403.2	800530	398.9	800716	380.9	800829	358.4
800414	403.3	800602	397.9	800717	382.1	800901	291.9
800415	401.3	800603	397.7	800718	378.2	800902	282.0
800416	401.6	800604	397.2	800721	379.9	800903	371.4
800417	401.4	800605	398.7	800722	380.1	800904	377.0
800418	403.1	800606	398.5	800723	379.4	800905	324.8
800421	403.7	800609	397.7	800724	375.2	800908	308.4
800422	402.9	800610	398.7	800725	377.1	800909	291.6
800423	403.6	800611	397.2	800728	381.2	800910	318.5
800424	406.9	800612	396.7	800730	379.1	800911	370.0
800425	408.1	800613	399.1	800801	380.1	800912	255.6
800428	399.4	800616	394.6	800804	373.6	800915	335.0
800429	400.0	800617	394.6	800805	380.0	800916	272.1
800430	399.6	800618	393.7	800806	382.6	800917	280.0
800505	399.7	800619	393.7	800807	379.9	800918	197.3
800506	399.5	800623	393.5	800808	365.4	800919	292.5
800507	399.2	800625	390.8	800811	364.7	800922	241.2
800508	399.7	800627	389.6	800812	388.0		
800509	400.7	800630	387.9	800813	365.3		
800512	399.5	800701	387.5	800814	374.2		
800513	400.6	800702	383.4	800815	382.0		
800514	400.7	800703	386.1	800818	355.6		
800519	403.5	800704	386.2	800819	364.8		

6.14 Geochemical Data

Samples of fracture fillings and groundwater precipitates were taken as a part of the Macropermeability Experiment because an apparent "skin" of lower permeability rock immediately surrounding the drift became evident during preliminary data analysis. The sampling locations and methodologies, and the analyses planned for the samples are described in Chapters 2 and 3.

At present, the only analysis completed is the x-ray diffraction study of precipitates from water collected from borehole R05. This study involved the use of Cu Kα radiation on a finely powdered sample of the precipitates. The major characteristic peaks occurred at 27.4, 31.8, 45.5, 56.6, and 66.2 degrees 2 θ, all of which are indicative of halite (NaCl). Several minor peaks were observed but could not be unequivocably identified. These results indicate that halite deposits will probably predominate in fracture fillings induced by evaporation of groundwater entering the drift.

Data from the remaining geochemical analyses will be published in subsequent reports. Additional data on groundwater geochemistry have been published by Fritz, Barker, and Gale (1979).

ACKNOWLEDGMENTS

The authors are indebted to a large number of people who materially assisted in the conduct of the Macropermeability Experiment and in the production of this report. Steve Lundgren and Bill Wong provided expertise in equipment design; John Gale participated in the original design of the drift and borehole array; Bill Stromdahl and Hans Carlsson were able project and site managers at LBL and Stripa; Per Axel Halen provided invaluable support as mine manager at Stripa; Tom Doe assisted in the initial design studies and provided valuable consultation throughout the project; Lars Jakobson and Gerry West provided skilled equipment installation and maintenance assistance; and special thanks to the report preparation crew that transcribed the large amount of data and text into a finished product.

This work was supported by the Assistant Secretary for Nuclear Energy, Office of Waste Isolation of the U.S. Department of Energy under Contract DE-AC03-76SF00098. Funding for this project was administered by the Office of Nuclear Waste Isolation at Battelle Memorial Institute.

REFERENCES

Baird, D.C., 1962. Experimentation: An Introduction to Measurement Theory and Experiment Design, Prentice Hall, Inc., Englewood Cliffs, New Jersey.

Beers, Y., 1957. Introduction to the Theory of Error, Addison-Wesley Publishing Company, Reading, Mass.

Dean, J.A., 1973. Lange's Handbook of Chemistry, 11th Edition, McGraw-Hill Book Co., New York.

Ferris, J.G., D.B. Knowles, R.H. Brown, and R.W. Stallman, 1962. Theory of Aquifer Tests, U.S. Geological Survey Water Supply Paper 1536-E.

Forster, C. and J.E. Gale, 1980. A Field Assessment of the Use of Borehole Pressure Transients to Measure the Permeability of Fractured Rock Masses. Lawrence Berkeley Laboratory report LBL-11829, SAC-34, University of California, Berkeley.

Fritz, P., J. F. Barker and J.E. Gale, 1979. Geochemistry and Isotope Hydrology of Groundwater in the Stripa Granite; Results and Preliminary Interpretation. Lawrence Berkeley Laboratory report LBL-8285, SAC-12, University of California, Berkeley.

Gale, J.E., 1981. Results of Hydrogeology Borehole Testing at the Stripa Mine Site, Lawrence Berkeley Laboratory report LBL-13101, University of California, Berkeley (in preparation).

Huntsberger, D.V. and P. Billingsley, 1977. Elements of Statistical Inference, 4th Edition. Allyn and Bacon, Inc., Boston.

Jeffreys, H., 1978. Theory of Probability. Oxford: Clarendon Press, Oxford, England.

Kurfurst, P.J., T. Hugo-Persson and G. Rudolph, 1978. Borehole Drilling and Related Activities at the Stripa Mine. Lawrence Berkeley Laboratory report LBL-7080, SAC-05, University of California, Berkeley.

Long, J.C.S., P. A.Witherspoon, C. R. Wilson and A. O. DuBois, 1980. "Large Scale Permeability Testing at Stripa." In Third Invitational Well Testing Symposium, Lawrence Berkeley Laboratory report LBL-12076, Berkeley, California, March.

McPherson, M.J., 1979a. "Psychrometry: the Measurement and Study of Moisture in Air." Mining Department Magazing, Vol. 31, University of Nottingham, United Kingdom.

McPherson, M.J., 1979b. An Interim Report on the Airflow and Humidity Monitoring in the Ventilation Drift. Prepared for Lawrence Berkeley Laboratory, Berkeley, California.

Osborne, N.S., H.F. Stimson, D.C. Ginnings, 1939. "Measurement of Heat Capacity and Heat of Vaporization of Water in the Range 0°C to 100°C." J. Res. Natl. Bur. Std., vol. 23, p. 261.

Snow, D.T., 1965. A Parallel Plate Model of Fractured Permeable Media. Ph.D. Thesis, University of California, Berkeley, 331 pp.

Topping, J., 1962. Errors of Observation and Their Treatment. Monograph of the Institute of Physics and the Physical Society. Chapman and Hall, Ltd., London, 3rd edition, 119 p.

Witherspoon, P.A. and O. Degerman, 1978. Swedish-American Cooperative Program on Radioactive Waste Storage in Mined Caverns. Lawrence Berkeley Laboratory report LBL-7049, SAC-01. University of California, Berkeley.

Witherspoon, P.A., C. R. Wilson, J. C. S. Long, A.O. DuBois, J.E. Gale, and M. McPherson, 1979. "The Role of Large-Scale Permeability Measurements in Fractured Rock and Their Application at Stripa." Presented at the International Symposium on the Scientific Basis for Nuclear Waste Management, Boston, Massachusetts, November. Lawrence Berkeley Laboratory report LBL-9903, Berkeley, California, October.

Witherspoon, P.A., C.R. Wilson, J.C.S. Long, A.O. DuBois, J.E. Gale, M. McPherson, and R.M. Galbraith, 1980. "Large Scale Permeability Measurements in Fractured Crystalline Rock." Presented at the International Geologic Congress, Paris, France, July.

APPENDIX A. COMPUTATION OF NET MOISTURE PICKUP

A.1 Introduction

The computation of net moisture pickup (MP) involves a series of 11 calculations. For each equation, a description is given followed by a demonstration of the use of the equation as applied to the data of 6 June 1980. This date was selected because its data are representative of a stable period toward the end of the 30°C test. Additional information on the derivation of each equation is provided by McPherson (1979a). The sequence of steps in computing MP is illustrated by the flow chart in Fig. 15, Chapter 4.

A.2 Input Information

The input data consist of: (1) measurements of the wet bulb temperature (t_w) and the dry bulb temperature (t_d) in the inlet and exhaust ducts; (2) the barometric pressure in the inlet duct (P_I) (the exhaust duct is designated by the subscript E and the inlet duct by the subscript I); (3) the differential pressure head in inches of water (DH) between the inlet and exhaust ducts; and (4) the chart reading (CH) used in determining the air flow rate. The measurements for 6 June 1980 are as follows:

Inlet Conditions			Exhaust Conditions			
t_{wI}(°C)	t_{dI}(°C)	P_I(millibars)	t_{wE}(°C)	t_{dE}(°C)	DH(in)	CH
11.0	14.9	1042.5	23.9	30.4	0.10	77

The constants used in the determination of MP are: (1) the gas constant for water vapor, R_v = 461.7 J/kg- K; (2) the gas constant for air, R_a = 287.15 J/kg-K; (3) the specific heat of water vapor at constant pressure,

C_{pv} = 1.884 kJ/kg-K; (4) the specific heat of air at constant pressure, C_{pa} = 1.005 kJ/kg-K; and (5) the density of water (ρ_w) in the inlet and exhaust ducts. The density of water is a function of temperature. Using a table of the density of water for various temperatures (Dean, 1973), the following values of ρ_w at the inlet and exhaust were determined:

Inlet (t_{dI} = 14.9°C): ρ_{wI} = 999.1 kg/m^3

Exhaust (t_{dE} = 30.4°C): ρ_{wE} = 995.5 kg/m^3

A.3 The Procedure

Step 1. Calculation of the latent heat of vaporization of water (L)

The latent heat of vaporization of water (L) is the quantity of heat required to change a unit mass of liquid to vapor without a change in temperature occurring. The latent heat of water is calculated using the following empirical formula:

$$L = 3152.15 - 2.3772t, \tag{A1}$$

where L = latent heat of water (kJ/kg),

t = temperature (K).

To determine the accuracy of Eq. (A1), the percentage error

$$\delta L = \frac{|\text{actual value of L - L based on Eqn. (A1)}|}{\text{actual value of L}} (100)$$

was determined. The actual value of the latent heat of water (Osborne et al., 1939) for the range of 10°C to 50°C as well as the corresponding percentage error are presented in Table A1. These results show that Eq. (A1) is accurate to within 0.10% of the actual value of the latent heat of water, a very good agreement. Equation (A1) will therefore be used.

Table A1. Latent Heat of Water.

Temperature °C	Actual value of L (kJ/kg)	L based on Equation (A1) (kJ/kg)	σL (%)
10	2476.74	2479.05	.09
20	2453.21	2455.27	.08
30	2429.57	2431.50	.08
40	2405.76	2407.73	.08
50	2381.73	2383.96	.09

The latent heat of water will be calculated at the inlet and exhaust for the wet bulb temperature because the process is occurring at that temperature. Step 3, calculating the ratio of mass of water vapor to mass of dry air at saturated air condition (X_S) will be performed at this temperature for the same reason.

L_I = 3152.15 - 2.3772 (11.0 + 273.15) = 2476.669 kJ/kg.

L_E = 3152.15 - 2.3772 (23.9 + 273.15) = 2446.003 kJ/kg.

Step 2: Calculation of the saturation vapor pressure of water (e_{SW})

The saturation vapor pressure is derived on the basis of the Clausius-Clapeyron equation employing the previously presented empirical relationship for L. The saturation vapor pressure is the vapor pressure of water in air under saturated conditions. It will be used to calculate (X_S) in the next step.

$$e_{SW} = 610.6 \exp\left(\frac{17.27t}{237.3 + t}\right) \qquad \text{(A2)}$$

where t = temperature (°C).

The percentage error between the actual value of the saturation vapor pressure of water and that based on equation (A2) was found to be less than 0.10 for the temperature range 10°C to 50°C, signifying good agreement. The saturation vapor pressure will be calculated for the wet bulb temperature at the inlet and exhaust duct conditions:

$$e_{swI} = 610.6 \exp\left(\frac{17.27(11)}{237.3 + 11}\right) = 1312.284 \text{ Pa}$$

and

$$e_{swE} = 2956.083 \text{ Pa} \quad .$$

A.5 Step 3: Calculation of the ratio of the mass of water vapor to the mass of dry air for saturated air conditions (X_s)

The derivation of X_s is based on the ideal gas law:

$$PV = mRt$$

where

m = mass of gas,

P = total pressure,

V = volume,

t = temperature,

R = gas constant.

By considering a mass of 1 kg of dry air, the partial pressure of air and water at saturated air condition are:

$$P_a V = 1(R_a)\, t \qquad \text{(i)}$$

$$e_{sw} V = X_s (R_v) t \qquad \text{(ii)}$$

where the subscript "a" denotes air and the subscript "v" denotes water vapor. Solving (i) and (ii) for X_s where $P_a = P - e_{sw}$, the following equation results:

$$X_s = \frac{R_a}{R_v} \frac{e_{sw}}{P - e_{sw}} \quad . \tag{A3}$$

For the inlet:

$$X_{sI} = \left(\frac{287.15}{461.7}\right) \frac{1312.284}{104250 - 1312.284} = 0.00793 \ \frac{\text{kg - water}}{\text{kg - moist air}} \quad .$$

To determine X_s at the exhaust, P_E must be calculated from the differential pressure head:

$$P_E = P_I - \rho_{WE} g(DH)$$

or converting to appropriate units for the instrumentation used:

$$P_E = P_I - 0.24925 \rho_{WE}(DH)$$

where the units are:

$P_I = P_E = (Pa)$

$\rho_{WE} = (kg/m^3)$

$DH = (\text{inches of water})$

so:

$$P_E = 104250 - 0.24925\ (995.5)(0.10) = 104225.187 \text{ Pa}$$

Thus, at the exhaust:

$$X_{sE} = 0.01821 \text{ kg-water/kg-air}$$

<u>Step 4: Calculation of ratio of mass of water vapor to mass of dry air at ambient condition (X)</u>

The latent heat transfer (LE) is:

$$LE = L(\text{mass transferred}) = L(X_s - X) \tag{A4}$$

where L is the latent heat of evaporation computed earlier. This energy transfer is taking place at the wet bulb temperature.

At equilibrium, the amount of latent energy transfer is balanced by the amount of sensible heat transfer (q) due to the convection of air:

$$q = C_{pm}(\text{mass of moist air})(\text{change in temp.})$$

$$= C_{pm}(1 + X)(t_d - t_w)$$

where C_{pm} = specific heat of the moist air.

By calculating the sensible heat transfer of both the dry air (q_a) and the water vapor (q_v) individually and then equating the sum $q_a + q_v$ to the total sensible heat transfer (q), C_{pm} is found to be:

$$C_{pm} = \frac{C_{pa} + XC_{pv}}{1 + X} \quad . \tag{A6}$$

Equating (A5) to (A4) and using (A6), X is determined to be:

$$X = \frac{LX_s - C_{pa}(t_d - t_w)}{C_{pv}(t_d - t_w) + L}$$

for the inlet

$$X_I = \frac{(2467.669)(0.00793) - 1.005(14.9 - 11.0)}{1.884(14.9 - 11.0) + 2476.669} = 0.00633 \ \frac{\text{kg - water}}{\text{kg - air}}$$

and exhaust

$$X_E = 0.01546 \ \frac{\text{kg - water}}{\text{kg - air}} \quad .$$

A.7 <u>Step 5: Calculation of vapor pressure of water at ambient condition (e)</u>

The evaluation of e will lead to the determination of the density of moist air ($\rho_{m(act)}$) and the density of dry air ($\rho_{m(app)}$), two essential properties necessary in the calculation of the net moisture pickup. The vapor pressure of water at ambient condition is determined using the ideal gas law as in step 3. This leads to the following:

$$e = \frac{PX}{X + \frac{R_a}{R_v}}$$

so

$$e_I = \frac{(104250)(0.00633)}{0.00633 + \frac{287.15}{461.7}} = 1049.915 \text{ Pa}$$

and

$$e_E = 2528.510 \text{ Pa} \quad .$$

Step 6: Calculation of density of moist air ($\rho_{m(act)}$)

The density of moist air $\rho_{m(act)}$ is derived using the ideal gas law. For 1 kg of moist air:

$$\rho_{m(act)} = \frac{1}{V} = \frac{P}{R_m t} \quad . \tag{A7}$$

The following two equations are based on the ideal gas law:

$PV = (1 + X)R_m t;$

$PV = (P_a + P_v)V = (R_a + XR_v)t.$

Solving these equations for R_m and substituting the relationship for X determined in a similar manner to X_s in Eq. (A3):

$$R_m = \frac{R_a P}{P - \left(1 - \frac{R_a}{R_v} e\right)} \quad .$$

Substituting this term for R_m in (A7) leads to:

$$\rho_{m(act)} = \frac{P - \left(1 - \frac{R_a}{R_v} e\right)}{R_a t} \quad .$$

The density of moist air is computed at ambient air conditions and therefore the dry bulb temperature is substituted in the equation above.

$$\rho_{m(act)I} = \frac{104250 - \left(1 - \frac{287.15}{461.7}\ 1049.915\right)}{287.15\ (273.15 + 14.9)} = 1.256\ \frac{\text{kg - moist air}}{m^3} ,$$

and the exhaust:

$$\rho_{m(act)E} = 1.185\ \frac{\text{kg - moist air}}{m^3} .$$

Step 7: Calculation of the standard air flow rate (Q_{st})

Calibration curves were determined in the field for each air flow measuring device to determine the relationships between Q_{st} and the chart reading (CH). In preparing the calibration curves, the air flow was standardized for $\rho_{m(act)} = \rho_{st} = 1.20\ kg/m^3$. Figures A1 to A4 present the four calibration curves corresponding to the four changes in flow measuring devices that occurred during the Stripa ventilation drift study. Each calibration curve therefore corresponds to a given time period as indicated in Table 4.

The calibration curves were fitted to the calibration data by using the method of least-squares regression analysis. A fundamental assumption incorporated in regression analysis is that the values of the independent variable (i.e., CH) are nonrandom or known. In the process of determining the standard air flow, this implies that no error occurs in obtaining the chart reading. However, inspection of the actual chart recordings will show that the readings fluctuate by approximately ±1.25 CH because of turbulence in the air. Because of this the average value of the chart reading was assumed to be characteristic of the average air flow for the purpose of computing moisture pickup.

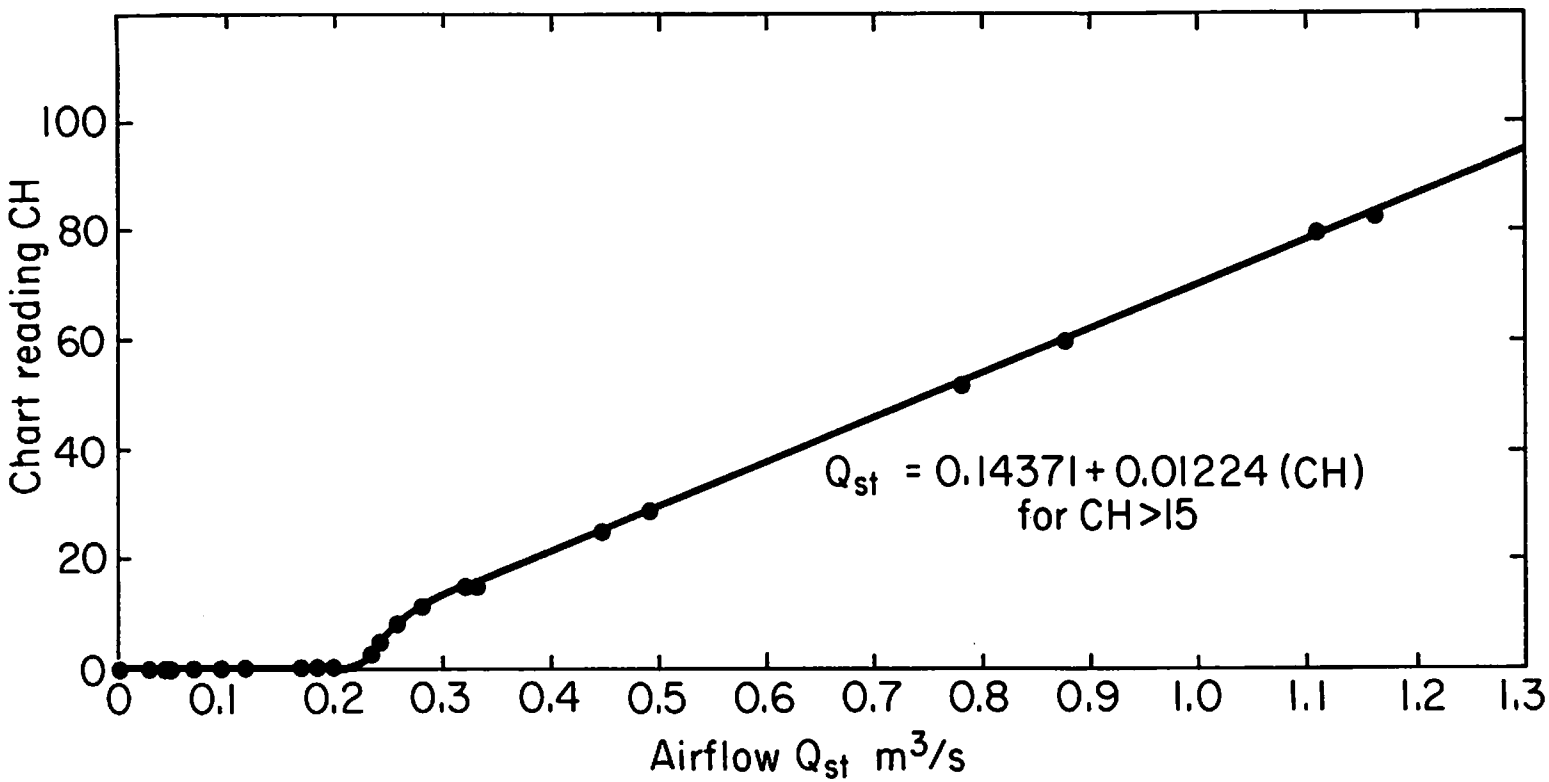

XBL 814-2810

Fig. A1. Air flow monitor calibration for test period of August 1979 to 22 April 1980.

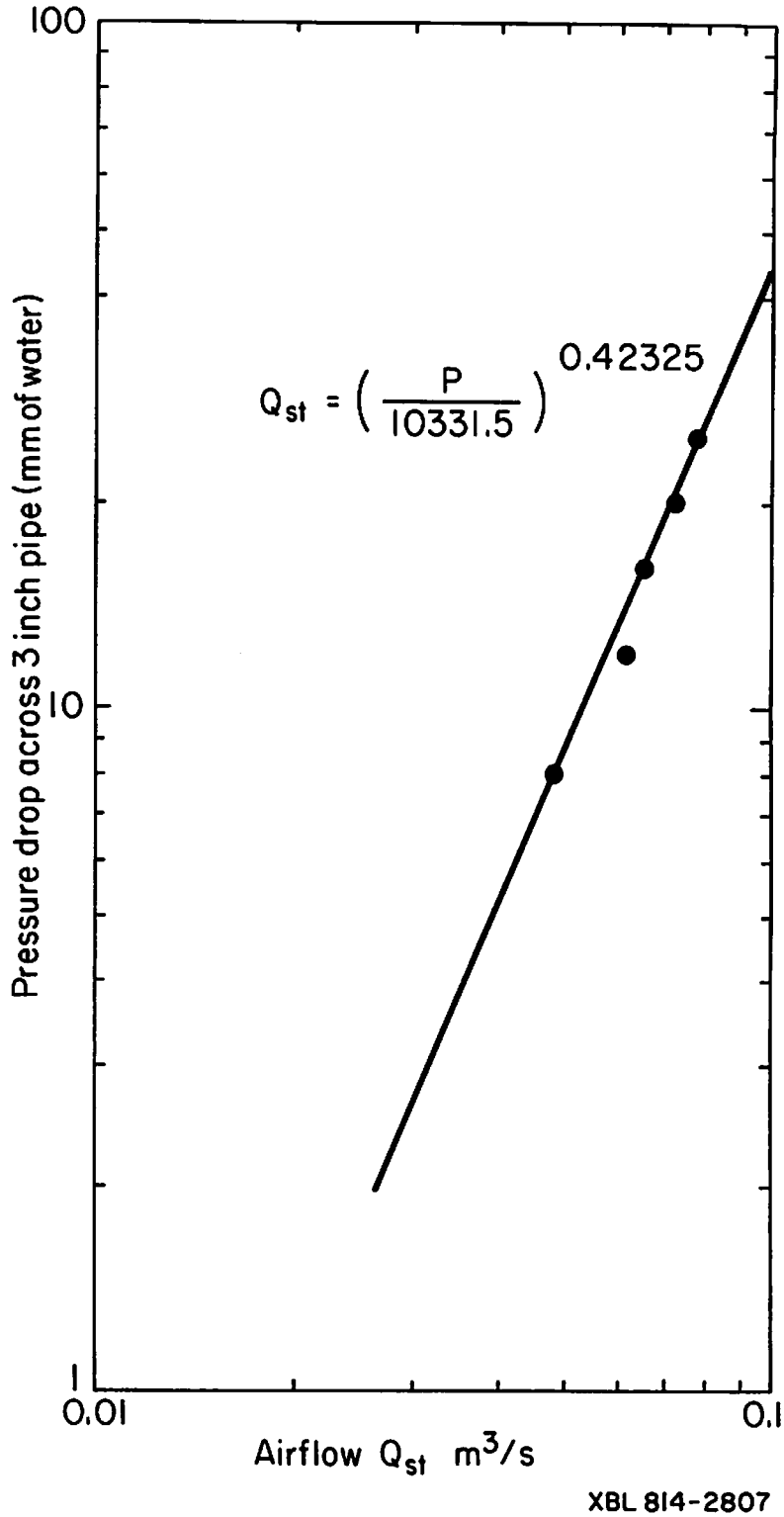

Fig. A2. Air flow monitor calibration for test period of 14 May 1980 to 27 May 1980.

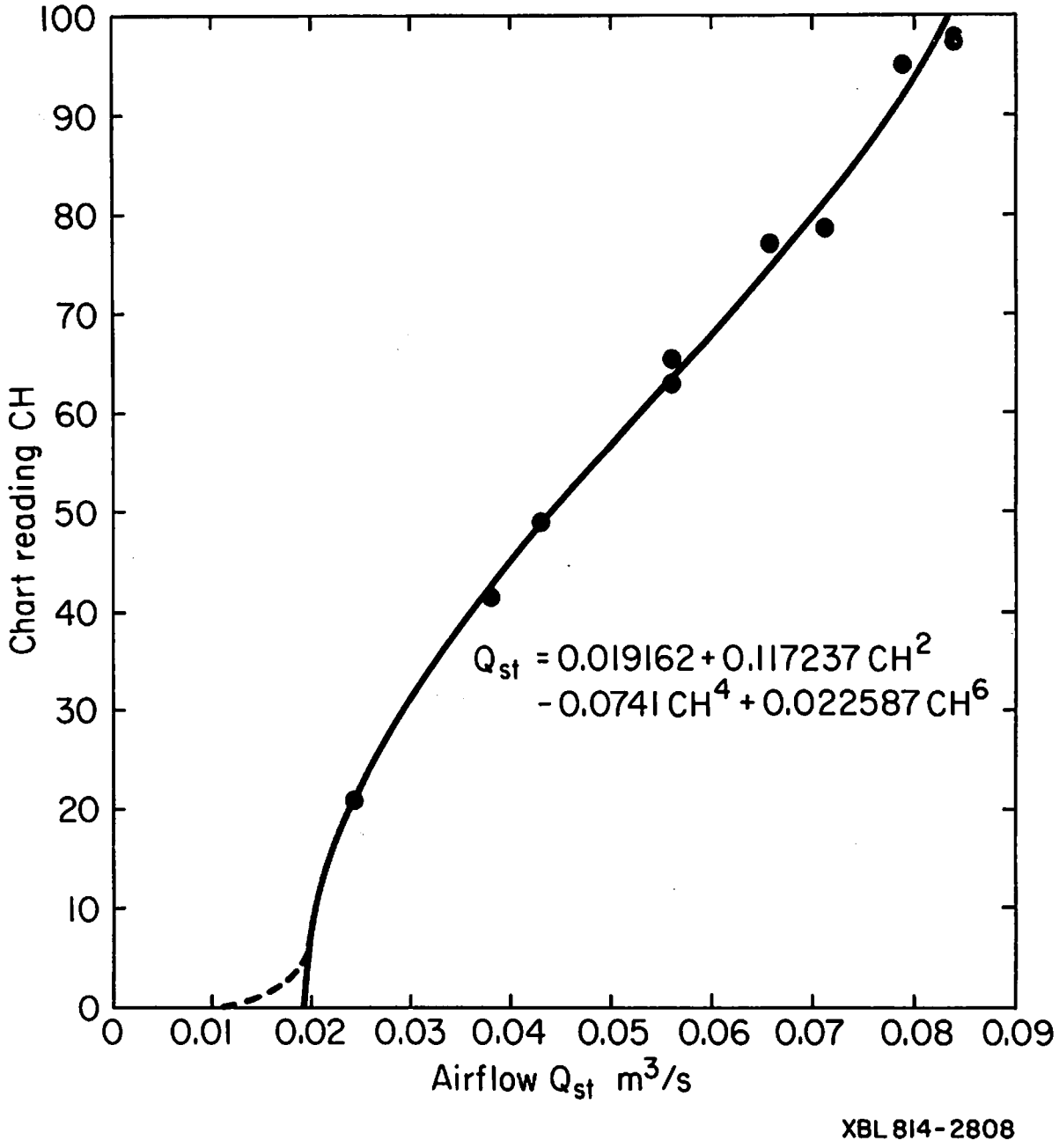

Fig. A3. Air flow monitor calibration for test period of 28 May 1980 to 29 July 1980.

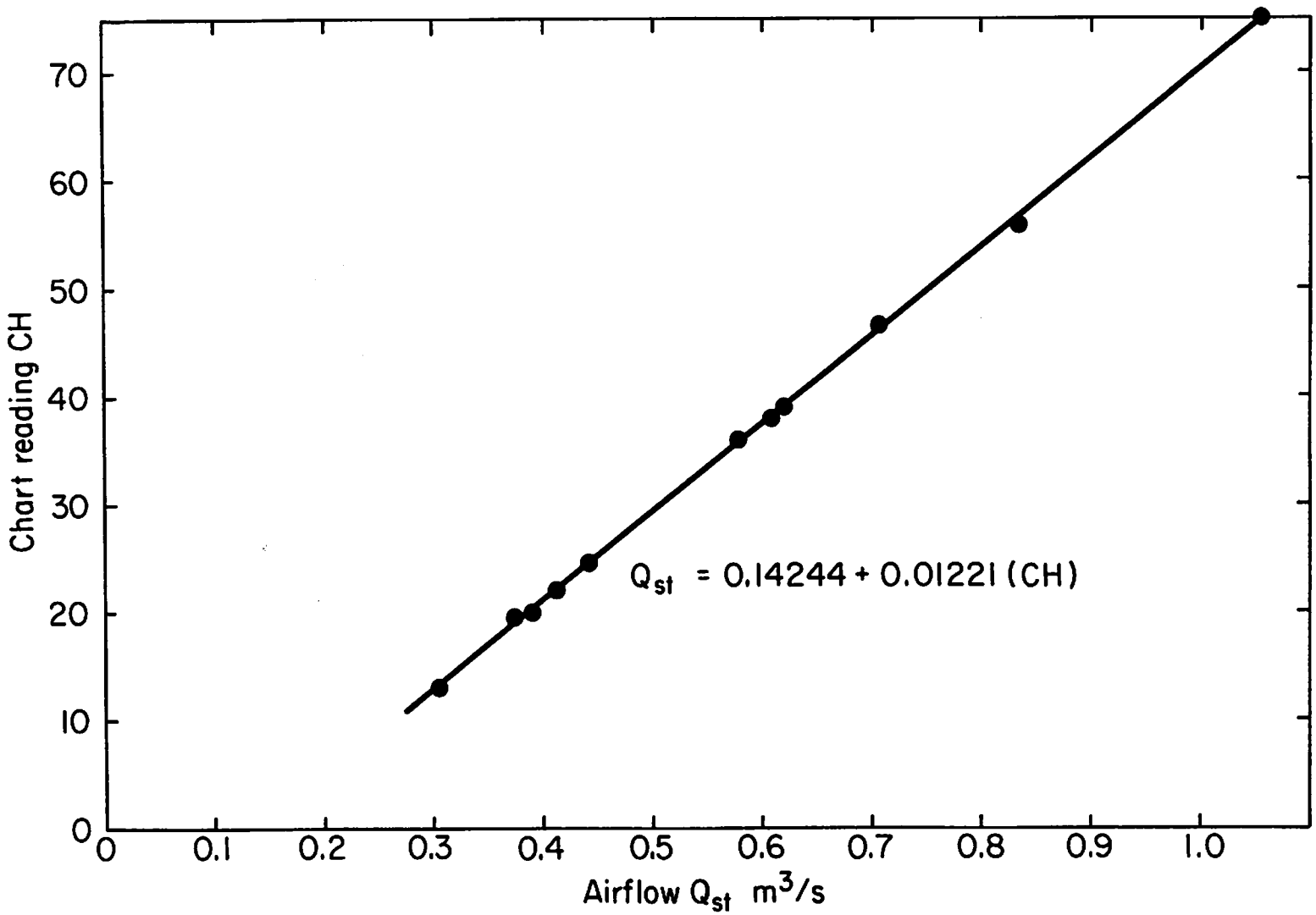

XBL 814-2809

Fig. A4. Air flow monitor calibration for test period of 2 August 1980 to 22 September 1980.

The standard air flow for 6 June 1980 can be calculated from the following equation (see Fig. A3):

$$Q_{st} = 0.019162 + 0.117237\left(\frac{CH}{100}\right)^2 - 0.0741\left(\frac{CH}{100}\right)^4 + 0.022587\left(\frac{CH}{100}\right)^6 \quad .$$

From the data, CH = 77. Therefore:

$$Q_{st} = 0.019162 + 0.117237(0.77)^2 - 0.0741(0.77)^4 + 0.022587(0.77)^6 =$$

$$= 0.0673 \text{ m}^3/\text{s} \quad .$$

<u>Step 8: Calculation of actual air flow (Q_{act})</u>

The actual air flow is:

$$Q_{act} = Q_{st}\sqrt{\frac{\rho_{st}}{\rho_{m(act)}}} \quad .$$

This equation is based on the fact that the chart reading is proportional to the square root of the velocity head (McPherson, 1979b). So:

$$Q_{actI} = 0.0673\sqrt{\frac{1.2}{1.256}} = 0.0658 \text{ m}^3/\text{s}$$

and:

$$Q_{actE} = 0.0677 \text{ m}^3/\text{s}$$

<u>Step 9: Calculation of density based on dry air fraction $\rho_{m(app)}$</u>

The density of dry air is derived in a manner similar to that for the density of moist air. The density of dry air is found to be:

$$\rho_{m(app)} = \frac{P - e}{R_a\, t_d} \quad .$$

Therefore:

$$\rho_{m(app)I} = \frac{104250 - 1049.915}{(287.15)(273.15 + 14.9)} = 1.248 \text{ kg/m}^3$$

and:

$$\rho_{m(app)E} = \frac{104225.185 - 2528.510}{(287.15)(273.15 + 30.4)} = 1.167 \text{ kg/m}^3 \quad .$$

Step 10: Calculation of equivalent liquid water flow rate (v)

The equivalent liquid water flow rate (v) can be calculated from the following mass flow relationship:

$X \cdot$ [mass flow of dry air] = mass flow of water = ρ_w[volumetric moisture flow rate]

or:

$$X \cdot [\rho_{m(app)} Q_{act}] = \rho_w v$$

so:

$$v = \frac{X\rho_{m(app)}Q_{act}}{\rho_w} (60 \times 10^6)$$

where v = (ml/min) and the other terms have SI units.

So:

$$v_I = \frac{0.00633(1.248)(0.0658)}{999.1} 60 \times 10^6 = 31.21 \text{ ml/min}$$

and:

$$v_E = 73.69 \text{ ml/min.}$$

A.13 Step 11: Calculation of net moisture pickup (MP)

$$MP = v_E - v_I = 73.69 - 31.21 = 42.48 \text{ ml/min.}$$

APPENDIX B. EQUATIONS FOR SENSITIVITY OF NET MOISTURE PICKUP TO VARIOUS INPUT PARAMETERS

The equations used in determining the sensitivity of the net moisture pickup to the intial input parameters will be presented. If no subscript (E or I) appears in the equation, the equation is applicable at both the exhaust and inlet.

B.1 Sensitivity with Respect to t_d

$$\frac{\partial MP}{\partial t_{dE}} = \frac{\partial v_E}{\partial t_{dE}} \quad \text{and} \quad \frac{\partial MP}{\partial t_{dI}} = -\frac{\partial v_I}{\partial t_{dI}}$$

where $$\frac{\partial v}{\partial t_d} = \left(\frac{v}{X}\right)\frac{\partial x}{\partial t_d} + \left(\frac{v}{Q_{act}}\right)\frac{\partial Q_{act}}{\partial t_d} + \left(\frac{v}{\rho_{m(app)}}\right)\frac{\partial \rho_{m(app)}}{\partial t_d}$$

$$\frac{\partial X}{\partial t_d} = \frac{-\left(2C_{pa}C_{pv}\,(t_d-t_w) + C_{pa}L + C_{pv}LX_s\right)}{\left(C_{pv}\,(t_d-t_w) + L\right)^2}$$

$$\frac{\partial Q_{act}}{\partial t_d} = -\frac{1}{2}\frac{Q_{act}}{\rho_{m(act)}}\frac{\partial \rho_{m(act)}}{\partial t_d}$$

$$\frac{\partial \rho_{m(act)}}{\partial t_d} = -\frac{\rho_{m(act)}}{t_d}$$

$$\frac{\partial \rho_{m(app)}}{\partial t_d} = -\frac{1}{R_a t_d}\frac{\partial e}{\partial t_d} - \frac{(P-e)}{R_a t_d^{\,2}}$$

and

$$\frac{\partial e}{\partial t_d} = \frac{p\left(\frac{R_a}{R_v}\right)}{\left(X + \frac{R_a}{R_v}\right)^2}\frac{\partial X}{\partial t_d}$$

B.2 Sensitivity with Respect to t_w

$$\frac{\partial MP}{\partial t_{wE}} = \frac{\partial v_E}{\partial t_{wE}} \quad \text{and} \quad \frac{\partial MP}{\partial t_{wI}} = -\frac{\partial v_I}{\partial t_{wI}}$$

where
$$\frac{\partial v}{\partial t_w} = \left(\frac{v}{X}\right)\frac{\partial X}{\partial t_w} + \frac{v}{\rho_{m(app)}}\frac{\partial \rho_{m(app)}}{\partial t_w},$$

$$\frac{\partial X}{\partial t_w} = \frac{L}{C_{pv}\left(t_d - t_w\right) + L}\frac{\partial X_s}{\partial t_w} - 2.3772\,\frac{\partial X}{\partial L} + \frac{L\left(C_{pa} + C_{pv}X_s\right)}{C_{pv}\left(t_d - t_w\right) + L^{\,2}}$$

$$\frac{\partial X_s}{\partial t_w} = \frac{R_a}{R_v}\,\frac{P}{\left(P - e_{sw}\right)^2}\,\frac{\partial e_{sw}}{\partial t_w}$$

$$\frac{\partial e_{sw}}{\partial t_w} = \frac{(17.27)(237.3)}{237.3 + (t_w - 273.15)^{\,2}}\,e_{sw}$$

$$\frac{\partial X}{\partial L} + \frac{X_s C_{pv}(t_d - t_w) + C_{pa}\,(t_d - t_w)}{\left(C_{pv}(t_d - t_w) + L\right)^2}$$

$$\frac{\partial \rho_{m(app)}}{\partial t_w} = -\frac{1}{R_a t_d}\,\frac{\partial e}{\partial t_w}$$

and
$$\frac{\partial e}{\partial t_w} = \frac{P\left(\frac{R_a}{R_v}\right)}{\left(X + \frac{R_a}{R_v}\right)^2}\,\frac{\partial X}{\partial t_w}$$

B.3 Sensitivity with respect to P

$$\frac{\partial MP}{\partial P_E} = \frac{\partial v_E}{\partial P_E} \text{ and } \frac{\partial MP}{\partial P_I} = -\frac{\partial v_I}{\partial P_I}$$

where $$\frac{\partial v}{\partial P} = \frac{v}{X}\frac{\partial X}{\partial P} + \frac{v}{Q_{act}}\frac{\partial Q_{act}}{\partial P} + \frac{v}{\rho_{m(app)}}\frac{\partial \rho_{m(app)}}{\partial P}$$

$$\frac{\partial X}{\partial P} = \frac{L}{C_{pv}\left(t_d - t_w\right) + L}\frac{\partial X_s}{\partial P}$$

$$\frac{\partial X_s}{\partial P} = -\frac{R_a}{R_v}\frac{e_{sw}}{\left(P - e_{sw}\right)^2}$$

$$\frac{\partial Q_{act}}{\partial P} = -\frac{Q_{act}}{2\rho_{m(act)}}\frac{\partial \rho_{m(act)}}{\partial P}$$

$$\frac{\partial \rho_{m(act)}}{\partial P} = -\frac{1}{R_m t_d}$$

and $$\frac{\partial \rho_{m(app)}}{\partial P} = \frac{1}{R_a t_d}$$

B.4 Sensitivity with respect to CH

$$\frac{\partial MP}{\partial CH} = \frac{\partial v_E}{\partial CH} - \frac{\partial v_I}{\partial CH}$$

where $$\frac{\partial v}{\partial CH} = \frac{v}{Q_{act}}\frac{\partial Q_{act}}{\partial CH}$$

$$\frac{\partial Q_{act}}{\partial CH} = \sqrt{\frac{\rho_{st}}{\rho_{m(act)}}}\frac{\partial Q_{st}}{\partial CH}$$

and $\frac{\partial Q_{st}}{\partial CH}$ depends on the calibration curve used.